Lattice QCD at Finite Baryon Density with an Implementation of Dynamical Fermions

Susan Elizabeth Morrison

Thesis submitted to
the University of Glasgow
for the degree of Doctor of Philosophy
in September 1997

Department of Physics & Astronomy,
Kelvin Building,
University of Glasgow,
Glasgow, G12 8QQ

ProQuest LLC.
789 East Eisenhower Parkway
P.O. Box 1346
Ann Arbor, MI 48106 – 1346

This Thesis is dedicated to my Mother and Father in recognition of their constant support and encouragement, to my sister Linda for her friendship and to David, who helped me to put things in perspective.

Acknowledgements

I would like to thank the many people in the Department of Physics and Astronomy who have helped to make my Postgraduate studies in Glasgow such a pleasurable experience. I particularly enjoyed my tutorials on Quantum Field Theory with Professor Moorhouse during the first year of my PhD. I have benefited greatly from the patient guidance and encouragement of my supervisor Dr. Ian Barbour. I also appreciated the advice of Dr. Christine Davies.

The Glasgow Postdocs: Hugh Shanahan, Arifa Ali-Khan, Sara Collins and Joachim Hein have proved to be an invaluable mine of information and I have highly valued their friendship. I am also grateful to Dr. Gerry Lowe for lending me his excellent notes on Quantum Field Theory and for his assumed role as my "mentor".

I have enjoyed the company of the Postgraduate students including Steven, Douglas who helped me considerably during my first year; Nektarios, Paul and Mark G. with whom I have shared numerous discussions; Scott for his lively enthusiasm and of course David for his contributions which are too numerous to mention.

It has been a great source of stimulation to work in collaboration with Professor John Kogut, Dr. Maria-Paola Lombardo and Dr. Ely Klepfish all of whom have contributed significantly to my understanding of finite density QCD.

Finally I would like to thank Professor Frithjof Karsch and Manfred Oevers for their collaborative work in exploring the monomer-dimer approach to simulating finite density QCD at infinite coupling.

This work was funded by the Particle Physics and Astronomy Research Council (PPARC).

Declaration

In this thesis Chapters 1 and 2 are introductions to lattice QCD at non-zero chemical potential. Chapter 3 describes Lee-Yang zeros analysis and two eigenvalue routines, one of which I proposed for implementation in the finite density QCD simulation algorithm. Chapters 4, 5, 6 and 7 are all my own original work. The work in Chapter 4 was done in collaboration with Dr. M.-P. Lombardo, Dr. E. Klepfish and Prof. J. B. Kogut. Chapters 5 and 7 involved collaboration with Prof. J. B Kogut. Chapter 6 involved collaboration with Dr M. P. Lombardo and Prof J. B. Kogut although I also benefited from discussion with Dr. S. Hands. All of the work in this thesis was done in conjunction with my supervisor Dr. I. M. Barbour.

Abstract

Simulations of Lattice QCD at non-zero chemical potential (finite baryon density) have been performed with the inclusion of dynamical fermions. The fundamental difficulty in simulating QCD at finite density and investigating the colour deconfinement and chiral transitions quantitatively is that the Grassmann integration over the fermion fields is complex as a result of the introduction of the chemical potential in the Dirac matrix. The complex nature of the QCD finite density action prohibits the use of naive probabilistic methods in evaluating the functional integral. Early simulations which avoided the problem of the complex action by looking at the theory in the quenched approximation where the determinant is set to a constant value gave unphysical results. In the quenched theory the onset of chiral symmetry restoration which should be determined by the mass of the lightest particle with non-zero baryon number, did not occur at a chemical potential equal to one third of the proton mass ($\mu = m_p/3$) as expected, but appeared to occur at one half of the pion mass ($\mu = m_\pi/2$) - a value which would extrapolate to zero in the chiral limit. The accepted explanation for the pathologies of the quenched theory is that the inclusion of the complex fermion determinant in the theory is essential. This thesis describes unquenched simulations of Lattice QCD at finite baryon density on 6^4 and 8^4 lattices. The problem caused by the non-Hermitian nature of the fermion matrix at $\mu \neq 0$ is circumvented by a method first proposed by Barbour and collaborators [1] which involves expressing the Grand Canonical Partition Function (GCPF) as an ensemble average of the fermion determinant at zero chemical potential. The GCPF is expanded in powers of the fugacity variable $e^{\mu/T}$ (where T is the physical temperature). The method is an example of a **reweighting** technique. The Lee-Yang zeros of the partition function are analysed to probe the phase structure of the theory.

The method is applied at infinite gauge coupling ($\beta = 0$) where analytic results from the strong coupling expansion and from mean-field theory are available as

well as numerical results from the monomer-dimer algorithm. The analytical arguments of Gibbs which pertain to the quenched theory are further developed and applied to give an improved Lee-Yang zeros analysis which allows determination of a critical point, μ_c, in agreement with that predicted by strong coupling expansions and monomer-dimer simulations. We do observe, however, two unphysical critical points:- μ_o, the onset for the free quark number density and the saturation threshold, μ_s, both of which are coincident with pathological onsets observed in the quenched QCD simulations. An analysis of the probability distributions for particle number supports our physical interpretation of the critical point μ_c, and offers a new interpretation of μ_o which confirms its unphysical nature.

The method is also applied at intermediate gauge coupling $\beta = 5.1$. For these simulations $S_G \neq 0$ so that the gauge fields are no longer random (as they were in the strong coupling simulations). We present evidence for $Z(3)$ tunnelling which confirms that our system is in the confined phase at $\mu = 0$. The onset in the fermion number density and energy density is investigated. The zeros analysis developed for the strong coupling simulations is applied here also. The dependence of the onset on the bare quark mass is investigated to determine whether the scaling can be associated with a Goldstone pion. We demonstrate for the first time that the pathological onset first observed in the quenched theory persists when dynamical fermions are implemented using the Glasgow reweighting method.

To address the question of whether the reweighting procedure is sufficiently effective in its implementation of dynamical fermions an exploratory study of the 3 dimensional Gross-Neveu model at $\mu \neq 0$ was performed. Although this model does not confine it does exhibit chiral symmetry restoration and has a massless pion in the chiral limit. This model does not have a complex fermion determinant when $\mu \neq 0$ (it is actually positive definite) therefore exact simulations are possible and have been performed by Hands *et. al.* [2] Thus it was possible to provide a direct comparison between fermion number densities obtained using the exact method with those obtained using our reweighting method with a statistical ensemble generated at zero chemical potential. This is analogous to the procedure we adopt in QCD. In the Gross-Neveu model is was also possible to choose an update chemical potential (at which the ensemble is generated) which is non-zero therefore we performed simulations for update chemical potentials both above and below the known critical value. An independent estimate of the critical chemical potential was obtained from the Lee-Yang zeros. The simulations were repeated for two different four-fermi couplings and comparison was made with the published exact results.

Having established the persistence of the early onset of the chiral/deconfinement transition in full QCD which we associate with the mass poles of the fermion propagator on isolated configurations a new approach to finite density lattice QCD simulations has been investigated. This approach involves adding a perturbatively irrelevant four-fermion interaction term to the lattice QCD Lagrangian. This theory which we call χQCD has the advantage that chiral symmetry breaking and the generation of a dynamical quark mass occurs **configuration-by-configuration** and the pion and sigma excitations are explicitly free of μ dependence. In addition it is possible in χQCD to simulate directly in the chiral limit (zero bare quark mass). χQCD simulations were performed on a 4^4 lattice at $\beta = 0.5$, on a 6^4 lattice at $\beta = 5.0$ and on an 8^4 lattice at $\beta = 4.0$. The onset in the fermion number density for a range of four-fermion couplings was determined. The Lee-Yang zeros have also been analysed. We have seen that for the range of four-fermi couplings explored, χQCD simulations do not appear to suffer from the severe μ_o pathologies seen in standard QCD. Certainly additional analytical and numerical work is required to see if χQCD really produces only physical results. In particular, it will be necessary in future work to explore the interplay between the gauge coupling and the four-fermi coupling in order to determine the range of couplings for which QCD dynamics is dominant.

The computations were performed on the C90 machines at the Pittsburgh Supercomputing Centre (PSC) and the National Energy Research Scientific Computing Centre (NERSC) which is located at Ernest Orlando Lawrence Berkeley Laboratory.

Contents

Chapter 1

Introduction

1.1 Motivation

The principal motivation for simulations of QCD at finite density is to confirm that QCD is the correct theory of the strong interactions. Although there is strong evidence that this is the case certain outstanding questions remain, as yet, unanswered. For example does QCD predict the pattern of chiral symmetry breaking observed in nature?

On the basis of elementary physics arguments we should be able to demonstrate that there is a chiral phase transition which is directly related to the mass of the lightest baryon. Although colour confinement is strongly inferred from the scaling of the strong coupling constant we still await a rigorous proof of confinement which generalises to the continuum limit. We also await numerical evidence for colour deconfinement at finite baryon density for non-vanishing chemical potential in the chiral limit ($m \to 0$). We would also like to understand the interplay of chiral symmetry breaking and deconfinement.

Aside from fundamental physics considerations the study of the phase structure of QCD has a wide range of applicability as explained below and illustrated in Fig. 1.1.

Simulations of the QCD phase transition at **finite temperature** are relevant to

- **Cosmology** – the existing theories of the early universe suggest that the latest phase transition since the big bang was the one of confinement of quarks and spontaneous breaking of the chiral symmetry. Possible effects associated with this phase transition are baryon creation and fluctuations in the baryon

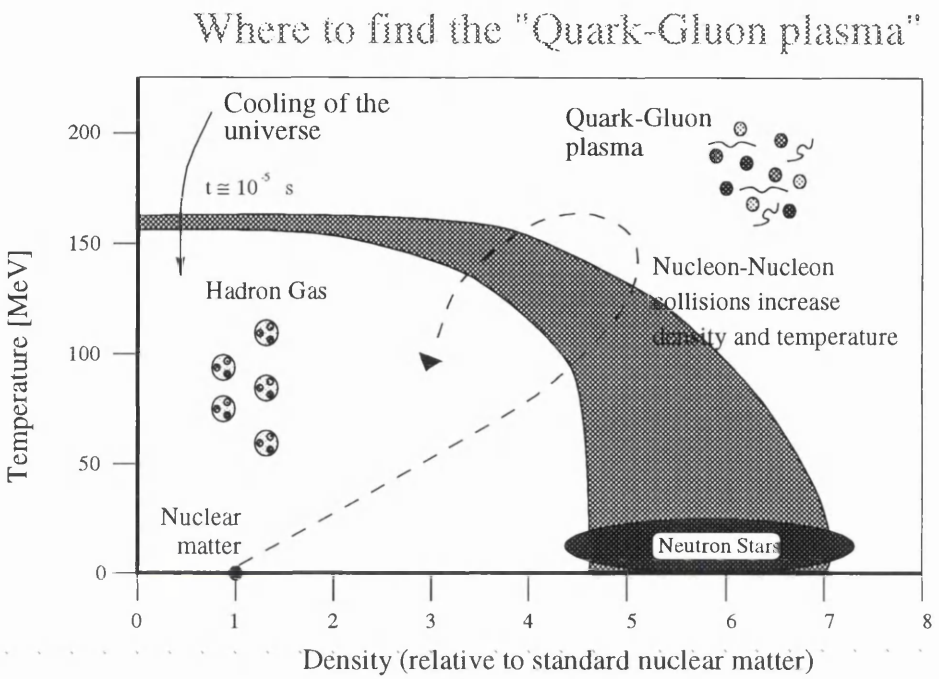

Figure 1.1: Phase diagram illustrating the temperature and density regimes where we expect the quark-gluon plasma to be found.

density, which could be the seeds of galaxy formation. Possible consequences of a strongly first-order transition are the generation of additional entropy and increased expansion in the supercooled phase of the universe due to the release of latent heat. This phase transition could also induce perturbations in the cosmic microwave background radiation which is the photon spectrum produced due to the recombination radiation emitted when hadrons are first formed [3, 4].

- **Heavy ion collisions** – the experimental evidence for a formation of the quark-gluon plasma is expected from the BNL Relativistic Heavy Ion Collider and CERN Large Hadron Collider. The energy densities of $(2 - 10\ \mathrm{GeV/fm}^3)$ that can be reached in these experiments may be sufficient to create, for a short time, the energy per nucleon and the densities sufficient to probe the transition into the deconfined phase [5]. Zero or vanishing net quark number densities occur in the *central rapidity region* of heavy ion collisions. Therefore finite temperature studies ($\mu = 0$ axis of the phase diagram) can make useful predictions of thermodynamic quantities and other observables here.

The QCD phase transition at **finite baryon density** is applicable to:

1. **Heavy ion collisions** – the baryon-rich *fragmentation region* of these experiments requires a knowledge of the equation of state in the temperature–chemical potential plane (i.e. $\mu \neq 0$).

2. **Neutron stars** – the density of nucleons in the interior of a neutron star is much higher than ordinary nuclear density, and it is approaching the value at which the restoration of the chiral symmetry may occur [6, 3]. This is an example of a "cold" highly dense nucleon matter, which is the most challenging for a theoretical investigation. A knowledge of the equation of state for a neutron star would be useful for models of stellar structure.

1.1.1 Introduction

QCD is the $SU(3)$ non-abelian gauge theory of the strong interactions. The basic degrees of freedom are quarks and gluons which both carry colour charge. The quarks come in 6 flavours and three colours , but only the colour index participates in the local gauge symmetry. The most important feature of QCD is **asymptotic freedom**. A rigorous proof that the Yang-Mills theory confines quarks and gluons has still to be found but using the *renormalization group* it can be demonstrated that the strong coupling constant, α_s, varies with energy. At high energies $\alpha_s \ll 1$ so quarks behave like free particles and perturbation theory can be applied. However for low energy processes $\alpha_s \to 1$, quarks and gluons are confined to hadrons and non-perturbative methods are required. The parameter $\Lambda_{QCD} \sim 200 - 500$ MeV is the *confinement scale* and defines the crossover between the two regimes. For processes with a typical momentum scale $p \lesssim \Lambda_{QCD}$ non-perturbative techniques are required in order to calculate observables.

1.1.2 Lattice QCD

The Lattice formulation of QCD introduced by Wilson in 1974 provides us with a framework to study QCD non-perturbatively. It provides a renormalization scheme for Quantum Field Theory where gauge invariance is ensured for **any** finite lattice spacing and enables systematic calculation without the aid of Feynman diagrams. Lattice field theory is essentially a means of defining the Feynman path integral. The lattice renormalisation program on Feynman integrals in momentum space consists of

- **Regularization**:– the infinities in Feynman integrals are due to UV divergence. Expression of the path integral in terms of a **spacetime lattice** ren-

ders the momentum integration in the Feynman integrals finite by providing a natural cut-off at a momentum of the order of the inverse lattice spacing.

- **Renormalisation**:– the lattice structure is removed by going to the continuum limit where we let the lattice spacing tend to zero, keeping the physical quantities independent of the lattice structure by tuning bare parameters in a definite way.

Continuum Yang-Mills theory is defined on the *Lie algebra* of the gauge group and is unique. A distinctive feature of lattice gauge theory essential to its conceptual simplicity is the fact that the basic building blocks are the *elements of the Lie group* themselves. The group elements are assigned to the links of a hypercubic lattice (3 dimensions in space and one in time). In the path integral formulation of the model the group elements are freely integrated over. Since the group volumes are finite, path integrals are well-defined and have simple invariance properties. This allows gauge invariance to be stated precisely in the full fluctuating theory. In this respect the lattice model is conceptually simpler than the weak-coupling *perturbative formulation* based on the Lie algebra of the group. As in classical continuum theory, local gauge invariance on the lattice dictates the form of the interactions. By applying local gauge invariance and by insisting on the locality of interactions, lattice actions can be formulated which:

- have classical continuum limits which reproduce the Yang-Mills theory.
- have strong coupling limits for which quark confinement can be demonstrated explicitly.

1.2 Lattice Discretization

There are many different ways of discretizing a given continuum action for the lattice. It is important for universality that they do not lead to different continuum theories in the limit of the lattice spacing going to zero. In addition it is desirable to retain the symmetries of the continuum action in the lattice discretization.

The continuum action of QCD in Euclidean space is $S_{QCD}^{(cont.)} = S_G^{(cont.)} + S_F^{(cont.)}$ where the Yang-Mills gauge action is given by

$$S_G^{(cont.)} = \frac{1}{2} Tr \int d^4x \, F_{\mu\nu} F^{\mu\nu} \tag{1.1}$$

where

$$F_{\mu\nu} = \partial_\mu A_\nu(x) - \partial_\nu A_\mu(x) - ig[A_\mu(x), A_\nu(x)] \tag{1.2}$$

$$A_\mu(x) = \sum_{B=1}^{8} A_\mu^B(x)\frac{\lambda_B}{2} \tag{1.3}$$

$A_\mu(x)$ is an element of the Lie algebra of $SU(3)$ and the λ_B are the 3×3 Gell-Mann matrices which are the SU(3) group generators.

The Dirac fermionic action is

$$\begin{aligned} S_F^{(cont.)} &= \int d^4x\, \bar{\psi}(x)\left(\gamma_\mu(\partial_\mu + ig_o A_\mu) + m_o\right)\psi(x) \qquad (1.4)\\ \gamma_\mu\gamma_\nu + \gamma_\nu\gamma_\mu &= 2\delta_{\mu\nu}\ ;\ \gamma_\mu^\dagger = \gamma_\mu \end{aligned}$$

In the Feynman path integral formulation the QCD partition function is given by

$$Z = \int D\bar{\psi}\, D\psi\, DA\, e^{-S_{QCD}^{(cont.)}} \tag{1.5}$$

where the functional integration $D\bar{\psi}D\psi DA$ takes account of all possible quantum fluctuations of the fields.

In lattice theory the gauge field is represented by the group element connecting neighbouring lattice sites

$$U_\mu(x) = \exp\left(igA_\mu(x)a\right) \tag{1.6}$$

Our choice of lattice gauge action is dictated by the requirement of local gauge invariance under the transformation

$$U_\mu(x) \to \Omega(x)U_\mu(x)\Omega^{-1}(x + a\hat{\mu}) \tag{1.7}$$

where $\Omega \in SU(3)$ and is defined independently on each lattice site.

The simplest possible gauge invariant action is defined in terms of the elementary **plaquette** variable $U_{\mu\nu}^P(x)$ which is the trace of a directed product of gauge links around a closed loop joining a sequence of nearest neighbour sites.

$$U_{\mu\nu}^P(x) = U_\mu(x)\, U_\nu(x + a\hat{\mu})\, U_\mu^\dagger(x + a\hat{\nu})\, U_\nu^\dagger(x) \tag{1.8}$$

The Wilson gauge action for $SU(N_c)$ where N_c is the number of colours is defined to be

$$S_G \equiv \beta \sum_{x\mu;\,\nu>\mu} \left[1 - \frac{Tr}{6}\left(U_{\mu\nu}^P(x) + (U_{\mu\nu}^P)^\dagger(x)\right)\right] \tag{1.9}$$

It can be shown that by taking the naive continuum limit of the lattice gauge action we recover the Yang-Mills action. The matrix-valued lattice field tensor $\mathcal{F}_{\mu\nu}^L$ can be defined as

$$U_{\mu\nu}^P(x) = \exp\left(ig_o a^2 \mathcal{F}_{\mu\nu}^L(x)\right) \tag{1.10}$$

and one finds that in the continuum limit ($a \to 0$) the continuum field tensor is well approximated by the lattice field tensor $\mathcal{F}_{\mu\nu}^L(x) \to F_{\mu\nu}(x) + \mathcal{O}(a)$ and the lattice

gauge action, S_G is equivalent to the continuum gauge action, $S_G^{(cont.)}$ provided we make the identification $\beta = \frac{2N_c}{g_o^2}$.

1.2.1 Fermions on the Lattice

The fermion fields are associated with lattice sites and the continuum Dirac action is discretized by approximating the partial derivative by a finite difference:

$$\partial_\mu \psi_\alpha(x) \equiv \frac{1}{2a}\left[\psi_\alpha(x + a\hat{\mu}) - \psi_\alpha(x - a\hat{\mu})\right] \tag{1.11}$$

where ψ_α is a single component of the four component field ψ. The lattice form of the fermion action is

$$S_F = \sum_{x,y,\alpha,\beta} \bar{\psi}_\alpha(x) M_{\alpha\beta}(x,y) \psi_\beta(y) \tag{1.12}$$

where in the interacting case the fermion Dirac matrix M is given by

$$M_{\alpha\beta}(x,y) = \sum_\mu \frac{1}{2a}(\gamma_\mu)_{\alpha\beta}\left[U_\mu(x)\delta_{y,x+a\hat{\mu}} - U_\mu^\dagger(x)\delta_{y,x-a\hat{\mu}}\right] + m\delta_{yx}\delta_{\alpha\beta} \tag{1.13}$$

so the **dimensionless** quark propagator is

$$\left\langle \hat{\psi}_\alpha(x), \hat{\bar{\psi}}_\beta(y) \right\rangle = [M_{\alpha\beta}(x,y)]^{-1} \tag{1.14}$$

After Fourier transforming to momentum space and taking the continuum limit we obtain the following expression for the physical quark propagator (in the free field case) the poles of which correspond to physical particles.

$$\langle \psi_\alpha(x)\bar{\psi}_\beta(y)\rangle = \lim_{a\to 0} \int_{-\pi/a}^{\pi/a} \frac{d^4p}{(2\pi)^4} \frac{\left[-i\sum_\mu \gamma_\mu \tilde{p}_\mu + m\right]_{\alpha\beta}}{\tilde{p}_\mu^2 + m^2} e^{ip(x-y)} \tag{1.15}$$

where $\tilde{p}_\mu = \frac{1}{a}\sin(p_\mu a)$. The zeros of this sine function at the edges of the first Brillouin zone destroy the correct continuum limit – they give rise to fermion species doubling [7]. This fermion doubling is clearly seen by inspecting the inverse propagator for a massless free fermion

$$S^{-1}(p) = i\sum_\mu \gamma_\mu \frac{1}{a}\sin(p_\mu a) \;;\; -\pi/a < p_\mu \leq \pi/a \tag{1.16}$$

The periodicity of the sine function means that we have not one but sixteen poles in every Brillouin zone. This is illustrated in Fig. 1.2. Nielsen and Ninomiya [8, 9, 10] showed that the fermion doubling problem cannot be eliminated without breaking the chiral symmetry in the limit $m \to 0$.

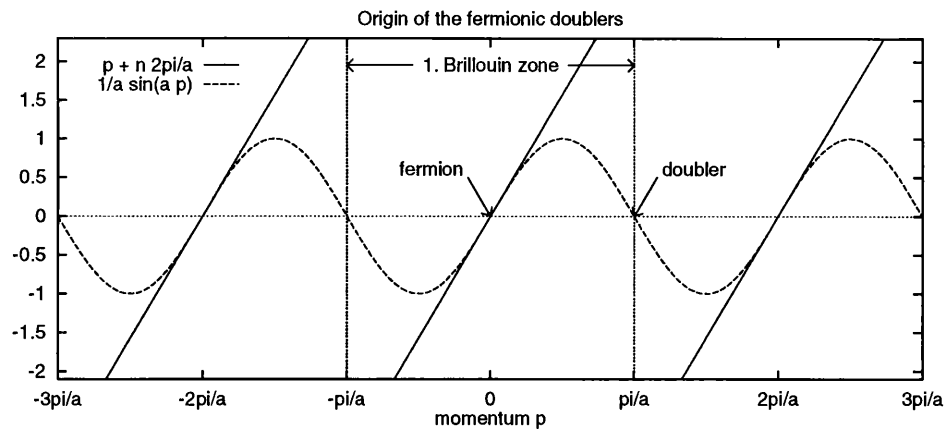

Figure 1.2: The origin of the fermionic doublers is clear from this plot of the inverse fermion propagator for the case of a massless free fermion.

1.2.2 Kogut-Susskind Fermions

A popular scheme for dealing with fermion doubling is "Wilson lattice fermions" whereby an irrelevant term is added to the action which gives an effective mass of $\mathcal{O}(1/a)$ to the 15 unwanted fermion doublers . Wilson fermions have the disadvantage that the irrelevant term explicitly breaks the chiral symmetry of the original lattice action. Since we are interested in the chiral phase transition we will use Kogut-Susskind staggered fermions which preserve a non-trivial piece of the full chiral symmetry.

The Kogut-Suskind fermion action eliminates the unwanted fermion modes by doubling the effective lattice spacing thereby reducing the Brillouin zone.

By making a local change of variables we arrive at an action which is diagonal in the Dirac indices thus the different fermion field components are decoupled and we keep only a single field component per site.

Starting with the naive fermion action with spin indices α, β shown explicitly (and where the lattice spacing, a=1, where not explicitly stated) :

$$\begin{aligned} S &= \frac{1}{2}\sum_{x,\mu}\left[\bar{\psi}_\alpha(x)(\gamma_\mu)_{\alpha\beta}\psi_\beta(x+\hat{\mu}) - \bar{\psi}_\alpha(x)(\gamma_\mu)_{\alpha,\beta}\psi_\beta(x-\hat{\mu})\right] \\ &+m\sum_x \bar{\psi}_\alpha(x)\delta_{\alpha\beta}\psi_\beta(x) \end{aligned} \tag{1.17}$$

The reduction of degrees of freedom is achieved by **spin diagonalization** where we perform a local change of fermionic variables

$$\psi_\alpha(x) = \Gamma_{\alpha\beta}(x)\chi_\beta(x) \;\; ; \;\; \bar{\psi}_\alpha(x) = \bar{\chi}_\beta(x)\Gamma^\dagger_{\beta\alpha}(x) \tag{1.18}$$

where in d spacetime dimensions $\Gamma(x)$ are diagonal $2^{d/2} \times 2^{d/2}$ unitary matrices

subject to the constraint

$$\Gamma^{\dagger}(x)\gamma_{\mu}\Gamma(x+\hat{\mu}) = \hat{\Delta}_{\mu}(x) \tag{1.19}$$

where $\hat{\Delta}_{\mu}(x) \equiv \eta_{\mu}(x)\mathbf{1}$. Note that $\hat{\Delta}$ should not be confused with any derivative operator. If we choose

$$\Gamma(x) = \gamma_1^{x_1}\gamma_2^{x_2}\gamma_3^{x_3}\gamma_4^{x_4} \tag{1.20}$$

where (x_1, x_2, x_3, x_4) are the components of the lattice site four-vector x, then the appropriate phases are

$$\eta_1(x) = \mathbf{1}\,;\; \eta_{\mu}(x) = (-1)^{x_1+x_2+\ldots x_{\mu-1}} \tag{1.21}$$

The above choice is not unique and there are a number of equivalent spin diagonalization prescriptions with different choices of $\Gamma(x)$, but due to the anti-commutation of the γ matrices ($\gamma_{\mu}\gamma_{\nu}\gamma_{\mu}\gamma_{\nu} = -1$ for $\mu \neq \nu$) the product of signs around any plaquette must satisfy the relation:

$$\Delta_{\mu}(x)\Delta_{\nu}(x+\hat{\mu})\Delta_{\mu}^{\dagger}(x+\hat{\nu})\Delta_{\nu}^{\dagger}(x) = -1 \tag{1.22}$$

After spin diagonalization and inclusion of gauge interactions the action reads

$$\begin{aligned} S_F^{(K.S.)} &= \frac{1}{2}\sum_{x,\mu,\alpha}\eta_{\mu}(x)\left[\bar{\chi}_{\alpha}(x)U_{\mu}(x)\chi_{\alpha}(x+\hat{\mu}) - \bar{\chi}_{\alpha}(x)U_{\mu}^{\dagger}(x-\hat{\mu})\chi_{\alpha}(x-\hat{\mu})\right] \\ &+ m\sum_{x,\alpha}\bar{\chi}_{\alpha}(x)\chi(x) \end{aligned} \tag{1.23}$$

By eliminating the Dirac matrix γ_{μ} we have decoupled the fermion field components thus we can reduce the number of fermion field *components* to a single one per site. Since the above action is diagonal in $\chi_{\alpha}(x)$ and is thus simply four copies of the same action written in terms of a one-component Grassmann variable $\chi_{\alpha}(x)$ and a space dependent sign $\eta_{\mu}(x)$.

The remaining four fermion species are interpreted as physical flavours in the continuum limit. Thus the lattice action reduces in the naive continuum limit to a sum of free fermion actions, one for each of the quark flavours:

$$S_f^{(K.S.)} \rightarrow \int d^4x \sum_{\alpha,\beta,f}\bar{\psi}_{\alpha}^{f}(x)\left(\gamma_{\mu}\partial_{\mu} + m\right)_{\alpha\beta}\psi_{\beta}^{f}(x) \tag{1.24}$$

where f is the flavour index which ranges from 1 to 4 and α, β are the spinor indices. Note that the staggered formulation has the disadvantage that in d spacetime dimensions it is restricted to a description of $2^{d/2}$ degenerate quark flavours.

The staggered fermion action (Eqn. 1.23) is local, Hermitian and invariant under the global $U(1)_1$ rotation:

$$\chi(x) \rightarrow e^{i\alpha}\chi(x)\,;\; \bar{\chi}(x) \rightarrow \bar{\chi}(x)e^{-i\alpha}. \tag{1.25}$$

In the massless case ($m = 0$) this symmetry becomes extended and we have the additional $U(1)_\epsilon$ symmetry defined by the transformations

$$\chi(x) \to e^{i\beta\epsilon(x)}\chi(x) \; ; \; \bar{\chi}(x) \to \bar{\chi}(x)e^{i\beta\epsilon(x)} \tag{1.26}$$

where $\epsilon(x) = (-1)^{x_1+x_2+x_3+x_4}$. The $U(1)_\epsilon$ invariance is a continuous remnant of the full chiral symmetry of the naive action and in the continuum limit, the full chiral symmetry of the free theory is restored.

The full $U(1)_\epsilon \otimes U(1)_1$ symmetry can be re-expressed in terms of independent rotations on odd and even lattice sites $U_o(1) \otimes U_e(1)$. In the ($m = 0$) case the even sites will be rotated by the angle $\alpha + \beta$ while the odd sites will be rotated by $\alpha - \beta$.

The spin and flavour quantum number assignments which have been suggested for the interpretation of the staggered fermion action in the continuum limit can be identified locally, in configuration space by assigning quantum numbers to the 16 degrees of freedom at the corners of unit hypercubes on the lattice [11]. We introduce the following formalism whereby we double the effective lattice spacing. We introduce a new field variable $\chi_A(y)$ defined in terms of $\chi(x)$ by

$$\chi_A(y) = \chi(2x + A) \tag{1.27}$$

where y is a four component site index on a **lattice of spacing 2a** and A is one of 16 four-vectors with each component either zero or one. If we define the sixteen 4×4 matrices Γ_A by

$$\Gamma_A^{\alpha a}(x) = \left(\gamma_1^{A_1}\gamma_2^{A_2}\gamma_3^{A_3}\gamma_4^{A_4}\right)^{\alpha a} \tag{1.28}$$

which form a basis for the linear vector space of 4×4 matrices. We can now define the quark fields associated with the hypercube identified with spatial coordinate y by

$$q^{\alpha a}(y) = \frac{1}{8}\sum_A \Gamma_A^{\alpha a}\chi_A(y) \; ; \; \bar{q}^{\alpha a}(y) = \frac{1}{8}\sum_A \bar{\chi}_A(y)\Gamma_A^{*\alpha a} \tag{1.29}$$

where α is a spin index and a is a flavour index. Both indices range from 1 to 4. By exploiting the orthogonality of the Γ_A:

$$\sum_A \Gamma_A^{\alpha a}\Gamma_A^{*\beta b} = 4\delta^{\alpha\beta}\delta^{ab} \tag{1.30}$$

and defining the finite difference operators:

$$\begin{aligned} \Delta_\mu f(y) &\equiv \frac{1}{4a}\left[f(y+\hat{\mu}) - f(y-\hat{\mu})\right] \sim \partial_\mu f(y) \\ \delta_\mu f(y) &\equiv \frac{1}{4a^2}\left[f(y+\hat{\mu}) + f(y-\hat{\mu}) - 2f(y)\right] \sim \partial_\mu{}^2 f(y) \end{aligned} \tag{1.31}$$

it is now possible to write the staggered action in the *free field case* in terms of the q variables on the lattice of spacing $2a$.

$$\begin{aligned} S &= \sum_{y,\mu} (2a)^4 \left[\bar{q}(y)(\gamma_\mu \otimes 1)\Delta_\mu q(y) + a\bar{q}(y)(\gamma_5 \otimes t_\mu t_5)\delta_\mu q(y)\right] \\ &+ m\sum_y \bar{q}(y)(1 \otimes 1)q(y) \end{aligned} \tag{1.32}$$

where $t_\mu = \gamma_\mu^*$. The *t matrices act only on flavour indices* while the γ matrices act only on spin indices (essentially in the above Eqn. the matrices to the left of the direct product act on spin while those to the right act on flavour). Transforming to momentum space we obtain the following expression for the free quark propagator

$$S(p) = \frac{\left\{\sum_\mu \frac{-i}{2a}(\gamma_\mu \otimes 1)\sin(2p_\mu a) + \sum_\mu \frac{1}{2a}(\gamma_5 \otimes t_\mu t_5)(1-\cos(2p_\mu a)) + m(1\otimes 1)\right\}}{\sum_\mu \frac{1}{a^2}\sin^2(p_\mu a) + m^2} \tag{1.33}$$

The fermion doubling problem has been circumvented since in this basis the momentum variable p_μ is only defined over the range $(-\pi/2a, \pi/2a)$ since the effective lattice spacing is now $2a$. In this case the only pole that occurs for the case m=0 is the physical one near $p_\mu = 0$ and the doubled species which previously appeared implicitly as extra poles near the edge of the Brillouin zone are now explicitly described by the *t algebra* acting on the flavour indices.

1.2.3 Numerical Computations for Fermions

Since they anti-commute, we cannot calculate numerically, using statistical methods, ensemble averages of products of fermion fields as we can for bose fields. However since the fermionic contributions to the action in QCD are **bilinear** in ψ and $\bar{\psi}$, we can use the identities below to perform the Grassmann integrals analytically:

$$\int D\psi\, D\bar{\psi}\, e^{\left(-\bar{\psi}_i M_{ij}\psi_j\right)} = \det M \tag{1.34}$$

$$\int D\psi\, D\bar{\psi}\, \psi_l\, \bar{\psi}_k\, e^{\left(-\bar{\psi}_i M_{ij}\psi_j\right)} = \left(M^{-1}\right)_{lk} \det M \tag{1.35}$$

where i, j represent spa

$$\begin{aligned} \int D\psi\, D\bar{\psi} &= \prod_{x,\alpha} d\psi_\alpha(x) \prod_{y,\beta} d\bar{\psi}_\beta(y) \\ \int D\psi\, D\bar{\psi} &= \prod_{x,\alpha} d\psi_\alpha(x) \prod_{y,\beta} d\bar{\psi}_\beta(y) \end{aligned} \tag{1.36}$$

It follows that the partition function in the interacting case is given by

$$Z = \int DU \det M(U)\, e^{-S_G} \tag{1.37}$$

Thus we obtain a new expression for the path integral formula for the euclidean correlation functions which is a simple statistical mechanical ensemble average with an effective action $S_{eff}(U) = S_G(U) - \ln \det M(U)$.

$$\langle \bar{\psi}(x)\psi(y)\rangle = \frac{1}{Z}\int DU M^{-1} \det M \, e^{-S_G} \tag{1.38}$$

The expectation value of the operator $\mathcal{O}$ is given by

$$\langle \mathcal{O}\rangle = \frac{1}{Z}\int [DU][D\bar{\psi}][D\psi]\, \mathcal{O}(U,\bar{\psi},\psi) e^{-s_G - \bar{\psi} M \psi} \tag{1.39}$$

and integrating out the fermionic fields gives

$$\langle \mathcal{O}\rangle = \frac{\int [DU]\, \mathcal{O}(U) \det M e^{-S_G}}{\int [DU] \det M \, e^{-S_G}} \tag{1.40}$$

Many Lattice QCD calculations use the **quenched approximation** which involves neglecting vacuum polarization i.e., ignoring the feedback from the quark field to the gluon field. This corresponds to setting $\det M = 1$ so that

$$\langle \mathcal{O}\rangle_{quen.} = \frac{\int [DU]\, \tilde{\mathcal{O}}(U)\, e^{-S_G}}{\int [DU]\, e^{-S_G}} \tag{1.41}$$

1.3 The Phases of QCD

The simplest possible phase diagram of QCD is shown in Fig. 1.3. The two thermodynamical variables which we control are the physical temperature, T, and the chemical potential, μ. The temperature controls the average kinetic energy of the quarks and gluons whilst the chemical potential controls the net quark number density, which is a measure of the excess of quarks over anti-quarks in the system, $(n_d \equiv n_q - n_{\bar{q}})$. In the confined phase the quark number density is simply related to the baryon number density, n_B, by $n_B = n_d/N_c$ where N_c is the number of colour degrees of freedom.

It is believed that at high temperature and/or high density nuclear matter should undergo a phase transition into a new state, the quark-gluon plasma. Thus we expect QCD to exhibit two distinct phases:

1. **Hadron gas phase** – a low temperature, low density phase where quarks and gluons are confined to hadrons.

2. **quark-gluon plasma phase** – a high temperature, high density phase where the quarks and gluons behave almost like free particles.

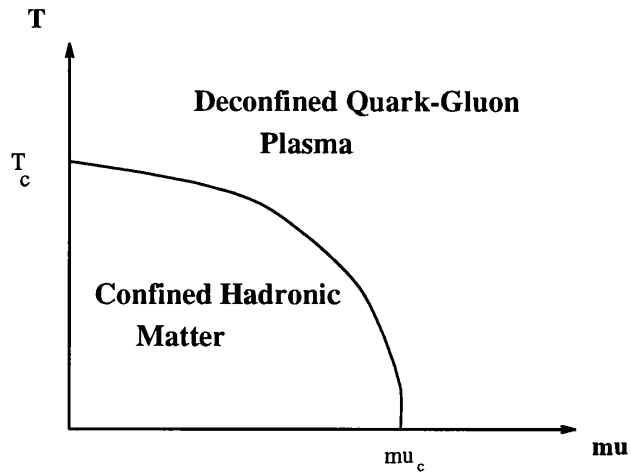

Figure 1.3: The simplest possible QCD phase diagram in the temperature - chemical potential plane. The critical temperature is T_c and the critical chemical potential is labelled mu_c.

A phase transition from the hadronic phase to the quark-gluon plasma phase can be induced by either adding thermal energy to the system or by squeezing nucleons together in a finite volume until a critical baryon density is reached. The question of whether there exists a sharp boundary between the above two phases is an open one. Lattice QCD simulations can be used to attack this question theoretically and relativistic heavy ion collision experiments offer the possibility of creating extremely hot and dense matter in the laboratory. From a theoretical point of view we would like to be able to predict both the order of the phase transition and the location of the phase boundary. Knowledge of the full equation of state for QCD in the temperature – chemical potential plane would allow us to make quantitative predictions for critical baryon densities and energy densities for the creation of the quark-gluon plasma in experiments. Moreover, studies of the phase structure of QCD are of fundamental importance in verifying that QCD is the correct theory of the strong interactions.

Considerable progress has been made in simulating lattice QCD at non-zero temperature and zero chemical potential [12]. We have learned that at vanishing temperature hadronic matter is characterized by two order parameters:

1. **Colour Confinement** – When colour deconfinement occurs the spectrum of states goes from the low temperature hadronic phase where colour is an exact but confined quantum number to a phase where coloured asymptotic states are possible

2. **Chiral Symmetry Breaking** – Chiral symmetry breaking in the hadronic phase is believed to be responsible for the vanishing mass of pions (which are identified as the Goldstone bosons of the chiral symmetry breaking) and the finite mass of baryons in the chiral limit ($m \to 0$). When chiral symmetry restoration occurs, the chiral condensate and the theory's *mass gap* vanishes.

At very high temperatures the asymptotic freedom of QCD implies that the theory becomes well approximated by free, fundamental quarks over ever-growing length and time scales.

Simulations of lattice QCD at **finite temperature** indicate that the two phase transitions, colour deconfinement and chiral symmetry restoration are coincident i.e., both occur at the same physical temperature T_c [12]. It seems that when the temperature is increased to the point where confinement is lost, the thermal fluctuations are sufficiently strong to evaporate the chiral condensate and eliminate the theory's dynamically generated mass gap. This is seen in both quenched simulations, which neglect vacuum polarization effects due to light quarks , and in exact simulations which include dynamical fermions.

Statistical QCD, as evaluated on a spacetime lattice is perhaps the only case in statistical physics where critical behaviour can be calculated from first principles dynamics without having to resort to an intermediate effective theory. The principal limitation of lattice QCD simulations is computer performance. Considerable progress has been made in finite temperature QCD simulations. Significant advances have resulted from finite size scaling methods and improved actions as well as improved computing power. The pure gluon theory with valence quarks (quenched theory) is close to being completely solved. The main features considered here are the deconfinement transition and the properties of the quark-gluon plasma. Below the deconfinement temperature T_c, the constituents of this system are colourless gluonium states (i.e. glueballs) but above T_c free coloured gluons are permitted. The equation of state for the $SU(3)$ pure gluon theory has been reliably extrapolated to the continuum (vanishing lattice spacing) using finite size scaling. The equation of state gives the energy density, ϵ, the pressure P and the interaction measure $(\epsilon - 3P)$ as functions of T. The phase transition is predicted to be weakly first order and the latent heat of deconfinement is found to be $\Delta\epsilon/T_c^4 = 1.40 \pm 0.09$ [13]. A critical temperature (in units of the string tension) σ of $T_c/\sqrt{\sigma} = 0.629 \pm 0.003$ has been estimated, which corresponds to $T_c \simeq 260$ MeV for the quarkonium string tension value $\sigma \simeq 420$ MeV . It has emerged that even at temperatures as high as $T \simeq 5T_c$, the thermodynamic variables are $10 - 15\%$ below

the ideal gluon gas (Stefan-Boltzmann) limit. These high temperature deviations cannot be accounted for by higher order perturbative corrections.

Despite the successes of the finite temperature studies of the quenched theory, the first simulations of full QCD which include the effects of dynamical light quarks have revealed significant differences from the predictions of the quenched theory. Although the equation of state for the full theory [14] is similar in form to that of the quenched theory with a large change in entropy density at the phase transition the critical temperature is $T_c \sim 150-200$ MeV, which is at least 30% lower than the quenched prediction. As mentioned above both quenched and full theories predict that at finite temperature and zero chemical potential the chiral symmetry restoration coincides with deconfinement, and that for non-zero bare quark masses used in simulations the sharpness of the two transitions is comparable. It remains to be confirmed whether in the limit of zero bare quark mass (which gives a massless Goldstone pion) the chiral transition is in the same universality class as the $O(4)$ spin model [15], as expected. The unquenched simulations are currently restricted to small lattices and we await additional computer power to allow a reliable extrapolation to the continuum limit comparable to that achieved in the quenched theory.

One of the main challenges for lattice QCD is to demonstrate a viable numerical approach for studying the phase structure at non-vanishing baryon density. Simulations at finite baryon density are complicated by the fact that the effective action resulting from the Grassmann integration over the fermions is complex for $\mu \neq 0$. In fact little progress has been made since a self-consistent lattice formulation for the theory was first proposed in 1983 [6], [16]. Early quenched simulations led to unphysical results whereby an infinitesimal chemical potential led to chiral symmetry restoration in the theory with massless quarks. The expectation was that the chiral symmetry should be restored at $\mu = \frac{m_B}{3}$ where m_B is the mass of the lightest particle with non-zero baryon number in the mass spectrum (the proton). Thus it is believed that a correct implementation of dynamical quarks in the simulations is essential to probe the true physics. In QCD at non-zero chemical potential it is possible that colour deconfinement and chiral symmetry restoration are separate. In fact many phenomenological nuclear models support this conjecture. If the deconfinement and chiral symmetry restoration were to be separated at finite density then we must consider the possibility of an intermediate phase characterised by deconfinement but where the chiral symmetry remains broken. Two popular examples of such phases include

- **constituent quark phase**– in naive quark models constituent quarks have masses close to one third of the nucleon mass and radii of around 0.3 fermi. It may be thermodynamically favourable for a constituent quark phase to form because the large nucleon-nucleon repulsion of the dense hadronic phase is eliminated by dissociation of nucleons into free smaller constituent quarks. This scenario is disfavoured by the presence of unconfined colour which would presumably be screened. From the ideas of percolation theory we might expect that as we increase the chemical potential thereby squeeze progressively more baryons into the system a first percolation threshold is reached when an infinite network of touching nucleons first appears so that a quark need not belong to a particular nucleon and the colour-colour correlation functions become long ranged. A second percolation threshold (at a larger μ) is reached when the constituent quarks themselves begin to overlap giving rise to chiral symmetry restoration.

- **diquark phase** a transition from nucleons to diquarks may occur because the diquarks have a relatively strong, attractive short-range spin-spin interaction which lowers their energy and holds them together in clusters significantly smaller than conventional nucleons. The diquarks are analogous to Cooper pairs in the BCS theory of superconductivity. The diquark model is motivated by hyperfine splitting patterns in hadronic spectroscopy. Perturbation theory and phenomenological arguments suggest a spin-spin interaction energy

$$H_s = -A \sum_{i,j} b_i^\dagger \sigma^a \lambda^B b_i b_j^\dagger \sigma^a \lambda^B b_j \tag{1.42}$$

where i, j labels the interacting quark, $b_i^\dagger$ is the quark creation operator, σ^a are the Pauli spin matrices and λ^B are the $SU(3)$ colour matrices. States of two diquarks can have colour 6 or $\bar{3}$ and spin zero or one. The most attractive diquark state of a u and d quark is the colour triplet spin zero combination $(\bar{3}, 0)$. In the proposed diquark phase where colour deconfinement has occurred there is still an energy gap and chiral symmetry breaking.

1.3.1 Approximate Chiral Symmetries of QCD

Spontaneous chiral symmetry breaking is one of the most fascinating features of the strong interactions. We know from a rich phenomenology in soft pion physics that chiral $SU(2) \otimes SU(2)$ is slightly intrinsically broken and, more importantly, spontaneously broken at zero temperature. Chiral symmetry is expected to be

restored both at high temperatures and at high nuclear densities (5 to 10 times the density of ordinary nuclear matter).

If QCD is to be a viable theory of strong interactions then it is imperative that it must reproduce the phenomenon of spontaneous chiral symmetry breaking. If it fails to do so then the consequences are serious since the spectrum predicted by QCD would possess **parity doubling** and no *very light* pions. This would contradict the experimental evidence. At present there is no rigorous proof that QCD does exhibit dynamical symmetry breaking with the pattern observed in nature but lattice Monte Carlo techniques give us the means to explore this scenario.

1.4 Spontaneously Broken Global Symmetries and Goldstone Bosons

Spontaneous breakdown of a continuous symmetry implies the existence of massless spinless particles [17]. Such scalar particles are known as *Goldstone bosons.* The work leading to the association of the pion as the Goldstone boson of spontaneously broken $SU(2) \otimes SU(2)$ chiral symmetry was completed prior to the existence of a specific theory of the strong interactions. The study of this phenomenon was initiated by Nambu [18, 19]. Further work by Goldstone, Salam and Weinberg [20, 21] provided proofs of the postulates. A deciding factor in the rapid acceptance of QCD as a theory of the strong interactions in 1973 was the fact that it explained the $SU(2) \otimes SU(2)$ symmetry as a direct consequence of the smallness of the up and down quark masses.

The importance of broken symmetries in particle physics began in 1957 when the Goldberger-Trieman relation was derived on the basis of a dynamical calculation of **pion decay** ($\pi \longrightarrow \mu + \nu$). Nambu's paper of 1960 pointed out that the axial-vector current is *exactly* conserved in the limit of zero pion mass. To take account of the fact that pions decay the initial assumption of model had to be modified to partial conservation of axial current (PCAC) whereby the divergence of the axial-vector current is small (of order ${m_\pi}^2$), except where a pion pole gives it a large matrix element. The spontaneous breaking of this approximate symmetry is associated with the appearance of an *approximately* massless pion. The fact that the particular broken symmetry involved is $SU(2) \otimes SU(2)$ was revealed only when processes involving more than one pion were modelled successfully by the Adler-Weisberger sum rule in 1965.

1.4.1 Chiral Symmetry in QCD

If the quarks were all massless there would be a very high degree of symmetry associated with QCD, but even for $m \neq 0$ symmetries are possible if two or more quark masses are equal. Three of the six quarks (c,b,t) are heavy in relation to the confinement scale Λ_{QCD} but the (u,d,s) quarks are light enough to have useful symmetries. In the chiral limit $m_q \to 0$, the left-handed and right-handed components of the quark fields decouple and have separate invariances.

Consider the Dirac equation for a massless particle $i\gamma^\mu \partial_\mu \psi = 0$. We can multiply by γ_5 from the left and use the anti-comutativity of γ_5 with γ^μ to obtain another solution which obeys $i\gamma^\mu \partial_\mu \gamma_5 \psi = 0$. These two solutions are superposed to form solutions, ψ_L and ψ_R of definite chirality. The right/left-handed fermion has spin aligned/anti-aligned relative to the momentum.

$$\psi_L = \Gamma_L \psi \; ; \; \psi_R = \Gamma_R \psi \tag{1.43}$$

where the matrices $\Gamma_L = \frac{1+\gamma_5}{2}$ and $\Gamma_R = \frac{1-\gamma_5}{2}$ are chirality projection operators. This can be translated to the Lagrangian formalism:

$$L_{QCD}|_{m=0} = -\frac{1}{4} F^a_{\mu\nu} F^{a\mu\nu} + \bar{\psi}_L \gamma^\mu D_\mu \psi_L + \bar{\psi}_R \gamma^\mu D_\mu \psi_R \tag{1.44}$$

for massless u and d chiral quarks with ψ_L and ψ_L chiral projections of the doublet $\psi = \begin{pmatrix} u \\ d \end{pmatrix}$ the appropriate symmetry operations are

$$\psi_L \to e^{(-i\Theta_L \cdot \tau)} \psi_L \; ; \; \psi_R \to e^{(-i\Theta_R \cdot \tau)} \psi_R \tag{1.45}$$

where τ^i $(i = 1, 2, 3)$ are the $SU(2)$ Pauli matrices and $\{\theta^i\}$ are the components of an arbitrary constant vector. Alternatively these can be expressed as vector and axial-vector isospin transformations

$$\psi \to e^{(-i\Theta_V \cdot \tau)} \psi \; ; \; \psi \to e^{(-i\Theta_A \cdot \tau \gamma_5)} \psi \tag{1.46}$$

where $\Theta_V = \frac{\Theta_L + \Theta_R}{2}$ and $\Theta_A = \frac{\Theta_L - \Theta_R}{2}$

This $SU(2)_L \otimes SU(2)_R$ or $SU(2)_V \otimes SU(2)_A$ symmetry in QCD is broken by quark mass terms

$$L_{mass} = -m_u \bar{u} u - m_d \bar{d} d = -m_u(\bar{u}_L u_R + \bar{u}_R u_L) - m_d(\bar{d}_L d_R + \bar{d}_R d_L) \tag{1.47}$$

so if $m_u = m_d \neq 0$ separate left and right handed invariances no longer exist although the vector isospin symmetry remains. In nature the fact that we do not observe parity doubling in the particle spectrum suggests that the axial symmetry

is a hidden symmetry (dynamically broken). The pion is the (approximate) Goldstone boson associated with the symmetry breaking $SU(2)_L \otimes SU(2)_R \rightarrow SU(2)_V$. Vectorial isospin symmetry involving simultaneous $SU(2)$ transformations of ψ_L and ψ_R remain an approximate symmetry of the particle spectrum as evidenced by the near equality in the masses of multiplets $(\pi^{\pm}, \pi^0), (p, n), (K^+, K^0)$ etc.

Note that these concepts can be extended by including the strange quark to give three massless quarks and an approximate $SU(3)_L \otimes SU(3)_R$ global symmetry. The dynamical breaking of this symmetry to vector $SU(3)$ would produce eight Goldstone bosons: $\pi^{\pm}, \pi^0, K^{\pm}, K^0, \bar{K}^0$ plus a neutral particle with the quantum numbers of the eighth component of the octet.

1.4.2 PCAC Relation

From a theory of chiral symmetry breaking which makes the simple assumption that the chiral symmetry is broken by the quark mass term only the following form of the PCAC relation can be derived (see for example [22])

$$f_\pi{}^2 m_\pi{}^2 = \frac{m_u + m_d}{2} \langle 0|\bar{u}u + \bar{d}d|0\rangle \tag{1.48}$$

where f_π is the pion decay constant measured in $\pi^+ \rightarrow l^+ + \mu_l$ and the experimental value is $f_\pi \simeq 93$ MeV. The point to note about this continuum relation is that it implies that the mass of the Goldstone pion is proportional to the square root of the bare quark mass. We will make use of this relation in lattice simulations when investigating the scaling of the onset of non-zero quark number density with the bare quark mass. Note that the scaling of the nucleon mass is assumed to have a linear dependence on the bare quark mass.

1.4.3 Chiral Symmetry Breaking and Quark Confinement on the Lattice

An explicit demonstration of quark-confinement **cannot be generated within perturbation theory** since perturbation theory is only applicable in the weak coupling ($g \rightarrow 0$) limit. However in lattice theory the form of the static $q\bar{q}$ potential, $V(R)$ can be studied using the expectation value of the *Wilson loop* for large Euclidean times. The phenomenon of quark-confinement in QCD suggests that for large separations of the quark-antiquark pair, $V(R)$ should have a linear R dependence up to distances where colour-screening due to vacuum polarization effects becomes dominant. In 1974 Wilson provided a lattice proof of confinement in the

strong coupling limit by studying the behaviour of a static quark and antiquark in a background field without dynamical fermions. Unfortunately his derivation was **not specific to the $SU(N)$ gauge group** and therefore also implied confinement for the $U(1)$ gauge theory of compact QED. Since for physical couplings we know that QED has a $1/R$ Coulomb potential it was deduced that there exists a QED phase transition between strong and weak couplings. Clearly Wilson's proof that QCD is confining in the strong coupling sector does not automatically prove confinement for physical (weak) couplings. It must therefore be demonstrated that there is no QCD phase transition to a weak coupling regime.

It can be demonstrated using lattice QCD in the large N_c and large d limit that chiral symmetry is spontaneously broken. However such proofs only apply to the strong coupling ($g \gg 1$) limit where the gauge action does not contribute and therefore they depend on non-universal features of the lattice QCD action. The $N_f \to 0$ limit (quenched approximation) is also implicitly taken in most of these calculations and this approximation has clear limitations since it neglects colour dynamical fermions (colour screening) and probably *overestimates* the tendency for chiral condensates to form. To provide a more accurate picture of the underlying physics it is necessary to investigate the chiral phase transition in the scaling region $g^2 \to 0$ and to include dynamical fermions in the simulations. It is instructive to note that in these strong coupling calculations it is the **disordered U–matrices** and not confinement that causes the chiral condensate to be non-zero (indicating chiral symmetry breaking). This can be demonstrated explicitly by repeating the strong coupling calculation using quarks in the adjoint representation of the gauge group and demonstrating that a non-zero chiral condensate still develops. In the adjoint representation the quarks are screened but **not confined** since a gluon can bind to an adjoint quark and make a colour singlet locally.

Chiral symmetry breaking has also been studied in the context of **four-fermion interaction models** where the chiral symmetry breaking is achieved via a *short range* interaction. In the Nambu-Jona Lasinio model the interaction is attractive and has zero range. If the strength of the four-fermion interaction is above a critical value then a chiral condensate forms and the fermions develop a **dynamical mass** (due to the interaction) non-perturbatively and a triplet of massless pions emerge as the Goldstone bosons of the spontaneously broken symmetry operators. Lattice studies of the Gross-Neveu model in three dimensions have demonstrated that the chiral symmetry transition predicted by mean-field theory can be successfully reproduced using lattice Monte-Carlo techniques. The principal feature of four-fermi

interaction models is that a short range interaction is sufficient for chiral symmetry breaking.

The coincidence of the deconfinement and chiral transitions at finite temperature is well established. However it is not a strict requirement that confinement implies chiral symmetry breaking. One argument which does claim that confinement implies chiral symmetry breaking is due to Casher [23]. He presents a mechanism which breaks chiral symmetry in a confining theory. Casher considers a state which consists of an isolated (massless) $q\bar{q}$ pair on top of the free Dirac vacuum. There exists a **long range** strong attractive force which forbids states where the quark and anti-quark are arbitrarily far apart. The following conditions of the confining force are assumed:

1. the attraction is spin independent.
2. the interaction energy is sufficiently strong to produce a bound $q\bar{q}$ pair in an **s-wave**.

Now consider a semi-classical description of a bound state which is formed by superposing paths in which the bound fermion must reverse its direction of motion. Since chirality is conserved, while the force cannot flip the spin the bound-state formation cannot be achieved because the attractive force cannot turn the fermion back. We must therefore reject the first assumption above and conclude that *a chirally invariant spin independent interaction cannot bind an isolated massless fermion pair.* Thus bound states imply chiral symmetry breaking.

1.4.4 Chiral Symmetry remnants in the Staggered Fermion Lattice Action

In the naive continuum limit the staggered fermion action Eqn. 1.32 possesses a $U(4) \otimes U(4)$ chiral symmetry for $m = 0$ since the first part of the kinetic term which involves $(\gamma_\mu \otimes 1)$ is diagonal in flavour and tends to the usual kinetic term of four Dirac fermion flavours while the second part is a lattice artifact involving $(\gamma_5 \otimes t_\mu t_5)$ (which vanishes in the continuum limit). This second part is troublesome since it departs from the desired continuum form at $\mathcal{O}(a)$ *breaking both Lorentz and flavour symmetries.* However the staggered fermion action does preserve a non-trivial piece of the full axial symmetry (involving the generator γ_5 in Dirac space) where the $U(4) \otimes U(4)$ continuous chiral symmetry of four massless flavours is broken down to $U(1)_o \otimes U(1)_e$. The symmetry generator is $\gamma_5 \otimes t_5$ under which the fields transform

as

$$q(y) \rightarrow e^{i\alpha(\gamma_5 \otimes t_5)} q(y) \;\; ; \;\; \bar{q}(y) \rightarrow \bar{q}(y) e^{i\alpha(\gamma_5 \otimes t_5)} \tag{1.49}$$

where α is a parameter independent of y. Note that near the continuum limit ($a \rightarrow 0$) or equivalently on a sufficiently large lattice we might expect the full flavour symmetry to be restored ie. the $U(1) \otimes U(1)_\epsilon$ symmetry of the action would be extended to an effective $SU(4)_L \otimes SU(4)_R$ (or $U(4)_L \otimes U(4)_R$ in the quenched theory) and this would be evidenced by the appearance of not one but ${N_f}^2 - 1 = 15$ massless Goldstone pions in the continuum limit.

It follows from Eqn. 1.32 that there is a conserved axial current $j_{\mu 5} \sim \bar{q}(\gamma_\mu \gamma_5 \otimes t_5)q$ and the Goldstone pion which transforms as a pseudoscalar flavour non-singlet is associated with $\bar{q}(\gamma_5 \otimes t_5)q$. In the chiral basis

$$t_5 = \begin{pmatrix} 1 & 0 & 0 & 0 \\ 0 & 1 & 0 & 0 \\ 0 & 0 & -1 & 0 \\ 0 & 0 & 0 & -1 \end{pmatrix}$$

so that we have two fermions with positive axial charge and two with negative axial charge. The resulting continuum theory contains no anomaly in this current.

1.5 Chemical Potential on the Lattice

Introduction of the lattice regularization of QCD and the Monte Carlo methods to simulate it have proved very successful in exploring finite temperature QCD including the prediction of a phase transition at $T_c \simeq 200 - 250$ MeV. Although there is a straightforward way of introducing finite temperature in lattice gauge theory calculations obtaining nonperturbative results in QCD at finite density is non-trivial. The problems stem from the introduction of the chemical potential on the lattice. As will be demonstrated below, the appropriate choice of action for $\mu \neq 0$ gives rise, in general, to a complex fermion determinant whereas Monte Carlo numerical simulations require a real determinant.

In direct analogy to classical statistical mechanics, non-vanishing quark number (baryon number) density ($n_q \neq 0$) can be described by the introduction of a non-zero quark chemical potential ($\mu \neq 0$) in the grand canonical partition function

$$Z(T, \mu) \equiv Tr \left\{ e^{[-(H - \mu N_q)/T]} \right\} \tag{1.50}$$

where H is the Hamiltonian and N_q is the quark number operator. The temporal extent of the lattice corresponds to *inverse temperature* i.e. $n_t a_t \sim \frac{1}{T}$, where n_t is the number of lattice sites and a_t is the lattice spacing in the temporal direction. The thermodynamic observables are calculated from the logarithmic derivatives of Z. At finite density we are interested in exploring the zero-temperature axis of the phase diagram hence we use symmetric, isotropic lattices where $n_s = n_t$ and $a_s = a_t = a$. For example the fermion number density is given by

$$n_q = \frac{T}{V}\frac{\partial \ln Z}{\partial \mu} = \frac{a^{-3}}{{n_s}^3 n_t}\frac{\partial \ln Z}{\partial (a\mu)} \tag{1.51}$$

A fundamental requirement which we insist must be satisfied by our QCD action with $\mu \neq 0$ is that for free quarks (without the colour gauge interaction) we should recover the continuum expressions for the thermodynamical quantities such as fermion energy density and number density when we consider the limit $a \to 0$ for $T = 0$. The expected continuum results for a free Fermi gas of massless particles at $T = 0$ are:

$$\epsilon = \frac{\mu^4}{4\pi^2} \; ; \; n_q = \frac{\mu^3}{3\pi^2} \tag{1.52}$$

Experience from finite temperature studies suggests that one should also study the ideal fermi gas on a lattice at $\mu \neq 0$ to get an idea of finite size effects. This also serves as a check that the chosen form of the lattice action (part of the regularization scheme) gives sensible answers in the continuum limit.

Using the continuum scheme based on the Feynman path-integral formulation the partition function is given by

$$Z(1/T, \mu) = \int [d\psi \, d\bar{\psi}] \exp\left\{ \int_0^{1/T} d^4x \, \psi(\gamma^\mu \partial_\mu - m + \mu\gamma^0)\psi \right\} \tag{1.53}$$

Introducing a spacetime lattice with the anticommuting spinor variables ψ defined on the sites gives the corresponding lattice partition function

$$Z(1/T, \mu) = \int \prod_n d\psi_n \, d\bar{\psi}_n \, e^{-S} \tag{1.54}$$

The naive form of the lattice action, S, for $\mu \neq 0$, obtained by following the same procedure on the lattice as used in the continuum case is:

$$S = a^3 \sum_x \left(ma\bar{\psi}_x\psi_x + \mu a \bar{\psi}_x\gamma_4\psi_x + \frac{1}{2}\sum_{\mu=1}^{4} \left(\bar{\psi}_x\gamma_\mu\psi_{x+\hat{\mu}} - \bar{\psi}_{x+\hat{\mu}}\gamma_\mu\psi_x\right) \right) \tag{1.55}$$

where the spinor field ψ is antiperiodic along the imaginary time axis.

The energy density can be calculated from the lattice partition function using the definition

$$\epsilon = -\frac{1}{{n_s}^3 a^3} \left. \frac{\partial \ln Z}{\partial (1/T)} \right|_{(\mu/T)=fixed} \tag{1.56}$$

After subtracting the vacuum contribution and taking the zero temperature limit we obtain the following lattice expression for the energy density:

$$\epsilon = a^{-4} \left(-\frac{1}{4\pi^4} \int_{-\pi}^{\pi} d^4p \frac{\sum_{j=1}^{3} \sin^2 p_j + (ma)^2}{(\sin p_4 - i\mu a)^2 + \sum_{j=1}^{3} \sin^2 p_j + (ma)^2} \right) - a^{-4}\{\mu \equiv 0\} \tag{1.57}$$

One can check that this expression is quadratically divergent [$(\mu/a)^2$] in the continuum limit. Thus the action Eqn. 1.55 leads to quadratic divergences even for free fermions. In the continuum limit the energy density, ϵ is found to be proportional to $\left(\frac{\mu}{a}\right)^2$ instead of the correct finite result $\epsilon \sim \mu^4$ (for massless fermions). The number density is also found to be inconsistent with the canonical μ^3 form.

The solution to this problem was first proposed by Hasenfratz and Karsch [16]. The correct lattice action is obtained by following the euclidean formulation of thermodynamics where the chemical potential acts like the fourth component of an imaginary, constant vector potential. They proposed an alternative form for the lattice action

$$\begin{aligned} S &= a^3 \sum_x \left(ma\bar{\psi}_x\psi_x + \frac{1}{2}\sum_{j=1}^{3} \left(\bar{\psi}_x\gamma_j\psi_{x+\hat{j}} - \bar{\psi}_{x+\hat{j}}\gamma_j\psi_x \right) \right. \\ &+ \left. \frac{1}{2}\left(e^{\mu a}\bar{\psi}_x\gamma_4\psi_{x+\hat{4}} - e^{-\mu a}\bar{\psi}_{x+\hat{4}}\gamma_4\psi_x \right) \right) \end{aligned} \tag{1.58}$$

This results in the term $(\sin p_4 - i\mu a)^2$ in Eqn. 1.57 being replaced by $\sin^2(p_4 - i\mu a)$, as in the continuum theory. The correct continuum μ^4 scaling is obtained, although due to fermion doubling the resulting energy density is 16 times the usual finite energy density of free fermions at zero temperature.

Note that the observed quadratic divergence discussed above is not a lattice artifact. It is, in fact, present in the continuum theory itself. In the continuum theory there are a number of procedures which can be used to get rid of the divergence e.g. disregarding the contributions of the contour integrals at infinity. As we have seen, the problem is tackled in lattice theory by making appropriate modifications to the action.

Gavai [24] started from a general form for the lattice action and obtained specific constraints for the class of actions which yield well-behaved thermodynamic observables in the continuum limit. He considered the free energy density of a quark gas in the absence of gauge interactions ($U = 1$). Consider the following general

Euclidean naive fermionic action where $F(\mu a)$ and $G(\mu a)$ are arbitrary functions of the chemical potential which we aim to determine

$$\begin{aligned} S_F &= \frac{1}{2}\bar{\psi}(x)\left\{\sum_{\mu=1}^{3}\left[\gamma_\mu\delta_{x,\tilde{x}-\hat{\mu}} - \gamma_\mu\delta_{x,\tilde{x}+\hat{\mu}}\right]\right. \\ &+ \left.\frac{a_s}{a_t}\left[\gamma_0\delta_{x,\tilde{x}-\hat{0}}F(\mu a_t) - \gamma_0\delta_{x,\tilde{x}+\hat{0}}G(\mu a_t)\right] + 2ma_s\delta_{x,\tilde{x}}\right\}\psi(\tilde{x}). \quad (1.59) \end{aligned}$$

The energy density is calculated from Eqn.1.56 by performing the contour integration in Eqn. 1.54 analytically and transferring to momentum space using

$$\psi(x) = \int_{-\pi}^{\pi}\frac{d^4p}{(2\pi)^4}\,\tilde{\psi}(p)\,e^{ipx} \quad (1.60)$$

and the corresponding expression for $\bar{\psi}(x)$. Thus we obtain the following expression for $\ln Z$ in momentum space

$$\ln Z = \sum_p ln\, det\, \Delta_p \quad (1.61)$$

where Δ_p is given by

$$\Delta_p = i\sum_{\mu=1}^{3}\gamma_\mu \sin(p_\mu a_s) + \frac{a_s}{a_t}\, i\gamma_0 R \sin(p_0 a_t + i\theta) + ma_s \quad (1.62)$$

and we have introduced R and θ which are defined by

$$R \equiv (FG)^{1/2} \;\;;\;\; \tanh\theta \equiv \frac{F-G}{F+G} \quad (1.63)$$

using the above we obtain for the energy density ($a_s = a_t = a$)

$$\epsilon = \frac{4}{{n_s}^3 n_t a^4}\sum_p\left[\frac{R^2\sin^2(p_0 a + i\theta)}{R^2\sin^2(p_0 a + i\theta) + \sum_{\mu=1}^{3}\sin^2 p_\mu a}\right] \quad (1.64)$$

The $T = 0$ limit is obtained by letting $n_t \to \infty$ and by subtracting the vacuum ($\mu = 0$) contribution. The final expression for the energy density (after performing a contour integral) is

$$\begin{aligned} \epsilon a^4 &= \frac{4}{{n_s}^3}\sum_p\left\{\left[\frac{\sum_{\mu=1}^{3}\sin^2 p_\mu a}{R^2 + \sum_{\mu=1}^{3}\sin^2 p_\mu a}\right]^{1/2}\Theta\left[\frac{F(\mu a) - G(\mu a)}{2} - \left[\sum_{\mu=1}^{3}\sin^2 p_\mu a\right]^{1/2}\right]\right. \\ &+ \left.\left[\frac{\sum_{\mu=1}^{3}\sin^2 p_\mu a}{1 + \sum_{\mu=1}^{3}\sin^2 p_\mu a}\right]^{1/2} - \left[\frac{\sum_{\mu=1}^{3}\sin^2 p_\mu a}{R^2 + \sum_{\mu=1}^{3}\sin^2 p_\mu a}\right]^{1/2}\right\} \quad (1.65) \end{aligned}$$

Now consider taking the limit $a \to 0$, $n_s \to \infty$ (keeping the volume $(an_s)^3$ fixed). The first term in Eqn. 1.65 contributes to the energy density if and only if

$$F(\mu a) - G(\mu a) \propto \mu a \text{ for small } \mu a \quad (1.66)$$

However the second and third terms always contribute in the given limit and lead to unwanted divergences unless $R = 1$. Thus the constraints on the general form of the action derived from the requirement that we should recover the appropriate continuum expression $\epsilon = 16\mu^4/4\pi^2$ for a massless free fermion gas in the non-interacting case in the $a \to 0$ limit are:

$$F(\mu a)G(\mu a) = 1 \tag{1.67}$$

$$F(\mu a) - G(\mu a) = 2\mu a + O\left(\mu^2 a^2\right) \tag{1.68}$$

The second condition is equivalent to $\frac{dF(\mu a)}{d(\mu a)}\Big|_{\mu a=0} \neq 0$. The naive choice for introducing the chemical potential (based on the continuum prescription) is equivalent to $F(\mu a) = 1 + \mu a$; $G(\mu a_t) = 1 - \mu a_t$ and clearly does not satisfy Eqns. 1.68 which is as we would expect since we have shown that this choice leads to divergences. The most straightforward choice which does satisfy our two conditions is

$$\begin{aligned} F(\mu a_t) &= e^{\mu a} \\ G(\mu a_t) &= e^{-\mu a} \end{aligned} \tag{1.69}$$

This choice is not unique, indeed Bilic and Gavai [25] have implemented an action with

$$F(\mu a_t) = \frac{1+\mu a}{(1-\mu^2 a^2)^{1/2}} \;\; ; \;\; G(\mu a_t) = \frac{1-\mu a}{(1-\mu^2 a^2)^{1/2}} \tag{1.70}$$

which gives results consistent with Eqn. 1.69.

As a consequence of the first of Eqns. 1.68 we see that for ($\mu \neq 0$) forward propagation of quarks is enhanced by the factor $F(\mu a)$ while the forward propagation of anti-quarks is suppressed by the factor $1/F(\mu a)$.

Let us now consider reintroducing the SU(N) gauge interactions in Eqn. 1.59. In this case we have $S_F = \bar{\psi}_x \, M_{x\tilde{x}} \, \psi$, where

$$\begin{aligned} M_{x\tilde{x}} &= \left\{ \sum_{\mu=1}^{3} \left[\gamma_\mu U_x^\mu \delta_{x,\tilde{x}-\hat{\mu}} - \gamma_\mu U_{\tilde{x}}^{\mu\dagger} \delta_{x,\tilde{x}+\hat{\mu}} \right] \right. \\ &+ \left. \frac{a_s}{a_t} \left[\gamma_0 U_x^0 \delta_{x,\tilde{x}-\hat{0}} F(\mu a_t) - \gamma_0 U_{\tilde{x}}^{0\dagger} \delta_{x,\tilde{x}+\hat{0}} \frac{1}{F(\mu a_t)} \right] + 2m a_s \delta_{x,\tilde{x}} \right\} \end{aligned} \tag{1.71}$$

For the interacting theory with $SU(N), N \geq 3$, **none** of the actions which satisfy Eqns. 1.68 lead to a real positive-definite fermion determinant (det M).(Note that for $SU(2)$, det M is real because the condition $\sigma_1 U \sigma_1 = U^\dagger$ holds). The fact that det M is non-Hermitian for $\mu \neq 0$ makes numerical simulation of QCD at finite density extremely difficult. The standard hybrid Monte Carlo algorithm requires a positive definite fermion determinant because $e^{-S_{eff}} = e^{-(S_G[U] - \ln \det M[U])}$ serves

as a transition probability in the updating process. In fact, det M can be made real and positive definite for $F(\mu a)$ complex by insisting that $|F(\mu a)| = 1$ for all μa but this leads to a complex chemical potential. One therefore needs an innovative method in order to perform numerical simulations at $\mu \neq 0$.

Simulations using the $SU(2)$ colour group at finite baryon density where the action is still real have been performed in the strong coupling limit ($g^2 = \infty$) and compared with analytical predictions obtained from a $1/d$ expansion combined with a mean field analysis. In the $SU(2)$ theory (where the fundamental representation is pseudoreal) the baryons are bosons in the same multiplet as the Goldstone boson and at $\mu = 0$ the theory has a $U(2N)$ chiral symmetry which is expected to break to $Sp(N)$. The analytic calculations [26] predicted a second-order chiral transition for $SU(2)$ (first-order transition for $SU(3)$) in the strong coupling, zero temperature limit. This prediction did not agree with the Monte-Carlo data but a more refined $1/d$, mean field analysis [27] which handled the mesonic and baryonic sector of the effective action more carefully and took into account the *spacetime asymmetry* introduced by a non-vanishing chemical potential gave results which were consistent with the Monte-Carlo data. In fact for the $SU(2)$ theory at $g^2 = \infty$, $T = 0$, $\mu \neq 0$ there is **no chiral symmetry restoring transition.** Although the chiral condensate $\langle\bar{\psi}\psi\rangle$ actually vanishes for all $\mu \neq 0$ in the limit $m \to 0$, the chiral symmetry remains unbroken due to the presence of non-vanishing **baryonic condensates.** Considering the $U_A(1) \otimes U_V(1)$ symmetry for staggered fermions note that the baryonic condensate breaks $U_A(1) \otimes U_V(1)$ completely whereas $\langle\bar{\psi}\psi\rangle$ breaks only $U_A(1)$. The spontaneous breakdown of the $U_V(1)$ symmetry is believed to be a direct consequence of the introduction of a chemical potential.

The complex Langevin algorithm is, in principle, capable of dealing with a complex probability measure such as that appearing in the $SU(3)$ theory but its convergence properties are poor and attempts to implement this algorithm have been unsuccessful to date.

Chapter 2

Lattice QCD at Non-Zero Quark Density

As outlined in Chapter 1 the fundamental difficulty in simulating QCD at finite density and investigating the transition quantitatively is that the effective action resulting from the Grassmann integration over the fermions is *complex* due to the introduction of the chemical potential in the Dirac matrix.

The complex nature of the QCD finite density action [6, 16] prohibits the use of naive probabilistic methods in evaluating the functional integral. Thus the standard simulation algorithms [28, 29, 30] for lattice QCD with dynamical fermions are inappropriate in this context. Exact studies are undesirable because they are extremely computationally intensive. Early simulations avoided the problem of the complex action by looking at the theory in the quenched approximation where the determinant is set to a constant value hence the effects of dynamical fermions are neglected. This approximation has problems in the chiral limit because it ignores the axial anomaly, but it is satisfactory for many practical calculations.

2.1 Overview of the Unphysical Results of Quenched Theory Simulations

Serious problems were first reported in quenched simulations of finite density QCD in 1986 [31] and the physical and mathematical reasons for this failure have been the focus of considerable debate ever since [32, 33].

In these early simulations the behaviour of the chiral condensate was studied at

fixed quark mass for various different values of the chemical potential, μ. At zero temperature we expect the deconfinement transition to occur at $\mu \simeq \frac{m_p}{3}$, where μ is the chemical potential and m_p is the proton mass [6]. This value corresponds to the lowest lying state with non-zero baryon number. The chiral condensate should serve as an order parameter for the transition. The behaviour was initially as expected *viz.* the chiral condensate remained constant up until a certain value of μ and then tended to zero as the chemical potential was increased.

We would expect that physical observables are μ independent up to some μ_c which is related to the threshold for baryon production. The problem encountered was that as the bare quark mass was decreased the μ at which the chiral condensate began to change also decreased towards zero.

In fact, the onset of chiral symmetry restoration appeared to occur at a chemical potential of half the pion mass, which would extrapolate to zero in the chiral limit ($m \to 0$). A study of the distribution of the eigenvalues of the lattice Dirac operator confirmed that the lowest mass state containing a net number of fermions (i.e. a quark or a baryon but not a meson which does not see μ) became massless as the bare quark mass was reduced to zero. The interpretation was that there existed either baryonic states which became massless in the chiral limit and had an energy equal to $\frac{3}{2}m_\pi$ or stable quark matter with low mass per baryon.

The result that μ_c is proportional to the pion mass is clearly unphysical. We expect $\mu_c \simeq \frac{m_p}{3}$ because the proton is the lightest state with non-zero baryon number. From this we are drawn to two possible conclusions:

- The quenched approximation is at fault implying it is strictly necessary to consider the complex action of full QCD at finite chemical potential.
- There could be intrinsic problems in the lattice formulation of fermions (possibly associated with fermion doubling) and chemical potential which would survive an unquenched treatment.

Further studies [34] of the quenched theory on larger lattices found similar behaviour. However, a recent study [32, 33] of the quenched theory which measured the condensate and the pion and nucleon masses, did find that, at intermediate and strong coupling, the theory is sensitive to the baryon mass but that it is pathological for $\mu > \frac{m_\pi}{2}$.

From an analytical study of the eigenvalues of the fermionic propagator matrix Gibbs [35] provided an argument explaining why, in the quenched theory, $\langle\bar{\psi}\psi\rangle$ is controlled by the *pion mass*. He showed that the eigenvalue spectrum calculated

on isolated configurations should contain poles in correspondence to the physical particle masses. In particular, the smallest mass state can be associated with the lowest eigenvalues. This state is obtained by squaring the propagator matrix, and defines the pion mass in QCD. The lowest eigenvalue of the propagator matrix appears to trigger the fall in $\langle\bar{\psi}\psi\rangle$ signalling the onset of the chiral transition. We shall return to this argument in Chapter 3.

It has also been suggested by several authors that the coincidence of the onset of the chiral symmetry restoration with one half of the pion mass might only have been a numerical accident, the correct relationship being $\mu_{onset} = \frac{m_p}{3} - \Delta$ where Δ is the contribution of the nuclear binding energy. If this scenario were true then the problems with finite density simulations would not be too serious. This conjecture has been tested by Kogut et. al. [33] but unfortunately their work confirmed the onset at $\mu = \frac{m_\pi}{2}$.

2.1.1 Random Matrix Models

In relation to the claim that the quenched approximation is responsible for the unphysical results for the chiral transition in QCD at finite density it was first suggested by Gocksch [36] that the quenched approximation is obtained as the limit of the number of flavours going to zero with an equal number of quarks and conjugate quarks i.e.., the limit of a partition function in which only the absolute value of the determinant enters. Recent work by Stephanov [37] within the framework of a random matrix model which incorporated the chiral and flavour structure of the Dirac operator has made this suggestion more explicit. He showed *analytically* that the quenched Dirac spectrum is obtained in the limit as both the number of quarks and conjugate quarks tend to zero. Since QCD does not have such conjugate quarks it seems that simulations of the quenched theory are inappropriate to QCD in this context. According to this scenario, in the quenched model the "early" onset for the number density would also correspond to the restoration of chiral symmetry because of the simultaneous occurrence of quarks and conjugate quarks in the system. It is predicted that the inclusion of dynamical fermions will result in a rearrangement of the eigenvalues such that the chiral symmetry will be restored at $\mu_c \simeq \frac{m_B}{3}$ as expected.

2.2 Lattice QCD at Non-Zero Chemical Potential with Dynamical Fermions

A method which circumvents the difficulty of investigating the finite density transition for dynamical fermions was proposed by Barbour and collaborators [1]. The method draws upon the classic work of Yang and Lee who showed that the distribution of the zeros of a partition function determines the equation of state for a many-body system. Our study of lattice QCD at finite density is based on expanding the Grand Canonical Partition Function (GCPF) as a polynomial in the fugacity variable ($e^{\mu/T}$).

2.2.1 Formulation of GCPF for a Statistical System

We shall consider the construction of the Grand Canonical Partition Function (Z) from its constituent Canonical Partition Functions (Z_n). The GCPF is formulated as follows

$$Z(\mu) = Tr\left(e^{-\beta(H-\mu.N)}\mathcal{P}\right) \tag{2.1}$$

where $\mathcal{P}$ is a projection onto gauge invariant states, H is the Hamiltonian and N is the fermion number given by

$$N = \int d^3x\, \psi^\dagger(x)\psi(x) \tag{2.2}$$

We re-express this by making use of use the following relation involving the Delta function

$$e^{\beta\mu N} = \sum_{n=-\infty}^{\infty} e^{\beta\mu n}\,\delta(N-n) \tag{2.3}$$

so that

$$Z(\mu) = \sum_{n=-\infty}^{\infty} e^{\beta\mu n}\, Tr(e^{-\beta H}\delta(N-n)\mathcal{P}) \tag{2.4}$$

We define a canonical partition function for an n fermion system as follows

$$Z_n = Tr\left(e^{-\beta H}\,\delta(N-n)\mathcal{P}\right) \tag{2.5}$$

so that the GCPF is

$$Z(\mu) = \sum_{n=-\infty}^{\infty} e^{\beta\mu n} Z_n \tag{2.6}$$

for a lattice of size ${n_s}^3$ by n_t and for N_c colours the maximum possible number of fermions in the system is $N_{max} = N_c {n_s}^3$ so that

$$Z(\mu) = \sum_{n=-N_{max}}^{N_{max}} e^{\beta\mu n} Z_n \tag{2.7}$$

The GCPF is represented on the lattice as a functional integration

$$Z = \int [dU][d\bar{\psi}][d\psi] \exp\left(S_G(U) - \bar{\psi} M(U,\mu)\psi\right) \tag{2.8}$$

Where S_G is the standard Wilson gauge action. The fermion fields are integrated out using the standard Gaussian integration technique to give

$$Z = \int [dU] \det\left(M(\mu,U)\right)\ e^{-S_G} \tag{2.9}$$

The fermion determinant, det M, can be expressed as a finite sum of gauge invariant loops of link fields, some of which wind around the lattice many times. We collect together all terms which contain the same number of loops, l, in the temporal direction

$$\det M = c_0 + \sum_{l=1}^{l_{max}} c_l\, e^{l\mu a n_t} + \sum_{l=1}^{l_{max}} c_{-l}\, e^{-l\mu a n_t} \tag{2.10}$$

where an_t is the temporal extent of the lattice and for an SU(N) gauge theory $l_{max} = N{n_s}^3$ where n_s is the spatial dimension of the lattice. Note that $c_l^* = c_{-l}$ because the loops which pick up a factor $e^{l\mu a n_t}$ are the complex conjugates of the loops which pick up a factor $e^{-l\mu a n_t}$. Only those quark loops which wind completely around the lattice will pick up factors of $e^{n_t a\mu}$ and $e^{-n_t a\mu}$ and these correspond to particles which propagate infinitely in time i.e. *real particles*. The quarks which double back in time forming closed loops which do not wind around the lattice pick up $e^{\pm n_t \mu}$ factors which cancel and these correspond to quark/antiquark creation and annihilation.

The c_n's are directly related to the canonical partition functions so that

$$Z_n \propto \int [dU]\, c_n\, e^{-S_G} \tag{2.11}$$

The coefficient $c_{l_{max}} = 1$ due to a gauge integral property on a product of gauge links. This coefficient corresponds to the Polyakov loop which is an order parameter for deconfinement in the case of the quenched theory.

2.3 Expansion of the Grand Canonical Partition Function

2.3.1 The Glasgow Method

The problem caused by the non-Hermitian nature of the fermion matrix at $\mu \neq 0$ can be circumvented by a method which involves the expansion of the grand-canonical partition function (GCPF) in powers of the fugacity variable $e^{\mu/T}$.

Consider the expression for the GCPF of lattice QCD

$$Z \sim \int [dU] \det\left(M(U,\mu,m)\right) e^{-S_g(U)} \tag{2.12}$$

The GCPF can be expressed as an ensemble average of $\det M$ at $\mu = 0$:

$$\begin{aligned} Z(m,\mu) &= \frac{\int [dU] \frac{\det M(\mu,m)}{\det M(\mu=0,m)} \det M(\mu=0,m)\, e^{-S_g[U]}}{\int [dU] \det M(\mu=0,m)\, e^{-S_g[U]}} \\ &= \left\langle \frac{\det M(\mu,m)}{\det M(\mu=0,m)} \right\rangle_{|_{\mu=0}} \end{aligned} \tag{2.13}$$

Note that it is generating the ensemble at $\mu = 0$ which allows us to avoid the problem of the complex action in the Hybrid Monte Carlo algorithm.

With the chemical potential included, the lattice Dirac operator with Kogut-Susskind fermions [6, 16] is:

$$M_{x,y}(\mu) = m\,\delta_{x,y} + \frac{1}{2}\left[\sum_{\nu=1,2,3} U_\nu \eta_\nu \delta_{x+\hat{\nu},y} - U_\nu^\dagger(y)\eta_\nu(y)\delta_{x-\hat{\nu},y}\right] \tag{2.14}$$

$$+ \frac{1}{2}\left[e^{\mu a} U_t(x)\eta_t(x)\delta_{x+\hat{t},y} - e^{-\mu a} U_t^\dagger(y)\eta_t(y)\delta_{x-\hat{t},y}\right] \tag{2.15}$$

This can be conveniently expressed in terms of matrices G and V where G contains all the spacelike links while V contains the forward and $V^\dagger$ the backward timelike links.

$$2iM_{x,y} = G_{x,y} + V_{x,y}e^{\mu} + V^\dagger_{x,y}e^{-\mu} + 2im\delta_{x,y} \tag{2.16}$$

Note that $G{=}G^\dagger$ and $VV^\dagger = 1$.

We can now define the propagator matrix in terms of these matrices [35]

$$P = \begin{pmatrix} -G - 2im1 & 1 \\ -1 & 0 \end{pmatrix} V \tag{2.17}$$

which is a matrix of dimension $6n_s^3 n_t$, for a $n_s^3 \times n_t$ lattice with $SU(3)$ gauge fields. Note that V **is an overall factor of** P.

The determinants of P and M are simply related:

$$\begin{aligned} \det(P - e^{-\mu}) &= \begin{vmatrix} -GV - 2imV - e^{-\mu} & V \\ -V & -1e^{-\mu} \end{vmatrix} \\ &= \det\left(GVe^{-\mu} + 2imVe^{-\mu} + e^{-2\mu} + V^2\right) \\ &= \det\left(\left(Ge^{-\mu} + 2ime^{-\mu} + V^\dagger e^{-2\mu} + V\right)V\right) \\ &= e^{-3\mu n_s^3 n_t} \det\left(G + 2im + V^\dagger e^{-\mu} + Ve^{\mu}\right) \\ &= e^{-3\mu n_s^3 n_t} \det M \end{aligned} \tag{2.18}$$

where we have used $\det V = 1$ and $V^\dagger V = VV^\dagger = 1$.

Since we have expressed $\det M$ in terms of the determinant of a matrix which is *diagonal* in $e^{-\mu}$ we can expand $\det M$ as a polynomial in e^{μ}

$$|2iM| = e^{3\mu n_s^3 n_t} |P - e^{-\mu}| \tag{2.19}$$

$$= e^{3\mu n_s^3 n_t} \sum_{n=0}^{6n_s^3 n_t} \omega_n e^{-n\mu} \tag{2.20}$$

Thus the determinant of the lattice Dirac operator is given by the characteristic polynomial of P.

Provided the $\langle \omega_n \rangle$ are determined to sufficient accuracy. we can measure the averaged characteristic polynomial over the ensemble generated at $\mu = 0$, and use this to provide an analytic continuation [1] for the GCPF to any non-zero μ. In order to obtain the fugacity expansion we must determine the eigenvalues of P.

The inverse of the propagator matrix is

$$P^{-1} = V^{\dagger} \begin{pmatrix} 0 & -1 \\ 1 & -G - 2im1 \end{pmatrix} \tag{2.21}$$

so

$$|2iM| = e^{-3\mu n_s^3 n_t} |e^{\mu} - P^{-1}| \tag{2.22}$$

$$= e^{-3\mu n_s^3 n_t} \sum_{m=0}^{6n_s^3 n_t} \omega_m^* e^{+n\mu} \tag{2.23}$$

we can use this to identify a symmetry in the expansion coefficients:

$$|P - e^{-\mu}| = e^{-6\mu n_s^3 n_t} |e^{\mu} - P^{-1}| \tag{2.24}$$

therefore

$$\omega_n = \omega^*_{(6n_s{}^3 n_t - n)} \tag{2.25}$$

i.e. ω_n gives the coefficient for a lattice with n fermions missing. The ω_n are closely related to the **canonical partition functions**, Z_n, for fixed particle number, n, on the lattice:

$$Z_n = \left\langle \frac{\omega_{(3n_s^3 n_t - n)}}{\det M(\mu = 0)} \right\rangle \tag{2.26}$$

where the normalisation factor arises from Eqn. 2.13

Since $(P^{-1})^{\dagger}$ is related to P by a unitary transform it can be shown that the eigenvalues of P have the symmetry: if λ is an eigenvalue then so is $1/\lambda^{\dagger}$.

The GCPF can now be expressed as

$$Z = \sum_{-3n_s{}^3 n_t}^{3n_s{}^3 n_t} < \omega_{|n|} > e^{n\mu} \tag{2.27}$$

2.3.2 Eigenvalues of the Propagator Matrix and $Z(n_t)$ Symmetry

In addition, since the matrix V is an overall factor of P, we can alter the timelike links on a single timeslice by $e^{2\pi i}$. We perform a unitary transform to spread this over all timelike links so that

$$V \longrightarrow V \times \text{ element of } Z(n_t) \tag{2.28}$$

This is then transferred to the eigenvalues, λ

$$|P - \lambda_i| = 0 \tag{2.29}$$

Therefore the eigenvalues themselves have a $Z(n_t)$ symmetry. This $Z(n_t)$ symmetry holds configuration by configuration. As a consequence of this symmetry, the characteristic polynomial for P is a polynomial in $e^{\mu n_t}$ with $(6n_s^3 + 1)$ complex coefficients. Thus we obtain an expansion for the GCPF in the fugacity, $e^{\mu/T}$

$$Z = \sum_{n=-3n_s^3}^{3n_s^3} < \omega_{|n|} > e^{n\mu n_t} = \sum_{n=-3n_s^3}^{3n_s^3} e^{-(\epsilon_n - n\mu)/T} \tag{2.30}$$

Since the probability for a given configuration of gauge fields to appear in our ensemble is equal to that of its complex conjugate the imaginary parts of the coefficients should average to zero. We **impose** the complex conjugation symmetry. As a consequence, the characteristic polynomial from a configuration (averaged with its complex conjugate) is invariant under $\mu \to -\mu$.

The major computational task in performing the GCPF fugacity expansion is the determination of all of the eigenvalues of P, a non-Hermitian, sparse matrix of dimension $6n_s^3 n_t$. We can exploit the $Z(n_t)$ symmetry of the eigenvalues because it is more efficient to diagonalize P^{n_t} than to diagonalize P. This introduces a $Z(n_t)$ degeneracy of the eigenvalues and effectively reduces the dimension of the matrix to $6n_s^3$. Note that although P is a sparse matrix P^{n_t} will be dense.

As described in detail in Chapter 2 we have investigated two methods of finding all the eigenvalues of P^{n_t}. The Lanczos technique with reorthogonalisation was used on 6^4 lattices but on 8^4 lattices the procedure involving balancing, reduction to upper Hessenberg form and then LU decomposition was more efficient.

2.3.3 Z(3) Tunnelling - Evidence for Simulating in the Confined Sector

The order parameter for deconfinement in the **pure gauge** theory is the expectation value of the Polyakov loop, $P(\vec{x})$, which describes the interaction of the gluons with

a static quark charge

$$P(\vec{x}) = Tr\left(\prod_{t=1}^{n_t} U_t(\vec{x},t)\right) \tag{2.31}$$

The expectation value of P gives the free energy, F_q, associated with a single static quark

$$|\langle P(\vec{x})\rangle| = e^{-F_q/T} = \frac{Z_{\bar{q}}}{Z_0} \tag{2.32}$$

where $Z_{\bar{q}}$ is the canonical partition function for a system with a single antiquark while Z_0 is the canonical partition function for a quarkless system. $P(\vec{x}) = 0 \Rightarrow F_q = \infty$ relative to the vacuum indicating that quarks are confined. However $P(\vec{x}) \neq 0$ implies that the free energy of an isolated quark is finite therefore the system must be deconfined.

In the pure $SU(N_c)$ gauge theory we have N_c equivalent vacua related by $Z(N_c)$ rotations in colour space. The $Z(N_c)$ centre symmetry consists of global gauge transformations which commute with the gauge group although they alter the quark fields. Note that $Z(N_c)$ is the only diagonal subgroup of $SU(N_c)$ which has unit determinant.

In simulations which include dynamical fermions, the Polyakov loop cannot be used as an order parameter for deconfinement. However in our dynamical simulations we can use $Z(3)$ tunnelling as an indication of whether we are in the confined sector. Tunnelling between the different $Z(3)$ vacua is much *more probable in the confined sector* than in the deconfined sector. To ensure that we are in the confined sector at $\mu = 0$ for the chosen lattice parameters we look for evidence of $Z(3)$ tunnelling. The the pure-gauge action as well as the integration measure are invariant under the $Z(3)$ transformation. This transformation should eliminate the triality non-zero coefficients. Just as for the $Z(n_t)$ symmetry, the $Z(3)$ symmetry is transferred to the eigenvalues of P^{n_t} via a unitary transform. This is equivalent to the transformation:

$$V \to V\, e^{\frac{2\pi i z_j}{n_t}} \text{ where } z_j = \frac{j}{3} \text{ for } j = 0,1,2. \tag{2.33}$$

Thus the GCPF can be written as:

$$Z(\mu) = \frac{\sum_{j=0}^{2} \int [dU][dU^\dagger]\, detM\left(\mu + \frac{2\pi i z_j}{n_t}\right) e^{-S_g[U,U^\dagger]}}{3\int [dU][dU^\dagger]\, detM(\mu = 0)\, e^{-S_g[U,U^\dagger]}} \tag{2.34}$$

Note that the $Z(3)$ symmetry does not hold configuration by configuration, but is a property of the *ensemble average*. We do not impose this symmetry - but we

look for it. Taking account of the $Z(3)$ symmetry the GCPF can be expressed as:

$$Z(\mu) = \sum_{n=-3n_s{}^3,3}^{3n_s{}^3} \langle \omega_n \rangle e^{\frac{-n\mu}{T}}. \tag{2.35}$$

Since our ensemble is generated at $\mu = 0$

$$Z(\mu = 0) = \sum_{n=3n_s{}^3,3}^{3n_s{}^3} < \omega_n >= 1 \tag{2.36}$$

and we monitor

$$S_m = \sum_n \langle \omega_n \rangle \text{ for mod(n, 3) = m ; m = 0, 1, 2} \tag{2.37}$$

Note that the sum, S_m is dominated by the first few (largest) coefficients of the expansion. In a confined system we expect

- $S_m = 0$ for $m = 1, 2$ which is a weak condition on the **triality one** and **triality two** coefficients.
- $S_m = 1$ for $m = 0$ which is a strong condition on the **triality zero** coefficients

The **triality zero** coefficients are associated with the canonical partition functions corresponding to **multiples of three quarks**. In the limit of infinite statistics and in a colour confined system we expect *only* canonical partition functions corresponding to multiples of three quarks to contribute to the GCPF i.e. in the limit of infinite statistics Z(3) tunnelling must be completely achieved. In our simulations we expect to see the magnitude of the triality one and triality two coefficients gradually decreasing as the statistics increase.

On any given *single configuration* the ω_n are *complex* but, since the conjugate configuration can occur with equal probability, their average is real. Their sign does fluctuate significantly between configurations. If the physical interpretation of the ω_n's as a measure of the relative probability of the associated canonical partition functions is valid then their **average must be real and postitive**.

2.4 Calculation of Observables

2.4.1 Definitions

Fermion number density is defined by:

$$\langle n_d(\mu, ma) \rangle \equiv \lim_{n_s \to \infty} \left[\frac{T}{{n_s}^3} \frac{\partial \ln(Z(\mu, m))}{\partial \mu} \right]_{a_s = a_t = a} \tag{2.38}$$

To define the fermion energy density we must subtract the energy density at $T = 0$ and $\mu = 0$:

$$\begin{aligned}\langle \epsilon_d(\mu, ma) \rangle &\equiv n\mu - \lim_{n_s \to \infty} \left[\frac{T}{{n_s}^3} \frac{\partial \ln(Z(\mu, m))}{\partial(1/T)} \right]_{a_s = a_t = a} \\ &+ \lim_{n_s \to \infty, n_t = n_s} \left[\frac{T}{{n_s}^3} \frac{\partial \ln(Z(\mu, m))}{\partial(1/T)} \right]_{a_s = a_t = a}^{\mu = 0} \end{aligned} \tag{2.39}$$

The chiral order parameter, $\langle \bar{\chi}\chi \rangle$, indicates whether or not chiral symmetry is broken: $\lim_{m \to 0} \langle \bar{\chi}\chi \rangle \neq 0$ in the chirally broken (probably also colour confined) phase whereas $\lim_{m \to 0} \langle \bar{\chi}\chi \rangle = 0$ when chiral symmetry is restored (quark-gluon plasma phase).

$$\langle \bar{\chi}\chi \rangle \equiv - \lim_{n_s^3 \to \infty} \frac{1}{n_s^3 n_t} \left[\frac{\partial}{\partial(m a_t)} \ln Z \right]_{a_s = a_t = a} \tag{2.40}$$

$\langle \bar{\chi}\chi \rangle$ is related to the usual chiral order parameter, the chiral condensate, via

$$\langle \bar{\psi}\psi \rangle_{4 flav.} = -\frac{1}{a^3} \langle \bar{\chi}\chi \rangle = \lim_{n_s^3 \to \infty} \frac{T}{n_s^3} \left[\frac{\partial}{\partial(m)} \ln Z \right] \tag{2.41}$$

2.4.2 Observables from Stochastic Estimators

The fermion number density, energy density and the chiral condensate can be evaluated using *stochastic estimators.* This procedure avoids the full inversion of the fermion matrix, M, which would be too computationally intensive. Instead the traces appearing in the expressions for expectation values of the observables are approximated by unbiased estimators. These are obtained by introducing N_η vectors of complex Gaussian random numbers $\eta^{(\mu)}$ with $(\mu = 1, 2, ..., N_\eta)$ of dimension equal to the dimension of M. The components of $\eta^{(\mu)}$ are distributed according to $e^{-(\eta^{(\mu)}, \eta^{(\mu)})} = e^{-\sum_x (\eta_x^{(\mu)\dagger} \eta_x^{(\mu)})}$ so that the diagonal matrix element with respect to the random vector is an unbiased estimator for the trace:-

$$Tr\{M^{-1}\} = \lim_{N_\eta \to \infty} \frac{1}{N_\eta} \sum_{\mu=1}^{N_\eta} \left(\eta^{(\mu)}, M^{-1} \eta^{(\mu)} \right) \tag{2.42}$$

We make use of the mathematical relation $\det M = e^{Tr \ln M}$ and consider differentiating with respect to arbitrary variable x:

$$\frac{\partial}{\partial x} \det M = \det M \, Tr \left(M^{-1} \frac{\partial M}{\partial x} \right) \tag{2.43}$$

We use this to obtain expressions for the observables in terms of the matrices V and $V^\dagger$ in the propagator matrix

$$\langle n_d \rangle = \lim_{n_s \to \infty} \frac{1}{{n_s}^3 n_t {a_s}^3 a_t} \left\langle Tr\, M^{-1} \left(a_t V e^{\mu a_t} + a_t V^\dagger e^{-\mu a_t} \right) \right\rangle \tag{2.44}$$

$$\langle \epsilon_d \rangle = \lim_{n_s \to \infty} \frac{1}{{n_s}^3 n_t a_t} \left\langle Tr\, M^{-1} \left(V e^{\mu a_t} - V^\dagger e^{-\mu a_t} \right) \right\rangle - \frac{N_c}{4a^4} + \frac{m}{4} \langle \bar{\psi}\psi \rangle |_{\mu=0} \quad (2.45)$$

$$\langle \bar{\chi}\chi \rangle = -\frac{1}{n_s^3} \langle (Tr M^{-1}) \rangle \quad (2.46)$$

2.4.3 Observables from GCPF Expansion Coefficients

Using the Glasgow method, we can readily obtain an independent estimate of the fermion number and energy densities directly from the coefficients of the GCPF expansion coefficients as follows:

Fermion number density:

$$\langle n_d(\mu) \rangle = \frac{\sum_{n=-3{n_s}^3}^{3{n_s}^3} n\, e^{-(\epsilon_n - n\mu)/T}}{\sum_{n=-3{n_s}^3}^{3{n_s}^3} e^{-(\epsilon_n - n\mu)/T}} \quad (2.47)$$

Fermion energy density:

$$\langle \epsilon_n(\mu) \rangle = \frac{\sum_{n=-3{n_s}^3}^{3{n_s}^3} \epsilon_n\, e^{-(\epsilon_n - n\mu)/T}}{\sum_{n=-3{n_s}^3}^{3{n_s}^3} e^{-(\epsilon_n - n\mu)/T}} \quad (2.48)$$

2.4.4 Alternative Methods

The Glasgow method involves an ensemble generated at $\mu = 0$. There is a possibility that this could introduce systematic errors due to insufficient overlap when measuring observables at μ significantly greater than the onset of non-zero number density although simulations on a 2^4 lattice indicate that as the statistics increase the results improve significantly. With the availability computing power of the order of Tera flops limited statistics should not pose a problem. It is important to be aware of the fact that although generating the ensemble at $\mu = 0$ is an exact method, accuracy could be lost if we have insufficient overlap with the true physical ensemble at $\mu \neq 0$. The Glasgow method is currently the most promising in the context the shortcomings of a number of alternative methods which have been implemented previously.

One alternative method involves generating the ensemble either with respect to the modulus of the real part of $\det M(\mu)$ or with respect to its absolute value [38, 39].

$$\det M \equiv e^{i\phi_M} |\det M| \quad (2.49)$$

and to include the phase in the measurement. Consider for example the expectation value of the pure gluonic quantity $\mathcal{O}[\mathcal{U}]$

$$\langle \mathcal{O}[U] \rangle = \frac{\langle \mathcal{O}[U] e^{i\phi_M} \rangle_{S_{eff}}}{\langle e^{i\phi_M} \rangle_{S_{eff}}} \quad (2.50)$$

Although this procedure is in principle correct, in practice, simulations at a fixed quark mass using these methods are well behaved only at low and high chemical potentials and not in the critical region: $\frac{m_\pi}{2} \leq \mu \lesssim \frac{m_p}{3}$. In this critical region the quantity $e^{i\phi_M}$ has very strong fluctuations in phase generated by $e^{-S_{eff}}$ so that it becomes very small and is not measurable. This behaviour can be understood by considering that most of the time the updating process produces incorrect configurations with inaccurate values of the observables and these contributions must be cancelled by a strongly fluctuating phase.

Gocksh [36, 40] used a **spectral density method** by binning the phase ϕ and measuring $\rho(\phi)$. The spectral density method was applied at infinite coupling and is discussed in detail in Chapter 3. On a 2^4 lattice, his results for μ_c are in broad agreement with mean-field theory. He studied the form of the density of states as a function of energy for different values of chemical potential and concluded that outside the critical region the density of states is sharply peaked at $\phi(U) \doteq 0$ therefore the phase is not important. However for $\mu \sim \mu_c$ the density of states is flat and there is an contribution from $\phi(U)$ at **all points** in the integration region hence the phase of the determinant must be accounted for. This observation explains the failure, in the critical μ region, of the methods involving updating with respect to the modulus of the determinant.

2.5 The Static Quark Model

Blum, Hetrick and Toussaint [41] have recently studied numerical simulations of lattice QCD in the limit that the quark mass and chemical potential are simultaneously made large. In that limit, the quark mass and chemical potential appear only in the ratio $(2ma/e^{\mu a})^{n_t}$ and the propagator matrix becomes

$$P = \begin{pmatrix} -2imV & V \\ -V & 0 \end{pmatrix}. \tag{2.51}$$

The corresponding fermion determinant is complex but trivial to evaluate which allows generation of very high statistics in their measurements and determine $\langle e^{i\phi} \rangle$ to sufficient accuracy.

For quenched QCD the high temperature transition is first order and they expected this behaviour to extend into the interior of the $T - \mu$ phase diagram. However their simulations showed that this transition becomes a **smooth crossover** at very small density (possibly for any nonzero density) and that, at low enough temperature, chiral symmetry remains broken at all densities.

Of course, as the authors point out,it is not at all clear that the static approximation has anything to do with real QCD. However, it is relevant that unexpected results follow in this simple model.

2.6 The Reweighting Procedure

The Glasgow algorithm is a particular example of a *reweighting procedure.* Such procedures are essentially based on the development of a Taylor series expansion of the GCPF around some update chemical potential, μ_0, at which the GCPF is normalised to be 1. In the general case the GCPF is defined as:

$$\begin{aligned} Z(m,\mu) &= \frac{\int [dU][dU^\dagger] \frac{\det M(\mu,m)}{W(\mu=\mu_0)} W(\mu=\mu_0) e^{-S_g[U,U^\dagger]}}{\int [dU][dU^\dagger] W(\mu=\mu_0) e^{-S_g[U,U^\dagger]}} \\ Z(m) &= \left\langle \frac{\det M(\mu,m)}{W(\mu=\mu_{up})} \right\rangle_{|_{\mu_0}} \end{aligned} \tag{2.52}$$

The expansion coefficients, w_n, of the GCPF are measured from an ensemble of configurations generated with respect to the Boltzmann weight $W(\mu=\mu_0)e^{-S_g[U,U^\dagger]}$ and are determined from the eigenvalues of the propagator matrix. A number of alternative $W(\mu=\mu_0)$'s have been tried in finite density simulations:

1. $W = |\det(M(\mu_0))|$ for some $\mu_0 \geq 0$.
2. $W = |real(\det(M(\mu_0)))|$ for some $\mu_0 \geq 0$.
3. $W = (\det(M_0 M_1 M_2))^{1/3}$ for $M_k = M(\mu = \frac{2\pi i k}{3n_t})$.
4. $W = |\det(M_0) + \det(M_1) + \det(M_2)|$ for $M_k = M(\mu = \mu_0 + \frac{2\pi i k}{3n_t})$.

The last two choices of W are constructed in an attempt to minimise the fluctuations in the triality non-zero coefficients so that the Z_n's are of comparable magnitude for n a multiple of three – these canonical partition functions are most relevant to the physical system. The last choice of update does serve to minimise the fluctuations but is difficult to implement.

The Glasgow algorithm uses $W = \det(M(\mu_0 = 0))$. This means that we have a reweighting factor $R_F = \frac{\det(M(\mu \neq 0))}{\det(M(\mu_0=0))}$. The reweighting procedure is most effective when $R_F \simeq 1$. This criterion is satisfied for $\mu \lesssim 0.5$ and for large μ, although R_F may be considerably less than 1, this is offset by the fact that the fluctuations are small for μ large. In the critical region (intermediate values of μ) the fluctuations in sign of the coefficients are large and $R_F << 1$. This means that measurements here are dominated by a few isolated configurations i.e. those for which $\det(M(\mu_0 =$

0)) is small. This implies that exact simulations of QCD at finite density using reweighting procedures may well require very high statistics to produce realistic estimates of observables in the critical region. Note also that as the dimensions of the lattice are increased the efficiency of the reweighting procedure diminishes. The effects of reweighting will inevitably affect the measurements of the observables using the *stochastic estimators*.

Chapter 3

Eigenvalues of the Propagator Matrix and Lee-Yang Zeros

The major computational task in performing the GCPF fugacity expansion is to find the eigenvalues of P, a non-Hermitian, sparse matrix of size $6n_s^3 n_t$. Due to the $Z(n_t)$ symmetry, it is more efficient to diagonalize P^{n_t}. This introduces a $Z(n_t)$ degeneracy and effectively reduces the dimension of the matrix to $6n_s^3$ but this smaller matrix is dense. We have investigated two methods of finding all the eigenvalues of P^{n_t}: firstly via Lanczos with reorthogonalisation and secondly via LR decomposition.

3.1 Non-Hermitian Lanczos Algorithm

The Lanczos method [42] is an eigenvalue technique which is applicable to large, sparse matrices. The method involves tridiagonalization of the given matrix, A. In general the Lanczos method is most useful when only a few of A's largest or smallest eigenvalues are required since information about A's extremal eigenvalues can often be obtained long before the tridiagonalization is complete. For our application we require all eigenvalues of the matrix P^{n_t} since they are used to obtain the coefficients of the GCPF and we need every coefficient. The main advantage of the Lanczos algorithm for finite density QCD simulations is that it minimises the storage requirements. Although P^{n_t} has many zero elements it is not sufficiently sparse to

make application of sparse matrix algorithms advantageous. Furthermore for our purposes the matrix sparsity decreases as the temporal extent of the lattice (n_t) is increased. Standard eigenvalue routines require storage of the full $6n_s^3 \times 6n_s^3$ matrix. The Lanczos method does not require storage of the full matrix. Rather it requires storage space for only about six Lanczos vectors. A matrix-vector multiplication subroutine is also required. Only the last two Lanczos vectors need be retained after each iteration and the rest can either be discarded or written to disk for subsequent use if calculation of the eigenvectors is required. The principal shortcoming of the Lanczos algorithm is failure induced by roundoff errors. Let A be the matrix whose eigenvalues are required and T be the tridiagonal matrix. We require a set of *Lanczos vectors*, $X = [x_1, x_2, ..., x_n]$. The elements of the tridiagonal matrix are obtained directly by applying a similarity transformation

$$T = X^{-1} A X \tag{3.1}$$

where

$$T = \begin{bmatrix} \alpha_1 & \beta_1 & 0 & 0 & 0 & 0 \\ \beta_1 & \alpha_2 & \beta_2 & 0 & 0 & 0 \\ 0 & \beta_2 & \alpha_3 & \beta_3 & 0 & 0 \\ 0 & 0 & \ddots & \ddots & \ddots & 0 \\ 0 & 0 & 0 & \ddots & \ddots & \beta_{n-1} \\ 0 & 0 & 0 & 0 & \beta_{n-1} & \alpha_n \end{bmatrix} \tag{3.2}$$

3.1.1 Orthogonalisation Vectors

$$\begin{aligned} X^{-1}AX &= T \\ \Rightarrow AX &= XT \end{aligned} \tag{3.3}$$

now

$$\begin{aligned} (AX)^\dagger &= (XT)^\dagger \\ X^\dagger A^\dagger &= T^\dagger X^\dagger \\ (X^\dagger)^{-1} X^\dagger A^\dagger (X^\dagger)^{-1} &= (X^\dagger)^{-1} T^\dagger X^\dagger (X^\dagger)^{-1} \\ A^\dagger (X^\dagger)^{-1} &= (X^\dagger)^{-1} T^\dagger \end{aligned} \tag{3.4}$$

In the special case where the starting matrix A is Hermitian ($A = A^\dagger$) and $T = T^\dagger$ then it follows that

$$\begin{aligned} A(X^\dagger)^{-1} &= (X^\dagger)^{-1} T \\ \Rightarrow (X^\dagger)^{-1} &= X \text{ from Eqn. 3.3} \end{aligned} \tag{3.5}$$

hence $x_i^\dagger x_j = \delta_{ij}$ so that when A is Hermitian we require only a single set of orthogonalisation vectors. However for our application, when $\mu \neq 0$ $P^{n_t} \sim A$ is non-Hermitian and as a consequence $(X^\dagger)^{-1} \neq X$ so we need a second set of orthogonalisation vectors $Y = [y_1, y_2, ..., y_n]$ such that $Y = (X^\dagger)^{-1}$ which satisfy

$$y_i^\dagger x_j = \delta_{ij} \tag{3.6}$$

therefore we now have two relations:

$$AX = XT \tag{3.7}$$

$$A^\dagger Y = YT^\dagger \tag{3.8}$$

Note that since $A \neq A^\dagger$ the $\alpha_i's$ and $\beta_i's$ can be complex.

The Lanczos equations which are used recursively to calculate α_i, β_i and x_i and y_i are obtained by equating columns in $AX = XT$ and $A^\dagger Y = YT^\dagger$ giving

$$Ax_j = \beta_{j-1}x_{j-1} + \alpha_j x_j + \beta_j x_{j+1} \tag{3.9}$$

for $j = 1, 2, ..., (n-1)$ where $\beta_0 q_0 \equiv 0$ and $\beta_n = 0$.

$$A^\dagger y_j = \beta_{j-1}^* y_{j-1} + \alpha_j^* y_j + \beta_j^* y_{j+1} \tag{3.10}$$

Equations 3.6, 3.9 and 3.10 are sufficient to determine all Lanczos vectors and the elements of the tridiagonal form.

The α's come from

$$\alpha_1 = y_1^\dagger A\, x_1 \tag{3.11}$$

The β's are obtained from

$$\begin{aligned} \beta_j x_{j+1} &= Ax_j - \beta_{j-1}x_{j-1} - \alpha_j x_j \equiv \hat{X}_i \\ \beta_j^* y_{j+1} &= A^\dagger y_j - \beta_{j-1}^* y_{j-1} - \alpha_j^* y_j \equiv \hat{Y}_i \end{aligned} \tag{3.12}$$

so that

$$\beta_i^2 = \hat{Y}_i^\dagger \hat{X}_i \tag{3.13}$$

successive Lanczos vectors are obtained recursively from

$$x_{i+1} = \frac{\hat{X}_i}{\beta_i}\ ;\ y_{i+1} = \frac{\hat{Y}_i}{\beta_i^*} \tag{3.14}$$

The stopping condition for an N - dimensional matrix is given by noting that $\beta_N^2 = 0$. If we assume exact arithmetic then the iterative procedure will end when we encounter $\beta_i = 0$ for some $i \leq N$. The algorithm will terminate before the full tridiagonal form has been obtained (for some $i = N - n$) if either we inadvertently

make a bad choice for the starting vectors whereby x_1 (y_1) is orthogonal to n of the right (left) eigenvectors of A or if there is an n-fold degeneracy in the eigenvalue spectrum of A. In a practical implementation of the Lanczos algorithm rounding errors mean that we never obtain a stopping vector β_{N-n} exactly equal to zero because of rounding errors. Rounding errors spoil the relationship in eqn. 3.6 i.e. orthogonality is lost thereby termination is ill-defined and the relationship between $A's$ eigenvalues and those of the tridiagonal form is complicated. To ensure accuracy and reliability of the algorithm we are forced to preserve the global mutual orthogonality of the x's and y's by reorthogonalising each new Lanczos vector against its predecessors. The reorthogonalisation step is

$$\begin{aligned} x_i &\rightarrow x_i - \sum_{j=1}^{i-1} (y_j^\dagger x_i) x_j \\ y_i &\rightarrow y_i - \sum_{j=1}^{i-1} (x_j^\dagger y_i) y_j \end{aligned} \tag{3.15}$$

Unfortunately the computational overhead associated with complete reorthogonalization is large. It is not always necessary to reorthogonalize after every step. In practice we choose x_1 and y_1 at random, say $x_1 = y_1 = \begin{pmatrix} 1 \\ 0 \\ \vdots \\ 0 \end{pmatrix}$ and it follows from the orthogonality condition that $y_i^\dagger x_1 = 0$ for $i \neq 1$ so we monitor this quantity for some $y_i^\dagger$ and if it's value exceeds 10^{-12} then we reorthogonalize. Practical experience tells us that the quantity $y_i^\dagger x_1$ will increase exponentially without reorthogonalization. The choice of starting vector will affect the magnitude of the α's and β's but there is no way of knowing in advance how the algorithm will evolve on the basis of a given choice for the starting vectors.

Once the tridiagonal form, T, has been generated we still have to find the eigenvalues. This is done via a standard QL algorithm with *implicit shifts*.

3.2 COMLR Algorithm

3.2.1 Balancing

Numerical algorithms for nonsymmetric matrices are considerably less reliable than algorithms for symmetric matrices. The possible reasons for this are

1. the matrix itself is defective so there is no complete set of eigenvectors.

2. the eigenvalues are very sensitive to small changes in the matrix elements.

The problems due to *ill-conditioned* matrices have been studied in detail by Wilkinson [43]. It is difficult to determine whether or not a nonsymmetric matrix is ill-conditioned but a good indication of a defective matrix is if two or more of the eigenvectors are almost parallel. It is particularly important for nonsymmetric matrices to minimise the rounding error in order to optimise the accuracy of the eigenvalues. The sensitivity of the algorithms to rounding error can be reduced by a procedure known as **balancing**. It is known that the errors in the eigensystem determined by numerical computation are related to the *Euclidean norm* of the matrix i.e. the square root of the sum of the squares of the matrix elements. Balancing involves using a sequence of similarity transformations to make corresponding rows and columns of the starting matrix have norms which are comparable in magnitude, thus reducing the overall norm of the matrix while leaving the eigenvalues unchanged. The actual algorithm employed uses diagonal matrices to achieve the similarity transformations and instead of summing the squares of matrix elements it sums the absolute magnitudes of the matrix elements. Balancing the norm is equal in effectiveness but superior in efficiency to balancing the Euclidean norm. The Balancing procedure has $O(N^2)$ operations for an $N \times N$ matrix and is inexpensive computationally. It is necessary to keep track of the order of the similarity transformations if the eigenvectors as well as the eigenvalues are required.

3.2.2 Reduction to Hessenberg Form

Prior to performing an iterative procedure to determine the eigenvalues the starting matrix is reduced to a simpler form. Our complex matrix is reduced to upper-Hessenberg form by stabilized elementary similarity transformations. An upper-Hessenberg matrix has zeros everywhere below the diagonal except the first subdiagonal row. For example for a 6×6 matrix looks like:

$$\begin{pmatrix} x & x & x & x & x & x \\ x & x & x & x & x & x \\ 0 & x & x & x & x & x \\ 0 & 0 & x & x & x & x \\ 0 & 0 & 0 & x & x & x \\ 0 & 0 & 0 & 0 & x & x \end{pmatrix} \tag{3.16}$$

The most effective procedure for reducing a matrix to Hessenberg form is analogous to Gaussian elimination with pivoting. The original matrix A is first balanced to

produce the matrix B. Let $B_1 = B$ and prior to entering the **rth stage** of the reduction B_1 has become B_r, which is upper-Hessenberg in its first $(r-1)$ rows and columns. The rth stage involves the following sequence of operations

1. In the rth column below the diagonal find the matrix element which gives the maximum value for the sum of the moduli of its real and imaginary parts. If the maximum value is zero then the rth stage is complete, otherwise denote by $\tilde{r}$ the row containing the above maximum element.

2. Perform the pivoting step by interchanging rows $\tilde{r}$ and $r+1$ then to make the permutation a similarity transformation interchange columns $\tilde{r}$ and $r+1$.

3. Now perform the multiplication stage:- for i=(r+2),(r+3),..,N, compute the multiplication factor

$$f_{i,(r+1)} \equiv \frac{b_{ir}}{b_{(r+1),r}} \tag{3.17}$$

and subtract $f_{i,(r+1)}$ times row (r+1) from row r then add $f_{i,(r+1)}$ times column i to column (r+1) to make the elimination a similarity transform.

A total of $N-2$ stages is required to complete the reduction. This corresponds to an operation count of approximately $5N^3/6$. The Hessenberg reduction stage is the most computationally intensive stage in determining the eigenvalues of our large matrix.

3.2.3 LR reduction

The eigenvalues are obtained from the Hessenberg form, H, by LR decomposition. The basic LR algorithm involves decomposing the starting matrix to a product of a lower triangular matrix, L, (which has non-zero elements only on the diagonal and below) and an upper triangular matrix, R (which has non-zero elements only on the diagonal and above).

$$H = LR \tag{3.18}$$

Then it follows that the matrix K defined by

$$K = L^{-1}HL \tag{3.19}$$

is similar to H and we can obtain a sequence of matrices each of which is similar to the original Hessenberg form H_1 i.e.

$$\begin{aligned} H_s &= L_s R_s \\ R_s L_s &= H_{s+1} \end{aligned} \tag{3.20}$$

It can be shown that if H_1 has roots of distinct moduli then, in general H_s tends to upper triangular form where the diagonal elements tend to the roots arranged *in order of decreasing modulus.* The algorithm is stabilised by using partial pivoting in the triangular factorization of each of the matrices.

H_1 is reduced to upper triangular form R_1 in $(N-1)$ major steps. The rth step involves the following steps

- Interchange rows r and $\tilde{r}$ by premultiplying by the permutation matrix $I_{r,\tilde{r}}$.
- Premultiply by an elementary matrix N_r which serves to annihilate the sub-diagonal elements of the rth column of the transformed matrix. N_r is equal to the identity matrix except for the non-zero sub-diagonal elements occupying the rth column.

Note the $\tilde{r}$ is chosen so that all elements of the elementary matrix N_r are bounded by unity. Thus we have

$$\begin{aligned} R_1 &= N_{(n-1)}I_{(n-1),(n-1)'}....N_2I_{2,2'}N_1I_{1,1'}H_1 \\ H_2 &= R_1I_{1,1'}N_1^{-1}I_{2,2'}N_2^{-1}...I_{(n-1),(n-1)'}N_{(n-1)}^{-1} \end{aligned} \tag{3.21}$$

Since H_1 is upper-Hessenberg, only N^2 complex multiplications are required to produce R_1 and a further N^2 complete the transform. Convergence is accelerated by origin *shifting.* If k is any constant then H-kI has eigenvalues $\lambda_i - k$. Eqns. 3.20 now become

$$\begin{aligned} H_s - k_sI &= L_sR_s \\ R_sL_s + k_sI &= H_{s+1} \end{aligned} \tag{3.22}$$

There is no need to add back the k_sI and we know that H_{s+1} is similar to $H_1 - \sum_{i=1}^{s} k_iI$. A strategy which has proved to be effective is to compute the eigenvalues of the 2×2 submatrix

$$\begin{pmatrix} h^s_{(n-1),(n-1)} & h^s_{(n-1),n} \\ h^s_{n,(n-1)} & h^s_{n,n} \end{pmatrix} \tag{3.23}$$

Then set k_s equal to the eigenvalue closer to $h^s_{n,n}$. It is recommended that the starting matrix H_1 is of upper-Hessenberg form since this means that all If H_1 is upper- Hessenberg then all subsequent H_s will also be upper-Hessenberg and this greatly reduces the computational effort and only the (N-1) sub-diagonal elements need be examined. There are two alternative stopping criteria:-

1. If a sub-diagonal element, $h^s_{(r+1),r}$, is deemed negligible then the eigenvalues of H_s are those of the leading principal minor of order r and the trailing

principal minor of order (N-r). Since our matrix is balanced we can assume that the element is negligible if

$$m(h^s_{(r+1),r}) \leq \epsilon \left[m(h^s_{(r+1),(r+1)}) + m(h^s_{r,r})\right] \tag{3.24}$$

where $m(h)$ is the sum of the moduli of real and imaginary parts of the matrix element h and ϵ is the machine precision.

2. The leading principal sub-matrix also decouples when two consecutive matrix elements are small even though, each individually is not small enough to effect decoupling. In this case the stopping criterion is

$$m(h^s_{(r+1),r})m(h^s_{r,(r-1)}) \leq \epsilon \left[m(h^s_{(r+1),(r+1)}) + m(h^s_{r,r}) + m(h^s_{(r-1),(r-1)})\right] \tag{3.25}$$

If the number of iterations required for any one root reaches 10 or 20 then and exceptional shift is used to promote convergence.

3.2.4 Method Comparison

The Lanczos method requires only half the storage of the LR reduction method and is more efficient for use on lattices of 6^4 and smaller. However the Lanczos method fails to find all eigenvalues on 8^4 lattices with the most likely explanation being accumulation of rounding errors. However the LR reduction method did prove to be successful on 8^4 lattices and in principle should be effective on larger lattices also. The LR algorithm has the additional advantage that it can be terminated after only half of the eigenvalues have been found since the eigenvalues emerge in order of decreasing modulus therefore the λ, $\frac{1}{\lambda^*}$ symmetry can be exploited. Improvements in performance of the LR algorithm are possible if a machine-specific optimised implementation of the BLAS (basic linear algebra subroutines) is available. Routines for balancing , reduction to upper- Hessenberg form and LR decomposition for a complex general matrix are available in the EISPACK and LAPACK numerical analysis software packages.

3.3 Lee-Yang Zeros

Our motivation in performing a grand canonical partition function expansion for finite density QCD is to learn about the phase structure of the theory. In nature phase transitions are manifested by singularities in the thermodynamic functions such as the magnetization in a ferromagnet or the pressure in a liquid-gas system.

Since we expect the partition function to be an analytic function of its arguments it is not immediately obvious how such singularities arise. In fact the singularities associated with phase transitions only emerge as we approach the thermodynamic limit (infinite volume for a fixed particle density) because it is known that the limit function of a sequence of analytic functions need not be analytic. Macroscopic bodies are indeed close to the idealized thermodynamic limit.

By studying the zeros of the GCPF we can visualize its properties and learn much about the occurrence of singularities in the thermodynamic limit. The landmark study of partition function zeros was performed by Lee and Yang [44, 45] who studied a simple statistical system of a lattice gas with attractive interactions (Ising ferromagnetic system). The Lee-Yang circle theorem states that for this particular system the roots of the partition function lie on a circle in the activity plane (e^{-2h} where h is the magnetic field). The magnetic field in this model is analogous to the chemical potential in finite density QCD.

Consider a (quantum mechanical) system of particles with hard cores occupying a finite volume V [46]. The particles will generally interact via some kind of potential. A finite volume can accommodate a maximum number of particles n_{max} and if for example the particles interact via a pairwise potential when n exceeds n_{max} so that two of them touch the free energy will become infinite and the partition function will vanish.

The grand canonical partition function comprises a sum of terms

$$Z(e^{\mu/T}, V) = 1 + c_1(V)e^{\mu/T} + c_2(V)e^{2\mu/T} + ... + c_{n_{max}}(V)e^{n_{max}\mu/T} \qquad (3.26)$$

corresponding to canonical partition functions and the coefficients c_n reflect the relative probability that the system will be in a state with n particles. If the expansion coefficients are to be interpreted as probabilities then in order to be physical they *must be real and positive.* Since all the expansion coefficients, c_n are positive the polynomial can have **no real positive roots**. We can however observe negative roots which are unphysical and, of course, complex roots. Yang and Lee showed that phase transitions are controlled by the distribution of roots of the GCPF in the complex fugacity ($e^{\mu/T}$) plane. *A phase transition occurs whenever a root approaches the real axis in the limit* $V \to \infty$.

Consider the parametric form of the equation of state in the infinite volume limit and let $z = e^{\mu/T}$

$$\frac{P}{kT} = \lim_{V\to\infty} V^{-1} \ln Z(z, V)$$

$$\frac{1}{v} = \lim_{V\to\infty} V^{-1} z \frac{\partial}{\partial z} \ln Z(z,V) \tag{3.27}$$

Then the Lee-Yang theorems can be stated as follows

- **THEOREM 1** The following limit exists for all $z > 0$

$$F_\infty(z) \equiv \lim_{V\to\infty} \frac{1}{V} \ln Z(z,V) \tag{3.28}$$

  This function is a continuous non-decreasing function of z.

- **THEOREM 2**

  If **R** is a region in the complex z plane that includes a segment of the positive real axis and contains *no roots* of the GCPF then in this region $V^{-1} \log Z(z,V)$ will converge uniformly to its limit as $V \to \infty$ and this limit is analytic for all z in **R**.

As a result of the second theorem it follows that in any region **R** the order of the partial derivative and the limit in eqn. 3.27 can be interchanged so that

$$\begin{aligned} \frac{P(z)}{kT} &= F_\infty(z) \\ \frac{1}{v(z)} &= z\frac{\partial}{\partial z} F_\infty(z) \end{aligned} \tag{3.29}$$

If region **R** includes the entire positive z axis then the system always exists in a single phase. However if a zero of the GCPF approaches a point, z_o on the real positive z axis then the system will have two phases : one in the region $z < z_o$ and one in the region $z > z_o$. P(z) must be continuous according to Theorem 1 but a discontinuity in $\partial P/\partial z$ would correspond to a first order phase transition while a discontinuity in $\partial^2 P/\partial z^2$ would indicate a second order phase transition.

Of course in practical lattice calculations we are not close to the thermodynamic limit $V \to \infty$ but as the lattice volume is increased, in general we expect the zero with the smallest imaginary part to approach the real axis. It will move towards a value on the real axis corresponding to the critical value. The finite volume scaling behaviour of this lowest zero can be used to determine the order of the phase transition. In a physically meaningful system which has positive GCPF expansion coefficients we do not expect any of the zeros to lie on the positive real axis. The coefficients will all be positive once the statistical average is complete. In our finite density simulations negative coefficients can arise due to limited statistics which can give rise to zeros on the real axis but these are spurious and must disappear in the limit of infinite statistics.

According to Itzykson et. al. [47] the occurrence of complex zeros that eventually stabilize along lines (or regions) on the complex plane does not in general indicate singularities in the thermodynamic quantities. They should in fact be interpreted as Stokes lines which separate different asymptotic behaviours of the partition function in the thermodynamic limit. They provided numerical evidence that along these lines of zeros the real part of the analytic continuation of the free energy will be continuous while the discontinuity in the imaginary part will be proportional to the density of the zeros.

Chapter 4

Lattice QCD at Strong Coupling

4.1 Motivation

The strong coupling limit of QCD provides us with an important testing ground for lattice Monte-Carlo simulations at finite density. Although we are ultimately interested in the weak coupling, continuum limit, the strong coupling limit is attractive for several reasons:

- the theory confines and spontaneously breaks chiral symmetry
- numerical results from monomer-dimer simulations are available
- analytic results from the strong coupling expansion and from mean field theory are available

No such analytic predictions are available in the scaling region (i.e. at intermediate coupling).

At infinite coupling the mean-field method predicts a *first order* transition at chemical potential μ_{mf} where

$$\mu_{mf} = \frac{1}{r}\sinh^{-1}(\lambda_0 r) - \frac{{\lambda_0}^2}{(d-1)r} \tag{4.1}$$

and

$$\lambda_0 = \frac{1}{r\sqrt{2}}\left(\sqrt{1+(d-1)^2 r^4} - 1\right)^{1/2} \tag{4.2}$$

for a lattice with d space-time dimensions where $r = n_t/n_s$.

m	$m_\pi/2$	$m_B/3$	μ_{mf}
0.06	0.29	1.01	0.59
0.12	0.41	1.03	0.63
0.32	0.66	1.10	0.75
0.52	0.84	1.17	0.87
0.72	0.98	1.24	0.97
0.92	1.10	1.31	1.07
1.02	1.16	1.34	1.11
1.50	1.39	1.50	1.30

Table 4.1: Comparison of mean-field predictions at infinite coupling for one half the pion mass (from Eqn. 4.4), one third of the baryon mass (from Eqn. 4.3) and the critical chemical potential (from Eqn. 4.1) for a range of bare quark masses.

The mean-field baryon and pion masses are given by [31]

$$m_B = \ln\left[\frac{1}{2}c^3 + \sqrt{1+\frac{1}{8}c^6}\right] \tag{4.3}$$

$$m_\pi = \ln\left[1+\frac{1}{2}(c^2-2d) + \sqrt{(c^2-2d)+\frac{1}{4}(c^2-2d)^2}\right] \tag{4.4}$$

where

$$c = (m+\sqrt{2d+m^2}) \tag{4.5}$$

The corresponding thresholds for a range of bare quark masses are listed in table 4.1. Note that μ_{mf} does not coincide with the mean-field baryon threshold $m_B/3$.

It has been argued that the discrepancy is related to the binding energy of nuclear matter which is large at infinite coupling. Bilic et al. [48] demonstrated explicitly that $1/g^2$ corrections diminish the discrepancy between μ_{mf} and the mass of the lightest baryonic state divided by N_c (the number of colours). Their results are summarised in table 4.2

Note also that mean-field pion threshold ($m_\pi/2$) and μ_{mf} are not well separated for bare quark masses $ma > 0.5$.

$6/g^2$	$m_b a/3$	$\bar{\mu} a$
0	0.972	0.571
1	0.936	0.586
3	0.850	0.617
5	0.735	0.648

Table 4.2: Strong coupling nucleon mass divided by N_c and the mean-field prediction for the transition value of the chemical potential versus the inverse gauge coupling squared. Table taken from Bilic et. al. [48] whose calculations involved finding a numerical solution to the mean-field equation for a $1/g^2$ corrected model of $SU(3)$ gauge theory with Kogut-Susskind fermions in the chiral limit ($m \to 0$).

4.2 Alternative Simulation Methods at Strong Coupling

In addition to the simulations using the Glasgow method which will be described in detail in this chapter, Gocksch [36, 40] and Karsch and Mütter [49] have developed methods to simulate finite density QCD and have measured the chiral condensate and the fermion number density at strong coupling ($\beta = 0$). Both of these methods gave results for μ_c as a function of the bare quark mass which were consistent with mean-field predictions (Eqn. 4.1). Gocksch used a *spectral density method* on a 2^4 lattice only. Extension of the spectral density method to larger lattices was not feasible. The Glasgow algorithm also gives $\mu_c \simeq \mu_{mf}$ on a 2^4 lattice but not on larger lattices. Karsch and Mütter applied a method where the GCPF is represented in terms of monomers, dimers and baryonic loops in which the dominant contributions to the partition function have positive weights. Their simulations were performed on an $8^3 4$ lattice. This method is only applicable at strong coupling and would have to be adapted in order to explore smaller bare quark masses $ma < 0.1$.

4.2.1 The Spectral Density Method

Gocksch applied a general method for simulating systems with a complex action , the "spectral density method", to $SU(3)$ lattice QCD at finite density and infinite gauge coupling. This method involves binning the phase of the determinant, θ, and measuring the density of states. He studied the form of the density of states as a function of energy for different values of chemical potential and concluded

that outside the critical region the density of states is sharply peaked at $\theta(U) = 0$ therefore the phase is not important, however for $\mu \sim \mu_c$ the density of states is flat and there is an contribution from $\theta(U)$ at **all points** in the integration region so that the phase of the determinant must be accounted for. To illustrate the method, consider an observable such as the chiral condensate given by the expectation value of some operator, O:

$$\langle O[U] \rangle = \frac{1}{Z} \int [DU]\, O(U)\, |\det M(U)|\, e^{\beta S_G + i\theta(U)} \tag{4.6}$$

where β is the inverse gauge coupling, S_G is the standard Wilson gauge action and $\theta(U)$ **is the phase of the determinant** of the fermion matrix, M(U). The expectation value can be re-expressed as:

$$\langle O[U] \rangle = \frac{\int_{-\pi}^{\pi} \langle O[U] \rangle\, dE\, \langle O \rangle_M\, \rho(E)\, e^{iE}}{\int_{-\pi}^{\pi} dE \rho(E)\, e^{iE}} \tag{4.7}$$

where we have introduced the **density of states,** $\rho(E)$, a periodic function of E with period 2π defined by

$$\rho(E) = \int [DU]\, \delta_P(\theta(U) - E)\, |\det M(U)|\, e^{\beta S_G} \tag{4.8}$$

where δ_P is a periodic delta function and $\langle O \rangle_M$ is the microcanonical average of the operator, O , defined by

$$\langle O \rangle_M (E) = \frac{1}{\rho(E)} \int [DU]\, O(U)\, \delta_P(\theta(U) - E)\, |\det M(U)|\, e^{\beta S_G} \tag{4.9}$$

Equation 4.7 is evaluated as a Riemann sum. The interval $[-E_{min}, E_{max}]$ is divided into overlapping sets with a given number of bins in each. This is essentially binning the phase $\theta(U)$. The density of states $\rho(E)$ is measured by considering the relative normalizations of adjacent sets using counts in the overlap bins. High statistics is required in each bin. In this method the Boltzman weight used in generation of configurations incorporates the modulus of the determinant

$$P(U)[DU] \sim |\det M(U)|\, e^{S_G} [DU] \tag{4.10}$$

and a Monte-Carlo procedure is performed in each set so that each value of the phase of the determinant is sampled separately and the contributions are added up coherently. This is most important in the critical region where the density of states is flat. In this region it is clear that simpler approaches, where we "*quench the phase*" by measuring the phase as part of the operator, will fail because of wild fluctuations in phase from configuration to configuration. This was discussed in Chapter 2. Application of the spectral density method to lattices larger than 2^4

would, unfortunately, be impractical because the method is too computationally intensive. We do however learn from the diagnostics of the simulations on the 2^4 lattices.

4.2.2 The Monomer-Dimer Algorithm

Simulations [49] using the monomer-dimer algorithm whereby the partition function is represented graphically in terms of monomers, dimers and baryonic loops estimate a critical chemical potential, μ_c which is in agreement with μ_{mf}. The partition function of a system of quarks and gluons in the infinite coupling limit is given by

$$Z = \int d\bar{\psi}\, d\psi \int dU\, e^{S_F} \tag{4.11}$$

where $\bar{\psi}$ and ψ denote the quark fields and U, the SU(3) gluon field. In the absence of the gluonic part of the action, e^{S_G}, it is possible to perform analytically the integrals over the SU(3) link variables. This is **only possible at infinite gauge coupling**. Starting with the standard lattice QCD action with four flavours of staggered fermions and performing the link integral we get

$$Z = \int d\bar{\psi}\, d\psi \, \exp\left[2ma \sum_x M(x)\right] \prod_{\langle xy \rangle} F(x,y) \tag{4.12}$$

where M(x) are associated with meson fields and F(x,y) contains dimer operators associated with M(x)M(y) and baryon-antibaryon fields. Non-vanishing contributions to the integrals over quark fields are obtained only if each site x of the lattice is occupied either by three mesons or by a baryon-antibaryon pair. The partition function can be written as a sum over monomer-dimer loop configurations K

$$Z = \sum_K w_K \tag{4.13}$$

The statistical weight, w_K, of a configuration is essentially controlled by $(ma)^{N_M}$ where N_M is the number of monomers. The baryonic loops which have troublesome **oscillating weights** are each replaced by two pure monomer-dimer configurations which are denoted "polymers". The Boltzmann weights in the new monomer-dimer-polymer system are non-negative for $\mu = 0$ and for $\mu > 0$ configurations *can* have negative weights (when certain dimers create an odd number of polymers along negative Polyakov loops) however it is argued that the *dominant contributions* arise from configurations with only positive weights. The important point is that the leading contribution at $\mu \neq 0$ comes from loops of minimal length ie. Polyakov loops of length equal to the number of sites on the lattice in the time direction.

The performance of the algorithm is expected to deteriorate as the lattice size is increased. Since the gauge fields have been integrated out exactly the fluctuations have been greatly diminished. The observables such as chiral condensate, fermion number density and energy density can be studied at fixed baryon number. Since a separate simulation is required at each value of the chemical potential it is not possible to obtain continuous curves for the observables as we do in standard hybrid Monte-Carlo techniques. The algorithm is unsuitable for simulating at small bare quark masses ($ma < 0.1$) because the update scheme means that acceptance rate is proportional to $(ma)^2$ which is clearly very small for small quark masses. The hybrid Monte-Carlo simulations allow us to push further towards the chiral limit ($ma \to 0$) and a typical bare quark mass would be $ma = 0.01$. The monomer-dimer algorithm is only applicable at infinite coupling since it relies on the analytic evaluation of the gauge fields. Note that **confinement is enforced exactly** in this model. Monomer-dimer simulations on 4^4 and 8^34 lattices predict a first order transition at a chemical potential consistent with the mean-field prediction. The fermion number density jumps from a tiny value to almost the saturation value at μ_c. The chiral condensate remains at its $\mu = 0$ value right up until μ_c where it crashes to zero.

4.2.3 Strong Coupling using the Glasgow Method

Consider again the expression for the GCPF

$$Z = \sum_{n=-3n_s{}^3}^{3n_s{}^3} e^{-(\epsilon_n - n\mu)/T} \tag{4.14}$$

The zeros of this polynomial are the Lee-Yang zeros of Z in the complex fugacity plane (or equivalently the complex e^μ plane). As we shall see, in the dynamical theory these zeros play a role analogous to that of the eigenvalues of P in the quenched theory when calculating the number density.

The fermionic determinant can be expressed explicitly as a function of μ by

$$\det(M(\mu, m)) = e^{-3\mu n_s^3 n_t} \det(P - e^\mu) \tag{4.15}$$

As before the lattice size is $n_s^3 n_t$ and P is the propagator matrix (independent of μ)[35]. We can compute $\det(M(\mu, m)$ in a basis where the propagator matrix is diagonal

$$\det(M(\mu, m)) = e^{-3\mu n_s^3 n_t} \prod_{k=1}^{6n_s^3 n_t} (\lambda_k - e^\mu) \tag{4.16}$$

We recognize that the zeros of the determinant in the e^{μ} plane are the eigenvalues of the propagator matrix. The symmetry of the eigenvalues of the propagator matrix $\lambda_{k+j} = e^{i2\pi j/n_t}\lambda_k$ for $j = 0$ to $n_t - 1$, together with the polynomial decomposition

$$\prod_{j=0}^{n_t-1}(e^{i2\pi j/n_t}\beta - x) = (\beta^{n_t} - x^{n_t}) \tag{4.17}$$

yields the equivalent representation

$$\det(M(\mu, m)) = e^{-3\mu n_s^3 n_t}\prod_{k=1}^{6n_s^3}(\lambda_k^{n_t} - e^{\mu n_t}) \tag{4.18}$$

and dictates the general structure of the characteristic polynomial $\det(M(\mu, m))$

$$\det(M(\mu, m)) = \sum_{k=-3n_s^3}^{3n_s^3} b_i e^{k\mu n_t} \tag{4.19}$$

Note the dependence on μ is now via the fugacity $f = e^{\mu n_t}$.

Hence, measurement of the average of the characteristic polynomials (normalised by $|M(0,m)|$) in the ensemble generated at update mass m and $\mu = 0$ will give $Z(\mu, m)$ explicitly as a function of μ at that mass.

This representation leads to a polynomial expansion of $Z(\mu)$ in powers of the fugacity whose coefficients are functions of the gluonic fields.

$$Z(\mu) = \sum_{k=-3n_s^3}^{3n_s^3} < b_i > e^{k\mu T} = \sum_{k=-3n_s^3}^{3n_s^3} Z_k f^k \tag{4.20}$$

This expansion is just that of the GCPF expanded in terms of the canonical partition functions, (CPF's), for a fixed number of quarks (anti-quarks) on the lattice. Thermodynamical averages, which can be calculated as logarithmic derivatives of the GCPF, are then given explicitly as functions of μ.

The relative value of the CPFs can also characterise the properties of the system. For example, the relative weight of the triality–bearing to the triality–zero CPFs can signal whether the system is in the confined or deconfined phase. In the confined phase the ensemble average of the triality–bearing CPFs must be zero. This leads to

$$Z(\mu) = \sum_{k=n_s^3}^{n_s^3} Z_{3k} f^{3k} \tag{4.21}$$

One can also explore the phase structure of the simulated system by examining the distribution of the zeros of the GCPF in the complex chemical potential (or fugacity) plane [44, 45] [47]. These zeros correspond to the singularities of the thermodynamic potential and will converge in the thermodynamic limit, $(L \to \infty)$ towards any critical μ in the physical domain.

In the following we also show that one can regard the zeros of the averaged characteristic polynomial as the "proper" ensemble average of the eigenvalues of the propagator matrix. This interpretation of the zeros as reflecting the ensemble average of the eigenvalues could be important in the explanation for the "unexpected" onset chemical potential in ensembles of limited statistics.

4.2.4 Observables

The starting point of our analysis is the GCPF Z computed with the Glasgow algorithm. Our raw data are the CPF's Z_n and our basic observables are the particle number density and the zeros of the GCPF in the complex fugacity plane.

Most of our discussions will consider the quark number density, defined as

$$\langle n_q(\mu,m)\rangle = \frac{1}{V}\frac{\partial \ln(Z(\mu,m))}{\partial\mu} = \frac{1}{V}\frac{\partial \ln < \det(M(\mu,m)) >}{\partial\mu} \tag{4.22}$$

Singular behaviour of the current can result from singularities in the density of baryonic states (particularly apparent in the zero-temperature limit). These singularities could be purely lattice artefacts and vanish in the continuum limit. However, they may instead reflect continuum spectral features, such as gaps in the spectrum or abrupt changes in the dispersion relation of the baryonic excitations. A chiral phase transition is one such possibility. A spectrum of chirally symmetric baryonic excitations will follow a gapless relativistic dispersion relation, contrary to the dispersion of particles with broken chiral symmetry. If the disappearance of the mass gap occurs together with the deconfinement transition, quark states will emerge instead of collective colourless baryonic excitations. Thus, the μ–dependence of n_q should determine the phase structure of dense baryonic matter, an alternative to the evaluation of the chiral condensate.

Differentiating the action with respect to μ reveals the operator form of the charge, and one sees that the current is the expectation value of the number of paths through the links in the time direction [6]. In this sense the current can be defined on isolated configurations, where it reduces to

$$n_q^i(\mu,m) = \frac{1}{V}\frac{\partial \ln(\det(M(\mu,m)))}{\partial\mu} \tag{4.23}$$

In the quenched ensemble $\ln(\det(M))$ is differentiated **before** taking the statistical average:

$$< n_q >^{quen.}(\mu,m) = \frac{1}{V}\left\langle \frac{\partial \ln(\det(M(\mu,m)))}{\partial\mu} \right\rangle \tag{4.24}$$

and we recognize that

$$< n_q(\mu,m) >^{quen.} = < n_q^i(\mu,m) > \tag{4.25}$$

In the following the μ and m dependence will be left implicit wherever this does not create ambiguities.

4.2.5 Failures on isolated configurations, and the quenched model

The early work by Gibbs [35] made it clear that the behaviour of some observables measured on isolated configurations at finite density can be pathological. Since the analysis of isolated configurations is a necessary step in any lattice simulation, the impact of his result may be broader that its original motivation which was to understand the pathologies of the quenched approximation.

Our renewed interest was prompted by two considerations. First, our results presented below show clear relics of the quenched pathologies discussed in Gibbs's paper : the onset μ_o where the number density n_q departs from zero is at half the pion mass. Second, published results on four fermion models [2] do not have such pathologies. However, both models share the same pattern of chiral symmetry breaking, and both models have Goldstone modes. Why, then, is there a difference at finite density? We decided to re–examine the behaviour of observables on isolated configurations in order to test the Gibbs scenario in a more general framework, and to gain some understanding of the process of statistical averaging in the two models.

First consider the behaviour of the quark number density on isolated configurations. The following expression for n_q^i follows from Eqns. 4.23, 4.16

$$n_q^i = -1 + \frac{1}{V} \sum_{i=1}^{6V} \frac{z}{(z - \lambda_i)} \tag{4.26}$$

(here and in the following we use Gibbs' notation $z = e^{\mu}$ [35]). In the zero temperature case the sum over complex poles can be conveniently done by contour integration, yielding:

$$n_q^i = \frac{1}{V} \sum_{1<|\lambda_i|<e^{\mu}} 1. \tag{4.27}$$

The threshold for the current n_q on isolated configurations is triggered by the lowest zero of the determinant. In turn, the zeros of the determinant are given by the eigenvalues of the propagator matrix.

From an analytical study of the eigenvalues of the fermionic propagator matrix in the **quenched theory**, Gibbs [35] concluded that the eigenmodes of the propagator matrix relate to the mass spectrum of the theory. The Gibbs argument requires the calculation of the hadronic spectrum on replicated lattices, i.e. lattices, with periodic boundary conditions on the gauge fields, which have been strung together d

times in the time direction. He considered the limit $d \to \infty$ in order to replace finite sums with contour integrations. The procedure is justifiable at zero temperature. The expression obtained for the inverse of the duplicated fermion matrix $G(t_1, t_2)$ is

$$G(t_1, t_2) = \sum A_a \lambda_a^{t_1 - t_2} \tag{4.28}$$

where A_a are the amplitudes (which can be related to the eigenvectors of the propagator matrix) and λ_a are the associated eigenvalues. The form of the inverse shows that the exponential decay at large separation is controlled by the eigenvalues λ_a hence we see that the eigenvalue spectrum calculated on isolated configurations should contain poles in correspondence to the physical masses. In particular, the smallest mass state can clearly be extracted from the lowest eigenvalues. This state is obtained by the squaring the propagator matrix, and defines the pion mass in QCD. The smallest mass state m_π is related to the lowest eigenvalue by:

$$m_\pi = 2 \ln |\lambda_{\min}| \tag{4.29}$$

This identification was clear in simulations done by Gibbs because the pion propagator was very similar configuration by configuration although, strictly speaking, masses are properties only of the statistical ensemble.

Gibbs argument has been reformulated and verified by Davies and Klepfish [34]. Pathologies of isolated configurations, the role of confinement and other issues, are also discussed in [32], [33]. All of these works confirm that on isolated configurations there is a singularity at a value of the chemical potential close to half the pion mass. This implies that in the quenched theory $\langle \bar{\psi} \psi \rangle$ is controlled by the *pion mass.* This was Gibbs's explanation for the quenched pathologies whereby the discontinuities in the chiral condensate and fermion number density were apparently associated with the pion. The eigenvalues in the quenched theory are analogous to the zeros in the dynamical theory which are obtained from the *averaged* characteristic polynomial where the coefficients on isolated configurations are a particular set of propagator matrix eigenvalues. Since on *one configuration* the eigenvalues (associated with particle masses) are formally equivalent to the zeros of the partition function in the statistical ensemble, it is conceivable that in a dynamical simulation with limited statistics we retain a remnant of "fake" critical points triggered by the masses in the QCD spectrum.

Therefore, the results on isolated configurations are qualitatively different from those expected of the statistical ensemble.

Some of the problems with the quenched model can be understood from Eqn.

4.25 :- the quenched number density is a simple average of the single-configuration number density estimate, and the quenched ensemble retains the pathological features observed on isolated configurations.

4.2.6 The statistical ensemble, and the full model

We can now focus on the interplay between the one configuration/quenched results and ensemble results. How can statistical averaging remove the problems observed on isolated configurations? Equivalently, how can the Glasgow averaging discussed above improve upon the quenched approximation?

Consider the fugacity expansion for Z, (Eqn. 4.20). By reinstating a factor $e^{3n_s^3 n_t \mu}$ we see that Z is a polynomial of degree $6n_s^3 n_t = 6V$ in the variable $z = e^{\mu}$. Z can then be written in terms of its zeros α_i in the z plane

$$Z = e^{3V\mu} \prod_{i=1}^{6V} (z - \alpha_i). \tag{4.30}$$

Recall that $Z = \langle det(M) \rangle$ and compare formulae 4.30 and 4.16 which we rewrite here

$$\det M = e^{3V\mu} \prod_{i=1}^{6V} (z - \lambda_i) \tag{4.31}$$

We see that the zeros of the partition function are the "proper" ensemble average of the eigenvalues of the fermionic propagator matrix, or, equivalently, of the zeros of the determinant.

Manipulations analogous to those of Eqns. 4.26 and 4.27 lead to the current

$$n_q = \frac{1}{V} \sum_{1<|\alpha_i|<e^{\mu}} 1. \tag{4.32}$$

Let's search for other critical points past the first onset. From Eqn. 4.32 we see that discontinuities in n_q are associated with a high density of zeros on circles with radius e^{μ_c} in the fugacity plane. More generally, the density of the moduli of zeros in the e^{μ} plane is the derivative of n_q with respect to μ, i.e. the quark number susceptibility. Interestingly, the relevant quantities controlling the critical behaviour of the current are indeed the moduli of the complex zeros. Clearly, discontinuities in n_q must be associated with a "high" density of zeros on circles with radius e^{μ_c}.

We would like to understand how the eigenvalues and the zeros are related. One obvious constraint on the distribution of the zeros is that in the confined sector we expect to see a $Z(3)$ symmetry arising from the triality non-zero coefficients averaging to zero so that only canonical partition functions containing multiples of

three quarks contribute to the thermodynamics. It is worth noticing that once the $Z3$ symmetry is enforced (Eqn. 4.21)

$$Z = e^{3n_s^3\mu} \prod_{i=1}^{2V} (z^3 - \beta_i). \tag{4.33}$$

The zeros in the complex plane z should then come in triplets, corresponding to cubic roots of certain complex numbers β_i. ***In principle*** (in practice things can be very different!) the effect of the $Z3$ symmetry can simply amount to a redistribution of phases with no effect on the moduli. That would not affect the critical behaviour, since the critical behaviour is triggered by the moduli themselves. The unphysical quenched onsets could certainly survive the $Z3$ symmetry of the full ensemble.

The zeros of the partition function drive the critical behaviour of the full model as the zeros of the determinant drive the critical behaviour of isolated configurations, hence of the quenched model. In the process of going from the zeros of the determinant to the zeros of the grand canonical partition function, the pathological results observed on isolated configurations should turn into the physics of the full model : the fake critical points should disappear, the real phase transitions of the full model should emerge. This must be achieved by correct **averaging** of the characteristic polynomial.

4.3 Simulation Results and Observables

As described in detail in Chapter 2 the Glasgow method provides us with the fugacity expansion of the Grand Canonical Partition Function.

$$Z = \sum b_n e^{\mu n/T} \tag{4.34}$$

Once Z is known, in principle one can compute all thermodynamical observables. In practice, we will focus our discussion on the number density n_q, and on the analysis of the complex zeros of Z in the e^{μ} plane.

The advantage of the Glasgow method lies in the fact that the configurations can be generated at zero chemical potential. In general we measure $Z = \left\langle \frac{detM(\mu)}{detM(\mu=0)} \right\rangle_{\mu=0}$ in which case the probability measure is $detM(\mu = 0)e^{-s_G}$. This is referred to as a **reweighting procedure**. At infinite gauge coupling $\beta = 0$ hence e^{-s_G} can be replaced by the identity and we can generate configurations either with the usual hybrid MonteCarlo procedure or alternatively choosing **random** SU(3) matrices. This is a convenient strategy since at infinite coupling the gauge action does not appear in the probability measure. Choosing random gauge fields corresponds to

different normalization for the partition function:

$$Z = \frac{\int [dU] \det M(\mu)}{\int [dU]} \tag{4.35}$$

A series of preliminary runs were performed on a 4^4 lattice to confirm that the results were independent of the algorithm chosen for the generation of the configuration. We finally selected a **random generation** procedure which produces decorrelated configurations.

We will present results on a 6^4 lattice for bare quark masses (ma) in the range 0.05 to 1.5 and on an 8^4 lattice for masses 0.08 and 0.1. The number of gauge field configurations analyzed varied from a small sample of 25 on the 8^4 lattice with $m_q = 0.08$, around 100 configurations on an 8^4 lattice with $m_q = 0.1$, and several hundred configurations on the 6^4 lattices.

In every case our raw data, i.e. the starting point of our analysis, are the coefficients, b_n, of the fugacity expansion (Eqn. 4.34).

4.3.1 The number density

The first simulations which calculated the number density with the fugacity expansions were performed by Barbour Davies and Sabeur on a 2^4 lattice [50]. Their results showed that the reweighting actually works on a 2^4 lattice – the onset in the number density moves gradually from zero to a value consistent with $m_p/3$ as statistics are increased. We reproduced these results as a first step in our study and proceeded to extend the simulations to a 6^4 lattice. The effectiveness of the reweighting proceedure demands higher statistics on larger lattices.

We first studied $m_q = 0.1$ where we can compare the results with the ones obtained in the quenched simulations, with the monomer–dimer simulation, and with the analytic results of the strong coupling expansions. Let's briefly review these results.

For $ma = 0.1$ the monomer dimer simulations [49] show a sharp transition at $\mu_c a = 0.69(\pm 0.015)$ which is consistent with the mean-field predictions.

The associated critical baryon-number density at the transition point is $n_c a^3 = 0.045(\pm 0.005)$ The strong coupling expansion predicts a strong first order transition at $\mu \simeq 0.65$. The small difference in μ_c could be probably accounted for by 1/d corrections.

In the strong coupling expansion there is however another feature which is not seen in the monomer dimer results: a *mixed phase* for $\mu_o < \mu < \mu_s$ where ordinary confined hadronic matter coexists with the saturated lattice phase.

The quenched results [32, 33] were characterized by a "forbidden region" ranging from $\mu_o = m_\pi/2 = 0.32$ to $\mu_s \simeq m_B/3 \simeq 1$.

μ_o and μ_s are close to the extrema of the *mixed phase* predicted by the strong coupling expansions mentioned above. In the hybrid Monte-Carlo quenched simulations there is **no remnant** of the critical point for the chiral symmetry restoration at $\mu_c \simeq 0.65$ predicted by the strong coupling expansion.

Our hope in doing the 6^4 calculations, was, of course, to see something completely different from the quenched calculations and very similar to the monomer-dimer results.

These expectations are only partially realized by the results. We do see a definite signature emerging for μ_c however the presence of the early onset μ_o is a *persistent feature* of the unquenched hybrid Monte Carlo simulation results. The baryon number density associated with μ_c in our simulations corresponds to approximately half the lattice fermion-saturation density i.e. $n_c a^3 \simeq 0.5$. This is inconsistent with the results of the monomer-dimer algorithm.

We first consider, in the light of the above discussion concerning the roles of the eigenvalues and the zeros of the GCPF, their distributions in the complex μ and e^μ planes. By contrasting the zeros of the GCPF with the poles of the determinant we can study the effect of the **Glasgow** *reweighting procedure.*

We can substantiate this interpretation of μ_c by examining the zeros of the grand partition function in the complex plane e^μ.

The numerical strategy suggested by the discussion leading to Eqn. 4.32 is straightforward: observe the distribution of the moduli of the zeros, or, equivalently, search for a strip of high densitiy in the e^μ plane. This criterion is numerically more convenient than the conventional Lee–Yang analysis, which only uses the zero whose imaginary part is closest to the real axis. It is also very natural since it says that the number density counts the density of states in the fermionic sector.

Fig. 4.1 shows a histogram of the distribution of the positive real parts of the eigenvalues in the complex μ plane. The distribution is obtained from configurations on an 8^4 lattice at a bare quark mass of 0.1. There is a clear signal that the number density becomes non-zero at $\mu \approx 0.3$ which is consistent with $m_\pi/2$. This is the quenched onset μ. The lattice is filled at $\mu = 0.95$.

The analogous distribution of the zeros of the GCPF is also shown in Fig 4.1. These zeros are those of the polynomial obtained by averaging the characteristic polynomials of the propagator matrix over the same 450 configurations. There is still a clear signal that the number density becomes non-zero at the same onset μ as that

of the quenched theory, however, a strong signal has developed via an intermediate peak in the distribution which is absent from that of the eigenvalues. As argued above, this band of increased density can be associated with a discontinuity in the number density. The fact that no further critical point was observed in the quenched calculations can be directly attributed to the **flat** eigenvalue distribution. The signal at μ_c in the zeros is entirely due to the Glasgow reweighting.

This difference in distribution between the eigenvalues and the zeros is found at all other bare quark masses. Fig. 4.2 shows our results at quark mass $m = 0.05$ while Fig. 4.3 shows results at $m = 0.08$.

Simulations at small bare masses are essential in order to explore the chiral limit. There, we expect the critical point to remain fairly constant and different from zero. For $ma < 0.5$, μ_{mf} and $m_{\pi/2}$ are well separated (see equations 4.1 and 4.4) hence we can distinguish μ_o from μ_{mf} for small masses. Large bare masses were used to investigate the scaling of the peak that we associate with μ_c in the zeros histograms. We insist that this peak should move in correspondence with Eqn. 4.1. The motion of the peak is more pronounced at larger bare quark masses. Simulation results for all bare quark masses were found to be in excellent agreement with Eqn. 4.1. For the larger masses the central peak shifts and broadens which is probably due to the fact that at large quark mass the transition is washed out. Interestingly, the current onset at larger quark mass is, apparently, smaller than half the pion mass – a surprisingly result since at $m_q = 1.5$ in the quenched model the critical region shrinks to zero – certainly this adds to the complication and the confusion associated with μ_o. However, even if the interpretation of the critical region at this stage is largely subjective, the estimate of the critical point μ_c seems reasonably sound.

Fig. 4.4 gives an overview of the location of μ_o and μ_c for six quark masses in the range $ma = 0.05$ to 1.5. The scaling of the central peak of the histogram is in remarkable agreement with the mean-field prediction calculated from Eqn. 4.1 and is consistent with the critical μ predicted by the monomer-dimer simulations. The peak corresponding to μ_o is consistent with the mean-field pion threshold for the smaller quark masses but significantly lower for $ma = 1.0, 1.5$ as noted above.

Figs. 4.5 and 4.6 show clearly the banded structure of the zeros distribution in the e^μ plane for two different lattice sizes and quark masses. As anticipated, we observe a dense line, which closely follows the prediction $|e^\mu| = e^{\mu_c}$. The innermost circle of zeros correspond to μ_o, hence to half the pion mass. The zeros fill up the puzzling critical region $\mu_o \to \mu_s$.

Compare Fig. 4.7 which gives the distribution of the real part of the zeros with Fig. 4.8 which gives the number density (on a 6^4 lattice with $m = 0.1$). Again the histogram for the zeros shows three distinct peaks: $\mu_o \simeq 0.3$ corresponding to the onset of net non-zero quark density; $\mu_c \simeq 0.7$ corresponding to the small discontinuity in the number density and the expected critical chemical potential; $\mu_s \simeq 1.0$ corresponding to the lattice saturation point. Comparison of the two plots shows that the derivative of the number density correlates well with the density of states (frequency histogram). Note the general trend of the number density results which are basically, indistinguishable from the quenched ones, except for the **small jump** at $\mu \simeq 0.7 \simeq \mu_c$ suggesting the **discontinuity** associated with the restoration of the chiral symmetry. This small hint of a discontinuity was not perceptibly larger on the 8^4 lattice.

One of the many intepretations proposed for the pathologies of lattice QCD at finite density is that the anomalous increase in number density at μ_o is temperature driven. There is no evidence for this in our simulations In Fig. 4.9, we show a detailed comparison of the results on 6^4 and 8^4 lattices, for $m_q = 0.1$ (note the different scales on the right and the left side). By zooming in on the onset region we observe that the number density starts to rise from zero at $\mu \simeq 0$. This effect is very small (note the scale) and it is temperature dependent. Clearly the number density is suppressed on the colder lattice. There is, however, no appreciable difference in the value of μ_o when we compare 6^4 and 8^4 lattices. This is at odds with the suggestion that the increase in the number density at μ_o reflects a thermal excitation of baryons. This result supports the belief that the rise at μ_o is unphysical, as in the quenched approximation. Of course we cannot rule out the possibility that the situation changes on larger lattices, and we refer to Refs. [32] and [33] for discussions on this point.

The most interesting point is that temperature effects are greatly lessened for $\mu > \mu_o$. Temperature effects become apparent again at μ_c, suggesting that μ_c is the threshold for a new phase.

In summary, we have seen how the small discontinuity observed in the fermion number density manifests itself in the histogram of zeros: the density of zeros is the *derivative* of the number density, so a small "discontinuity" in n_q corresponds to a distinct signal in the histogram of zeros.

Will more statistics eventually cancel the onsets at μ_o and μ_s? Even if we have not observed any dramatic effect by increasing the number of configurations, the persistence of μ_o could still be explained by insufficient statistics, especially since

Z_3 invariance has not been completely achieved yet, and since it is possible that the precision required to achieve the cancellation of the unwanted onset is prohibitively high. It is also possible that the polynomial representation for the GCPF is ill-conditioned [51].

4.3.2 Analysis of the Probability Distributions

Fermion number density fluctuations in the grand canonical ensemble can be used to identify the critical region and are amenable to study using our GCPF expansion.

Write

$$Z = \sum_{n=-3V}^{3V} W_n \tag{4.36}$$

If we choose to normalize so that $Z = 1$, then W_n is the probability that a system in a grand canonical ensemble has n fermions. Using the numerical results for the GPF above (see Eqn.(4.20), the shapes of the probability distributions $W_n = Z_n e^{\mu n_t n}$ for different chemical potentials can be drawn as a function of n, and the critical region can be studied using standard statistical mechanics analysis.

For a first order phase transition we can make qualitative predictions for the expected behaviour of W_n. For $\mu \neq \mu_{crit}$ we expect W_n to have a single sharp peak at some value of n. This peak should become infinitely sharp as $V \to \infty$. However at the critical point, $\mu = \mu_c$ we expect the probability distribution to become flat over a range of n's where each fermion number density in that range is equally probable. The situation corresponds to large fluctuations of density in the transition region which is a well-known characteristic of a first order transition. Note that we were able to relate the density of partition function zeros to the fermion number susceptibility our analysis of the simulation results.

Since we consider both quarks and anti-quarks in our statistical ensemble what we measure is the *net particle number* which is the number of particles minus the number of anti-particles. The number density can be written as

$$n_q = \frac{1}{V} \sum_{n=-3V}^{3V} n W_n \tag{4.37}$$

The chemical potential effectively enhances the propagation of quarks and inhibits the propagation of antiquarks. We expect that for $\mu = 0$ the distribution is symmetric about the origin, and $J_0 = 0$ since the number of quarks is equal to the number of anti-quarks. This is reflected in our results. For $0 < \mu < \mu_o$ although the peak of the distribution migrates away from the origin favouring quark propagation, the net fermion number remains negligibly small ($n_q < 0.01$).

The behaviour of the probability distribution for small chemical potential is shown in Fig. 4.10 . At $\mu = 0$ the distribution is symmetric around the origin, and $n_q = 0$ as expected. By slightly increasing μ the distribution becomes asymmetric, reflecting the enhancement (suppression) of the forward (backward) propagation. Positive and negative states are still both contributing to the probability distribution. The net J_0 moves immediately off zero, but it is very small. At $\mu = \mu_o$ the scenario changes completely since a **secondary maximum** develops at positive n, and the distribution distinctly moves into the positive n region. We show this behaviour for both $m_q = 0.1$ and $m_q = 0.08$ in Fig. 4.11. For $\mu > \mu_o$ the negative states are totally suppressed. This behavior is correlated with the sharp increase of n_q plotted before and should be related to changes in the theory's spectrum, perhaps reflecting pathologies of the quenched case such as the " funny pions" [33] or Stephanov's condensates [37].

For $\mu \simeq \mu_c$ which we believe corresponds to the expected critical region, we do indeed observe a broadening of the probability distribution consistent with a peak in the fermion number susceptibility and supporting the idea that μ_c is associated with a phase transition. We show this behaviour for both 6^4 and 8^4 lattices in Fig. 4.12.

Now consider the critical region :- we see the expected broadening of the probability distribution at μ_c (Fig. 4.12 , 4.13). Finite size effects become important again for $\mu > \mu_c$. Note, in particular, in Fig. 4.13, the sensitivity to μ on a very fine scale : the three central plots are for $\mu = 0.68, 0.683, 0.7$.

In Fig. 4.14 we summarize these observations by plotting W_0, the probability that the system has zero particle number, and the integrated probabilities $W^+ = \sum W_n, n > 0$; $W^- = \sum W_n, n < 0$. The logarithmic scale of the plot makes it easy to see that backward and forward propagations are enhanced and suppressed by the same factor at small μ. Correspondingly, the contribution of $n = 0$ must decrease. At $\mu = \mu_o$ $n = 0$ equals the overall contribution from > 0. For $\mu > \mu_o$ only positive n contribute to Z.

These results suggest that μ_o is the threshold for a phase with only positive propagation. Perhaps this observation is a clue to the nature of the phase $\mu > \mu_o$. Recall that mean field analysis predicts the threshold of the mixed phase (broken phase/ saturated phase) at $\mu \simeq \mu_o$. Future work should address possible relations between these observations.

We believe that μ_c indicates a physical critical point. All approaches (except the pathological quenched case) predict a transition or, at least, a clear change

in the behavior of observables here. From the point of view of this section it is relatively easy to understand the robustness of this result whereby the probabilities plotted here underlie all the observables discussed earlier and the "flatness" of the distributions, which locates the critical point, is a qualitative feature which should appear in all the numerical procedures.

4.3.3 Summary of Finite Density Lattice QCD at Strong Coupling

The simulations of QCD at strong coupling [52] which implement dynamical fermions using the Glasgow reweighting procedure on 6^4 and 8^4 lattices have demonstrated the persistence of the early onset, μ_o, of the transition first observed in the quenched theory. However the unquenched simulations give a signature corresponding to the expected μ_c as predicted by the strong coupling expansion. The value of μ_c predicted by the simulations is consistent with μ_{mf} (Eqn. 4.1) for all bare quark masses. This signature is absent in the quenched theory and is attributable to the averaging of the characteristic polynomial which is controlled by the reweighting procedure. As demonstrated for $ma = 0.1$, the small discontinuity observed in the fermion number density correlated with a very clear signature in the zeros. The density of the moduli of the zeros is analogous to the fermion number susceptibility. The susceptibility gives a much stronger signal for a discontinuity at μ_c.

The success of the monomer dimer approach (of use only at strong coupling) may be due to analytic integration first over the gauge fields, and then the fermion fields, giving an effective action with a reduced sign problem. Standard Hybrid Monte-Carlo algorithms integrate the fermion fields prior to the gauge fields. The Glasgow algorithm μ_c prediction is in agreement with the monomer-dimer algorithm, however in the latter there is no early onset and the critical fermion number density is $n_c a^3 \simeq 0.05$ in stark contrast to $n_c a^3 \simeq 0.5$ from the Glasgow algorithm.

The explanation of the persistence of μ_o in the hybrid Monte-Carlo simulations is essential to an understanding of the physics of the transition. It is conceivable that the colour deconfinement and chiral transitions are *separated* at finite density. This may suggest that both μ_o and μ_c are physical. A finite temperature study could be used to explore this scenario. We do however expect that the early onset, μ_o, should disappear in a correct calculation. Physical arguments support this view as well as the monomer–dimer and strong coupling expansions discussed here. It might be that a high statistics run of the present algorithm will cancel μ_o. In this case the

method would be impractical, but, at least, not conceptually wrong. If this were true, we should develop a strategy to monitor the convergence of the method to the correct statistical ensemble, and to remove unphysical contributions to observables due to partial "cancellations" of unwanted onsets. Although a limited increase in statistics revealed that the peak in the histogram of zeros corresponding to μ_o grew proportionally with the peak at μ_c it is still possible that the signal for μ_o will be "cancelled out" in the limit of infinite statistics *once the $Z(3)$ invariance has been completely achieved.*

Since it is believed that a correct implementation of dynamical fermions will eliminate μ_o it is possible that the necessary cancellation of the poles of the propagator by the zeros of the fermion determinant (for example in the expression for the chiral condensate Eqn. 2.46) has not been fully realized in the simulations. Incomplete cancellation could arise from either limited statistics or from the reweighting procedure itself. Using an ensemble generated at $\mu = 0$, together with reweighting with respect to the fermion determinant at $\mu = 0$ may not give sufficient overlap with an ensemble generated at $\mu \neq 0$ to correctly describe the true physics there. This explanation is suggested from the standard problems encountered by reweighting procedures. We have investigated this possibility by performing an exploratory simulation of the three dimensional Gross Neveu model [53] the results of which will be described in Chapter 6. If reweighting does pose a problem the Glasgow method can be improved if a better starting point were invented. This is a worthwhile direction to pursue.

At the present point, we have to accept that, at strong gauge coupling, ensemble averaging does not help to suppress the pathologies of isolated configurations. The results of a similar investigation at intermediate gauge coupling where the gauge action **does contribute** to the dynamics will be discussed in the next chapter.

It might well be that a satisfactory simulation of finite density QCD requires an algorithm which produces physical results on each configuration. This insight has motivated our study of χQCD [54], where an irrelevant four fermi term is added to the standard QCD action used here. χQCD has the advantage that chiral symmetry breaking and the generation of a dynamical quark mass occurs configuration-by-configuration and the pion and sigma excitations are explicitly free of μ dependence. In fact, as we shall demonstrate in Chapter 7 χQCD simulations do not suffer from the severe μ_o pathologies seen here [55], although additional work, both theoretical and practical, is needed to see if χQCD really produces only physical results. Research in this topic is in progress.

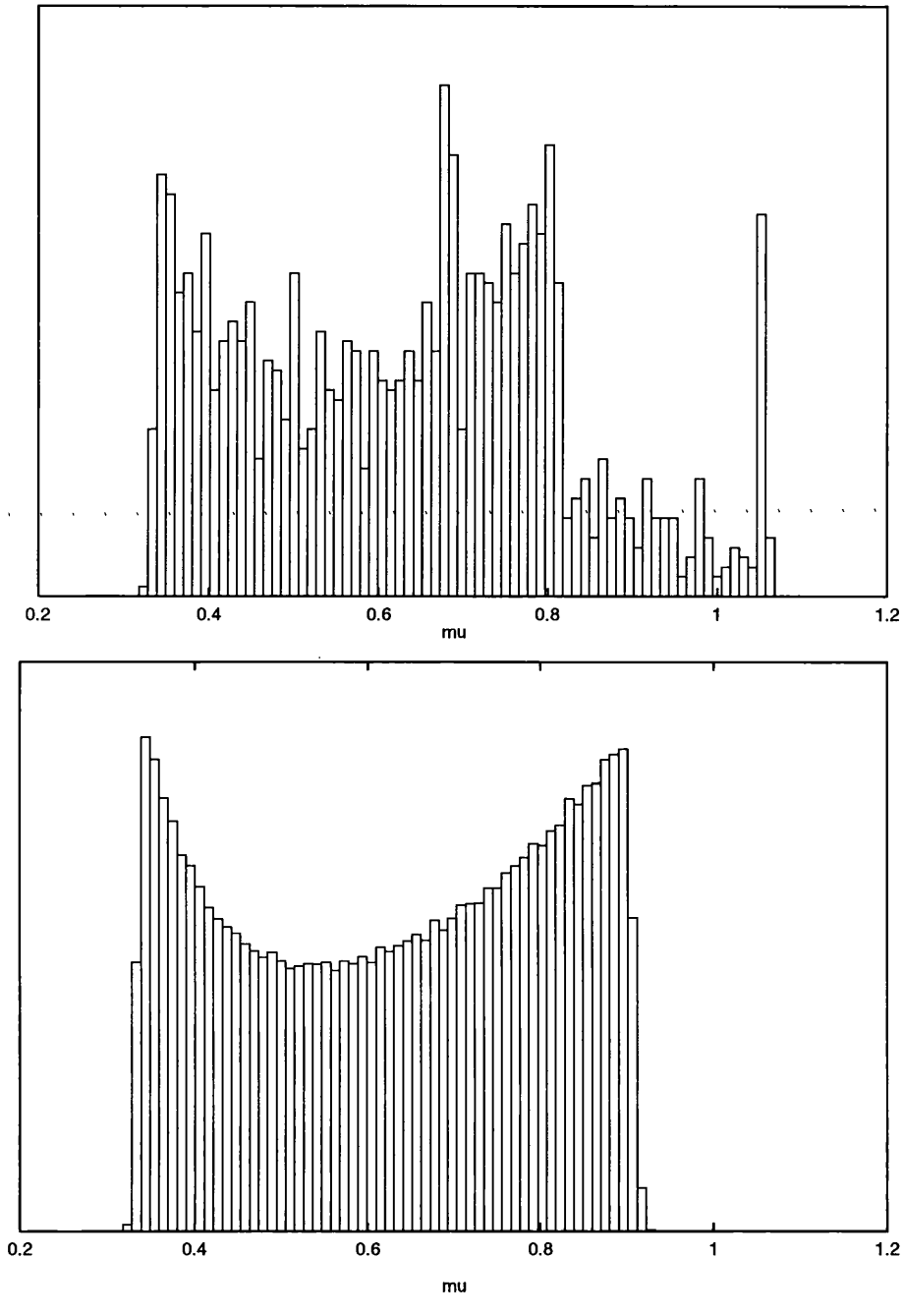

Figure 4.1: Histogram of the zeros of the full model (top), and Histogram of the zeros of the determinant (bottom), hence of the quenched approximation. Simulation with $m_q = 0.1$ and $\beta = 0.0$ on an 8^4 lattice.

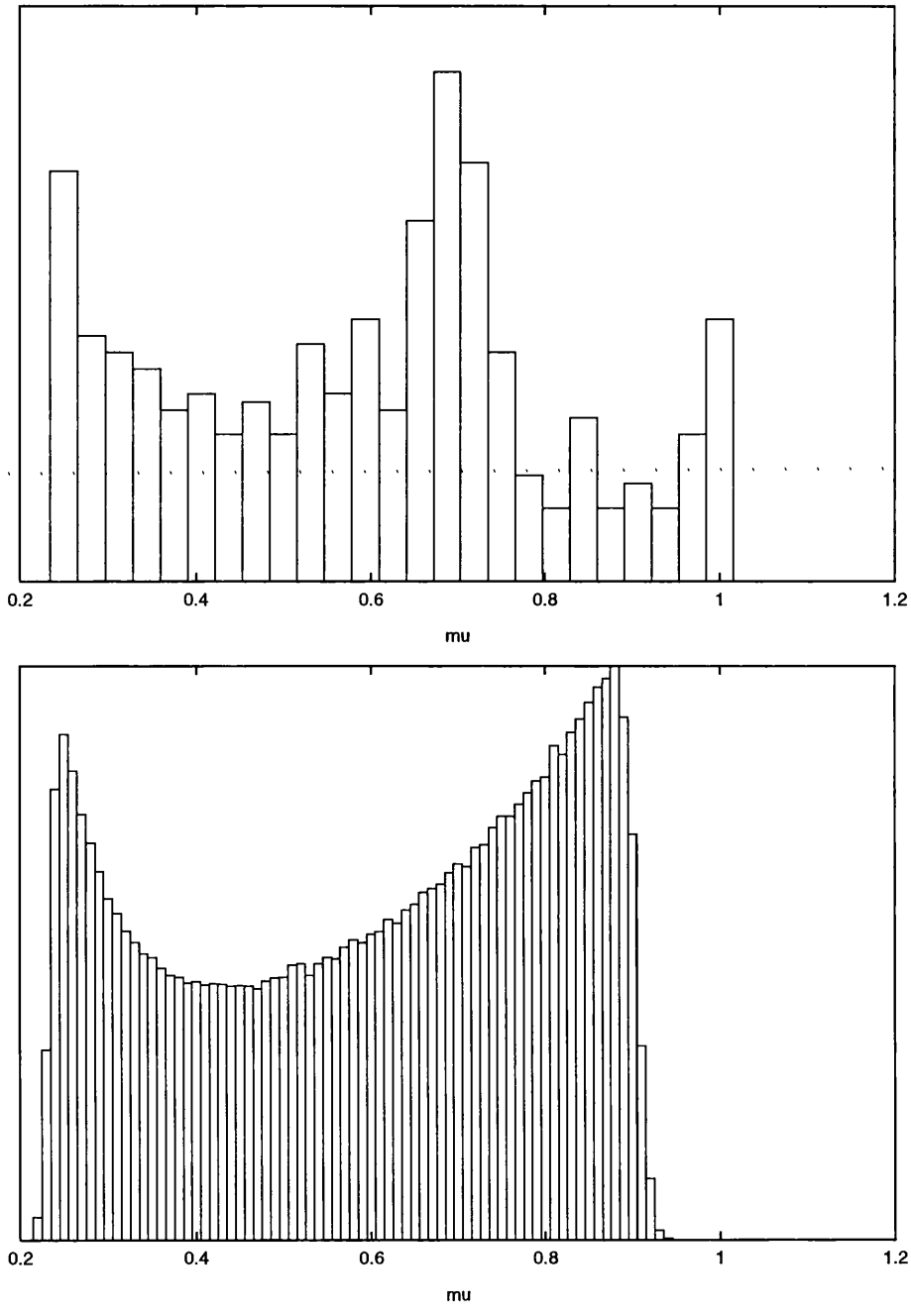

Figure 4.2: As in Fig. 4.1, but $m_q = 0.05$.

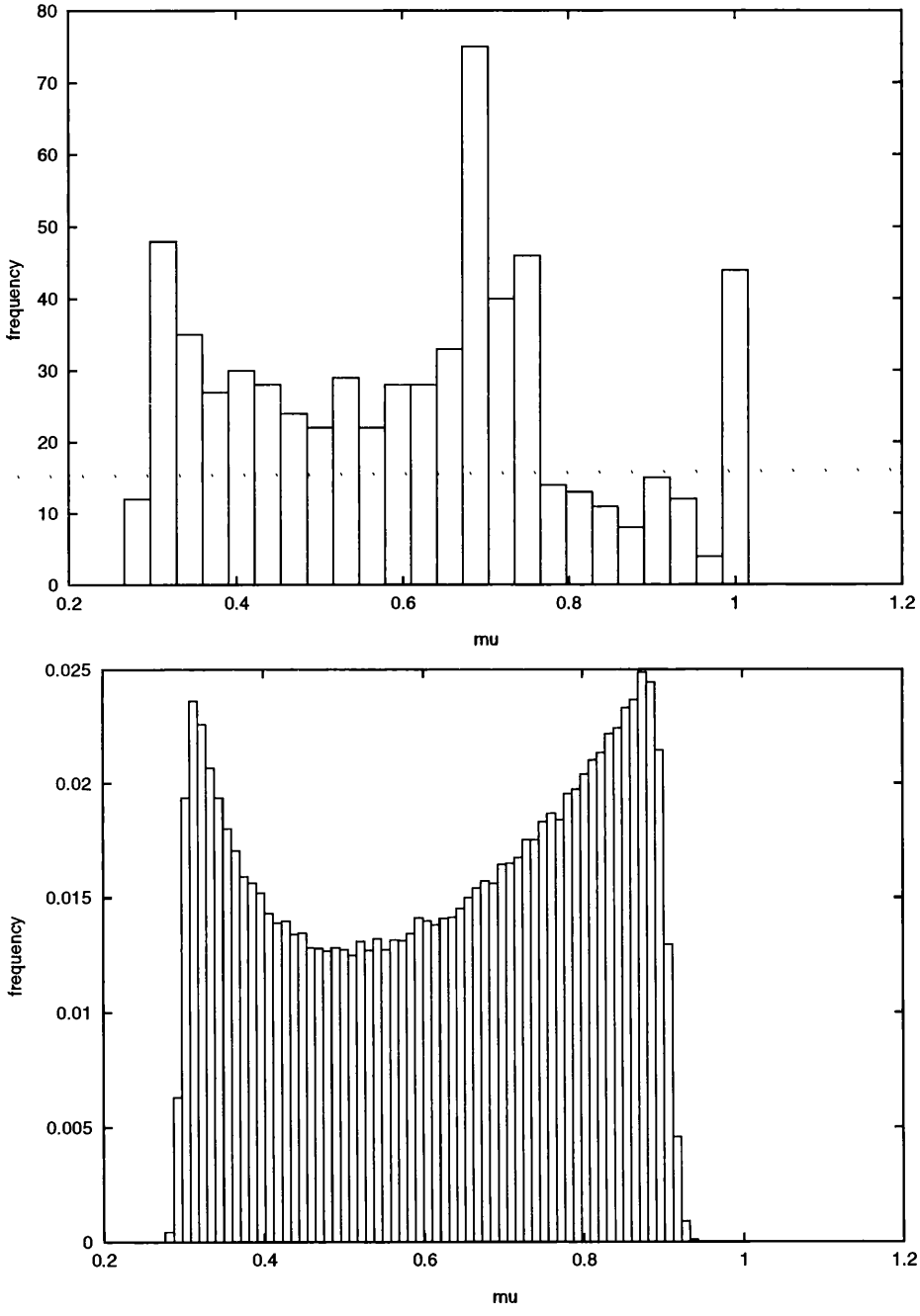

Figure 4.3: As in Fig. 4.1, but $m_q = 0.08$.

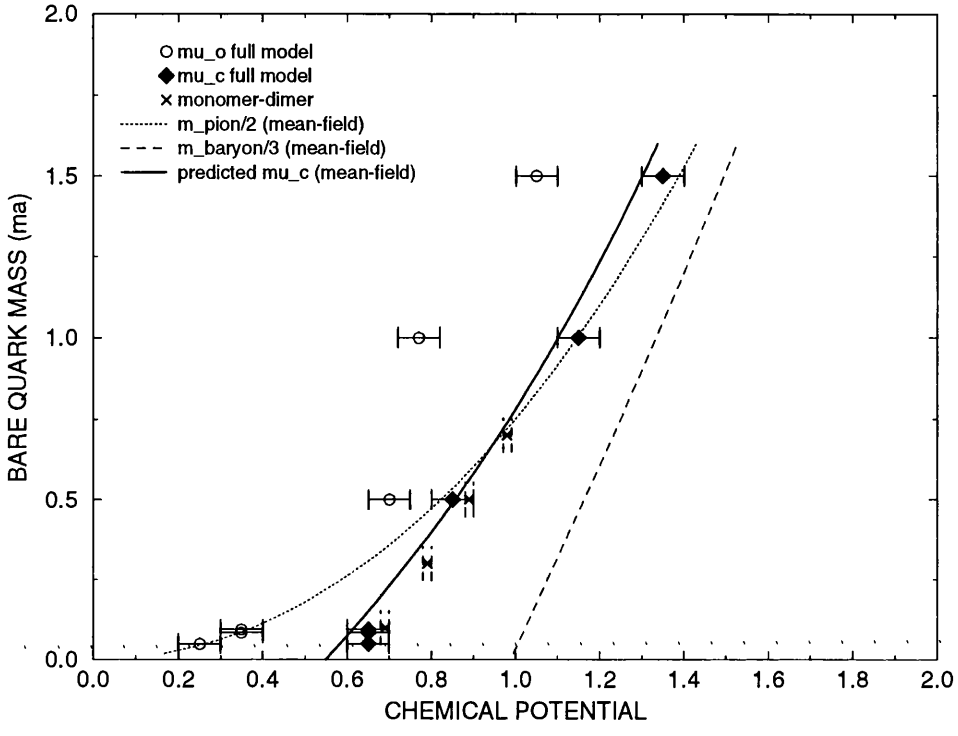

Figure 4.4: Summary of the $\beta = 0.0$ results for the critical point μ_c, and current onset μ_o. μ_c follows the prediction of the mean field analysis of ref.[4] (dashed line). The onset is close to half the pion mass at small mass, and below half the pion mass for $m_q > 0.5$.

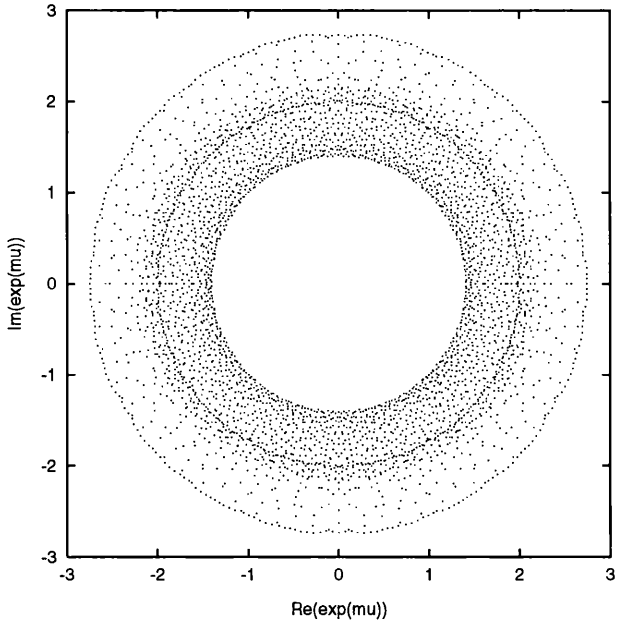

Figure 4.5: Zeros in the e^{μ} plane for 6^4 lattice with $m = 0.095$ and $\beta = 0.0$. The critical line is the thin line inside the denser region $e^{\mu} = e^{\mu_c}$

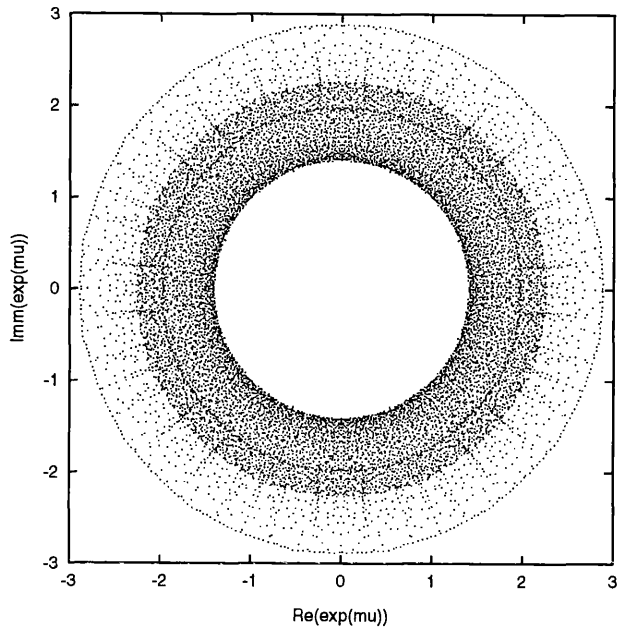

Figure 4.6: Zeros in the e^{μ} plane for 8^4 lattice with $m = 0.1$ and $\beta = 0.0$. The critical line is the thin line inside the denser region $e^{\mu} = e^{\mu_c}$.

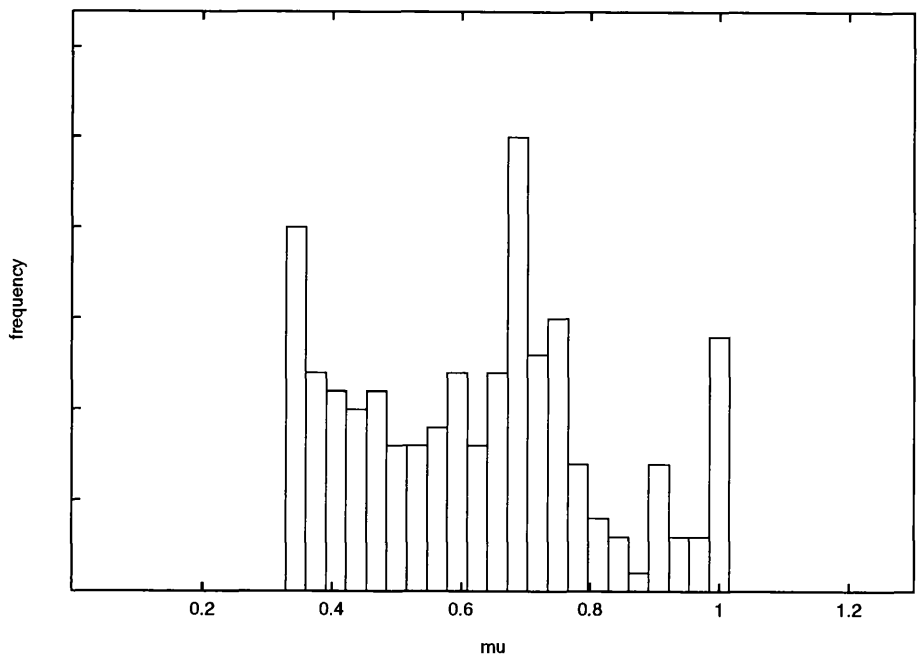

Figure 4.7: Histogram of zeros accompanying Fig. 4.8 ($m_q = 0.1$ and $\beta = 0.0$ on a 6^4 lattice). Note a) the peak at $\mu_c = 0.687(15)$ matching the small jump, to be contrasted with the monomer–dimer results $\mu_c = 0.69(1)$. b) the correspondence of the extrema of the histogram with the onset μ_o of the current and its saturation μ_s.

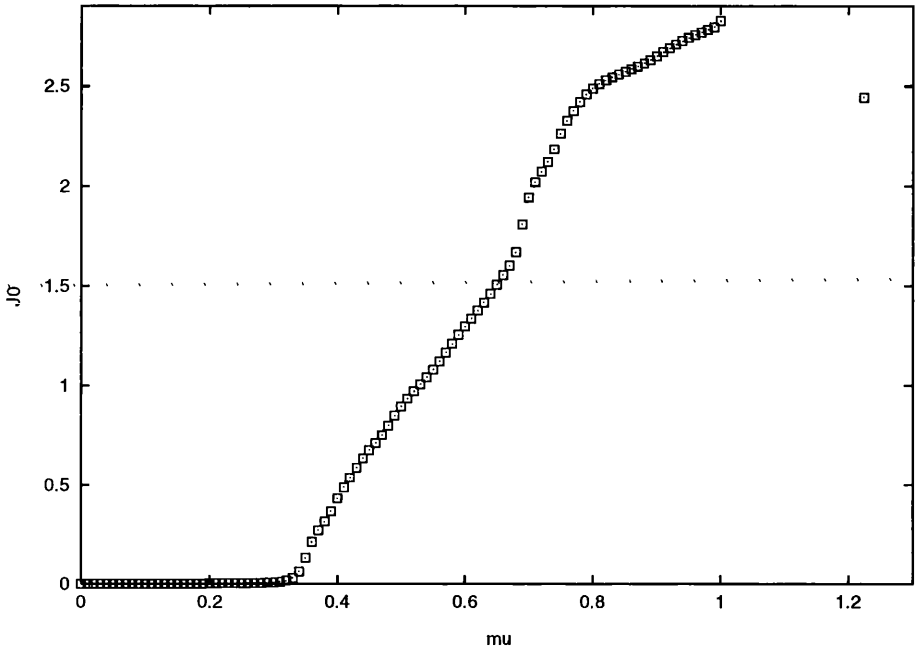

Figure 4.8: Quark number density from the Glasgow algorithm. $m_q = 0.1$ on a 6^4 lattice $\beta = 0.0$. The onset $\mu_o \sim 0.33$, and the saturation point $\mu_s \sim 1.0$, are the same as the ones observed in the quenched approximation. The critical point for chiral symmetry restoration measured in a monomer–dimer calculation is $\mu_c = 0.69(1)$, coincident with the little gap observed in our results. The same monomer–dimer results would, however, predict a very sharp transition with a critical density close to zero, in agreement with the results of the strong coupling expansion.

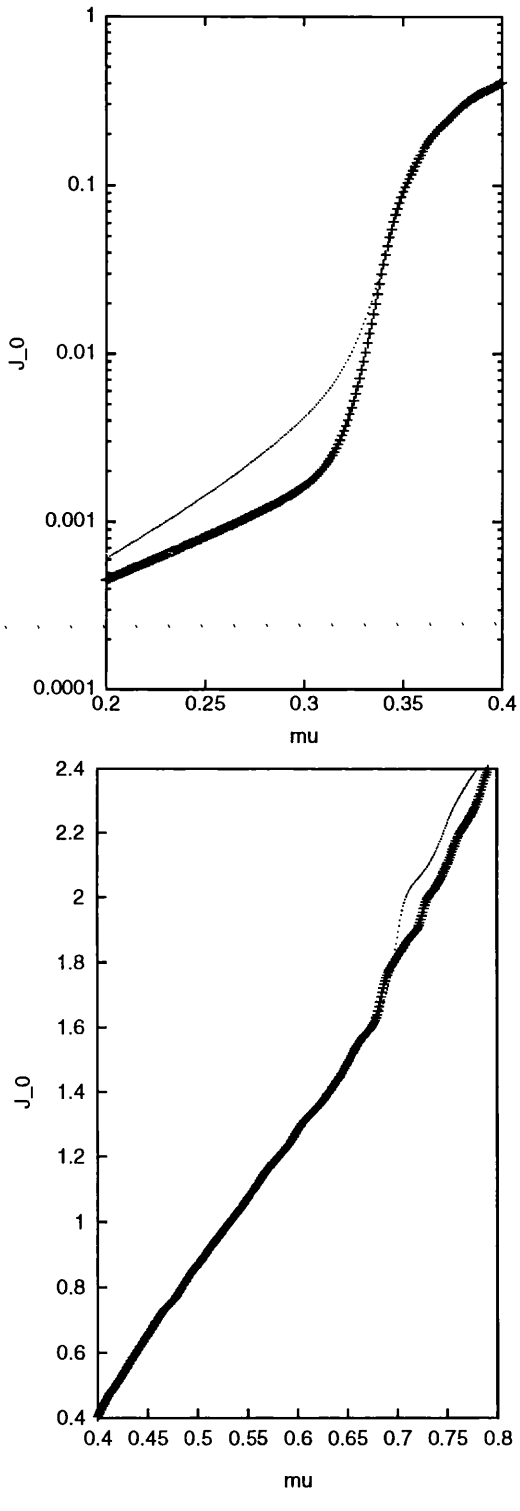

Figure 4.9: Finite size effects at $m_q = 0.1$ and $\beta = 0.0$. We show details of the critical regions around μ_o and μ_c for $m_q = 0.1$ for two different lattices. The thick lines are for the 8^4 lattice, the thin lines for the 6^4.

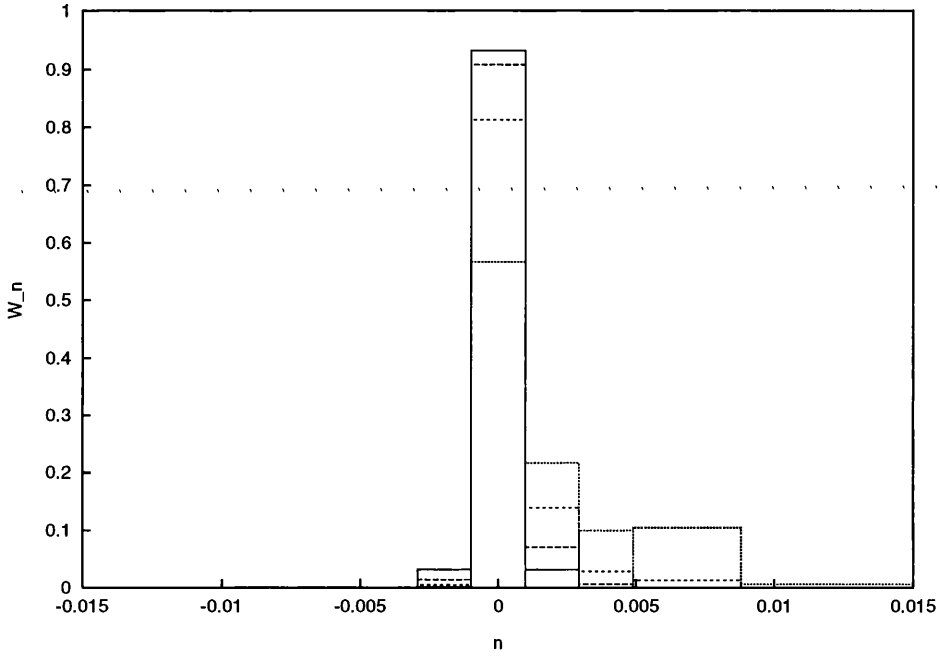

Figure 4.10: Probability distributions for small chemical potential at $m_q = 0.1$ and $\beta = 0.0$ on the 8^4 lattice. The solid line is $\mu = 0.0$, the dashed lines , from top to bottom at $n = 0$, are for $\mu = 0.1, 0.2, 0.3$.

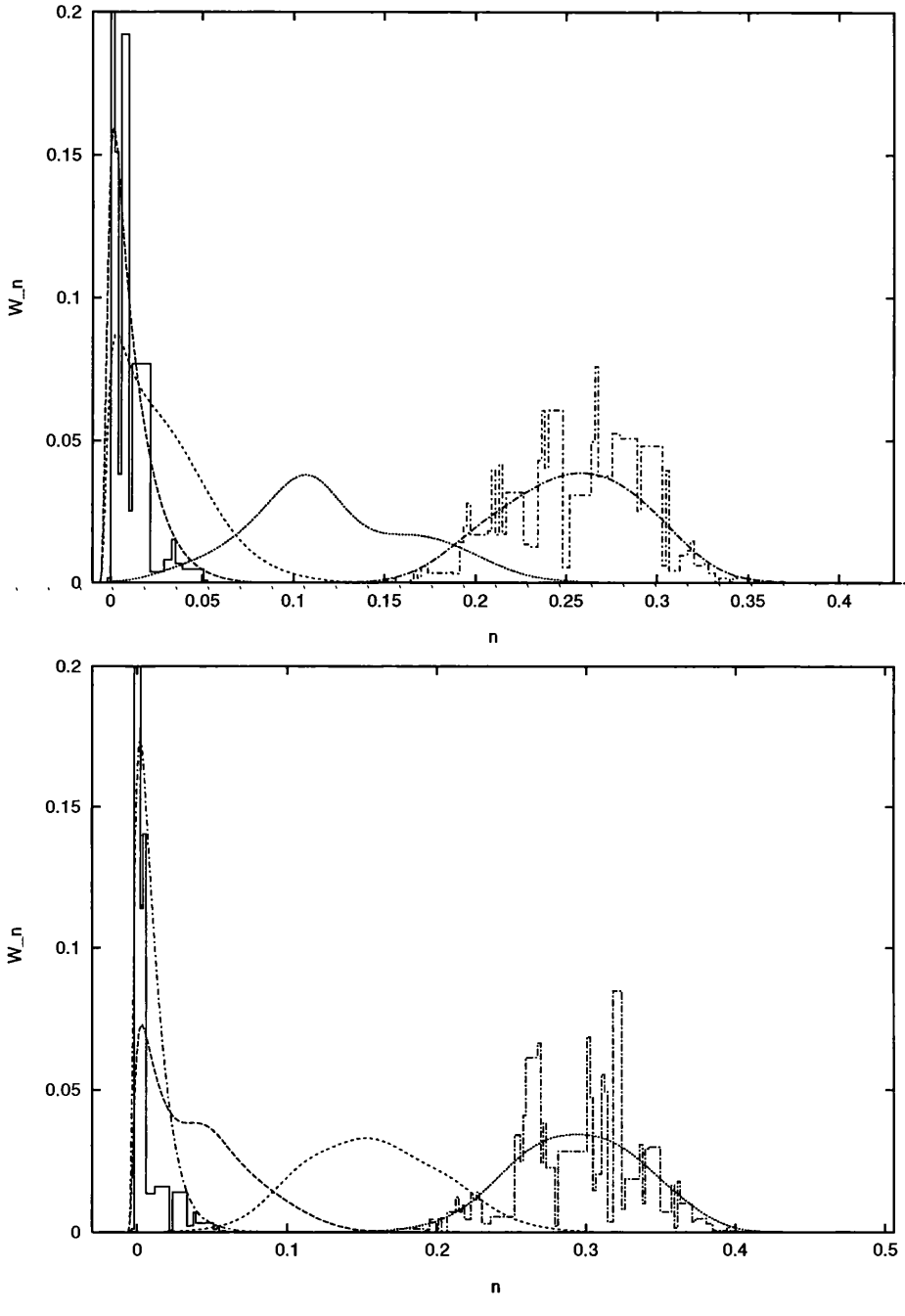

Figure 4.11: Probability distributions around the onset μ_o for $m_q = 0.08$ (top) and $m_q = 0.1$ (bottom) on an 8^4 lattice. The leftmost histogram (solid) at $m_q = 0.08$ is for $\mu = .28$, the rightmost is for $\mu = 0.34$. Bezier interpolations (from Gnuplot) are shown for $\mu = 0.28, 0.30, 0.32, 0.34$. At $m_q = 0.1$ $\mu = 0.32, 0.34, 0.36, 0.38$ from left to right. For both masses at μ_o the probability distribution moves on the positive n axes. Simulations were performed at $\beta = 0.0$

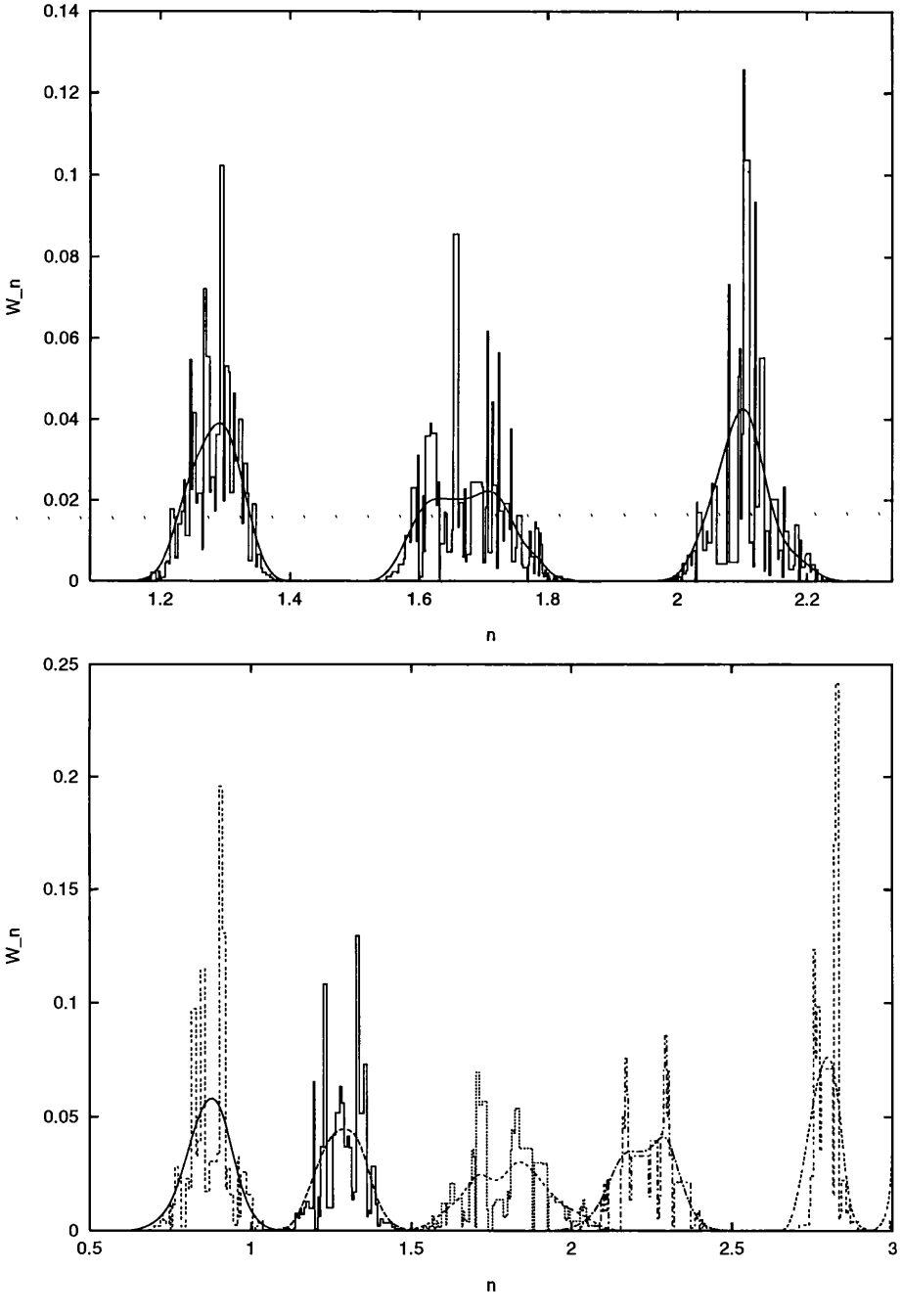

Figure 4.12: Probability distributions in the critical region at $m_q = 0.1$ and $\beta = 0.0$, on the 8^4 (top) and the 6^4 (bottom). μ is (0.6, 0.683, 0.75) , from left to right (top) , and (0.5. ,0.6, 0.695, 0.75 , 1.0) bottom.

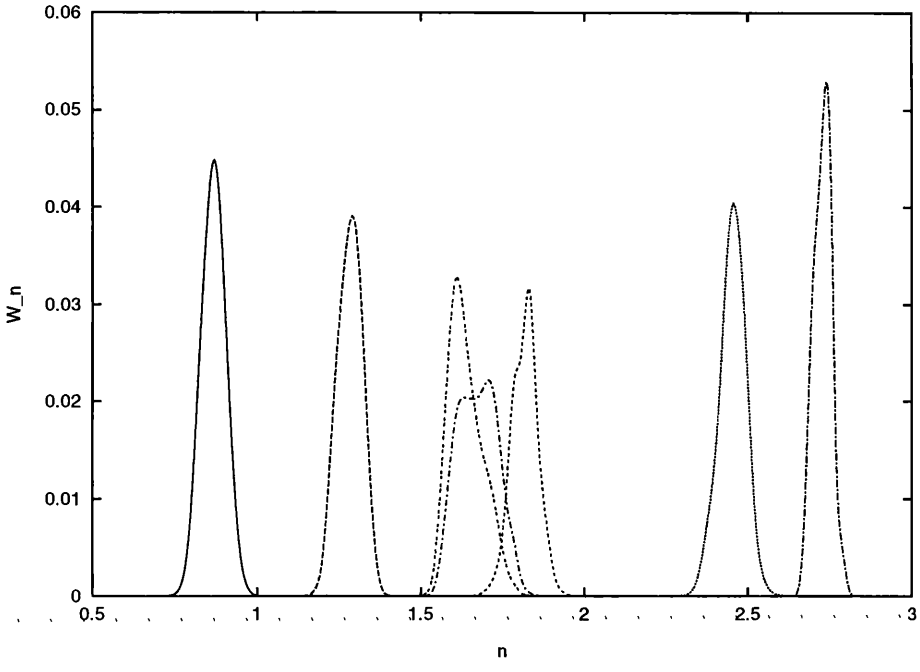

Figure 4.13: Probability distributions on the 8^4 lattice with $m_q = 0.1$ and $\beta = 0.0$, for μ = (0.5 , 0.6 , 0.68, 0.683, 0.7 , 0.8 , 0.9). Only the Bezier interpolations are shown. The complete results for several μ values can be seen in Fig. 4.12.

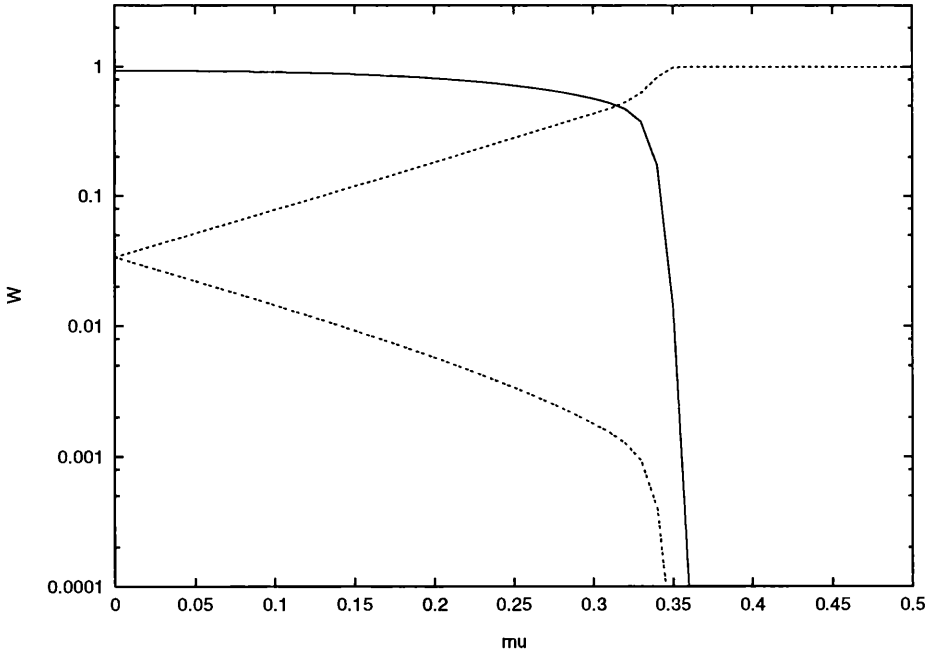

Figure 4.14: W_0 (solid) , and integrated probabilities W^+ and W^- (dash) at m_q = 0.1 and $\beta = 0.0$, on the 8^4 lattice

Chapter 5

Simulation Results at Intermediate Gauge Coupling

The simulations at strong gauge coupling have proved to be very informative. We have implemented dynamical fermions in the simulations using the Glasgow reweighting method and have demonstrated the persistence of the early onset of the phase transition . The strong evidence for the emergence of a signal for the expected transition at μ_c was very encouraging although the pathological onset at μ_o remained.

We have associated the early onset of the transition μ_0 with mass poles of the quark propagator on isolated configurations. Our understanding of how the poles in the region $\mu_o \leq \mu < \mu_c$ can be cancelled by the fermion determinant is far from complete. Such a cancellation would allow us to obtain a physical picture consistent with mean-field analyses and the strong coupling expansion.

The strong coupling simulations have offered us considerable diagnostic power but in order to explain continuum physics it will be necessary to perform simulations at intermediate gauge couplings and to gradually push further towards the continuum limit $\beta \to \infty$. For simulations at intermediate coupling $S_G \neq 0$ hence our gauge fields are no longer random (as they were in the strong coupling simulations). There are few analytical results available at intermediate coupling but the strong-coupling analysis of Bilic et. al. [48] predicted a critical chemical potential of $\mu_c \simeq 0.65$ for a gauge coupling of $\beta = 5.0$. We can use this as a guideline for the

expected critical point in our simulations.

Will the fermion number density and the partition function zeros suggest a similar picture to that occurring at strong coupling?

Taking account of the fact that we generate our configurations at $\mu = 0$ and perform an analytic continuation into the complex plane we selected our lattice parameters so that we were close to the deconfinement transition for the 6^4 lattice. We believe that such a choice is optimal for the Glasgow reweighting technique. To ensure that for our choice of lattice parameters we had a starting point in our simulation such that we were in the confined phase at $\mu = 0$ we monitored the $Z(3)$ tunnelling of the system. As explained in Chapter 2, the $Z(3)$ tunnelling is an order parameter for confinement where dynamical fermions have been included in the simulations. As Fig. 5.1 shows, at $\beta = 5.1$ and $m = 0.01$ on an 8^4 lattice we obtained a clear signal for Z(3) tunnelling whereby the sum of the triality zero coefficients shows a strong tendency to average to unity and the sum is bounded below whilst those of triality one and two coefficients each tend to zero and the sum is bounded above. This is consistent with simulating in the confined phase at $\mu = 0$ as expected at this coupling and quark mass. The strongest signal for tunnelling was obtained around the small n levels and the first few terms in the partition function expansion dominate the sum. Although some of the triality zero levels are determined with large statistical error, it is clear that their real parts are approximating to a continuous curve with respect to n, as seen in Fig. 5.3 for an 8^4 lattice at $\beta = 5.1$ and $ma = 0.01$.

The hybrid Monte-Carlo time evolution of $\ln|\det M|$ on an 8^4 lattice at $\beta = 5.1$ and $ma = 0.01$ is shown in Fig. 5.2. We have noticed from simulations close to the transition on a 6^4 lattice that if the system switches from the confined to the deconfined phase $\ln|\det M|$ increases. This is a direct result of the fact that in the confined phase the eigenvalues are relatively small compared to those in the deconfined phase. In the confined phase the eigenvalues cluster around the origin when plotted in the complex chemical potential plane. This gives a non-zero value for the chiral condensate.

5.0.4 Thermodynamic Observables

We obtained an estimate of the fermion number and energy densities directly from the coefficients of the expansion using the definitions in Eqns. 2.47 and 2.48. The results for 6^4 and 8^4 lattices at $\beta = 5.1$ and $ma = 0.01$ are plotted in Fig. 5.4. Clearly the onset at $\mu_o \sim 0.1$ is inconsistent with the prediction $\mu_c \sim 0.6$ and

it is possible that this is a remnant of the pathologies first seen in the quenched theory. Although the onset chemical potential differs very little on the 6^4 and the 8^4 lattice both the fermion number and energy density curves steepen in gradient on the larger lattice for $\mu > 0.7$. This is exactly the behaviour we would expect due to finite size effects. It is clear from the susceptibilities plotted for the 8^4 lattice in Fig. 5.5, that there is a distinct increase in gradient of number and energy densities signalled by a peak in the susceptibilities at $\mu \sim 0.65$. This is completely consistent with the analysis of the partition function zeros shown in Fig. 5.6. The zeros show the characteristic band of increased density which was closely associated with μ_c in the strong coupling simulations. As expected, the innermost circle of zeros is associated with the onset in the number and energy densities and the outermost circle is associated with the lattice saturation. The histogram of the real parts of the zeros reflects this behaviour with a peak at $\mu \sim 0.7 - 0.9$. It is possible that this peak is the true critical point (as suggested by our strong coupling simulations).

5.1 Scaling Behaviour

We have also checked the μ^3 scaling of the number density and the μ^4 scaling of the energy density which is the behaviour expected for a Fermi gas in the continuum limit. We expect the quark-gluon plasma to approximate a Fermi gas of quarks with zero dynamical mass. For the range of chemical potential where the scaling is continuum-like the two plots in Fig. 5.7 should have zero gradient and this seems to be a good approximation for $\mu \sim 0.7 - 0.9$. Note that the densities pertaining to a free lattice gas did not fit our simulation data. Clearly we would not expect to obtain continuum behaviour on small lattices but the observed scaling properties combined with the other evidence that some $\mu > \mu_o$ could be associated with μ_c constitute a self-consistent picture of the features of all of our finite density QCD simulations with our method of implementation of dynamical fermions.

5.1.1 Onset Dependence on Bare Quark Mass

The fermion number density on a 6^4 and 8^4 lattices with $\beta = 5.1$ and $ma = 0.01$ revealed that the early onset of deconfinement seen in the strong coupling simulations also occurs at intermediate coupling. We found $\mu_o \simeq 0.1$ which is much less than the expected μ_c and consistent with the results of the quenched theory. We therefore repeated our simulation for a range of quark masses on a 6^4 lattice in order to establish whether the scaling of μ_o with the bare quark mass

was consistent with either a baryon or a Goldstone pion controlling the transition. To do this we make use of the PCAC relation (Eqn. 1.48) which tells us that μ_o should be proportional to the square root of the bare quark mass if the scaling is consistent with a Goldstone boson. We expect μ_o to have a linear dependence on the bare quark mass if the scaling is consistent with a baryon. For a range of bare quark masses we have investigated [56] the chemical potential (the onset μ) required to make the level with 3 quarks equally probable with the zero quark level, i.e. $\mu_{onset} = (\epsilon_3 - \epsilon_0)/3$. This ad-hoc definition takes into account that it is these energy levels which are most accurately determined and allows errors to be estimated directly.

Fig. 5.8 shows the dependence of the onset μ on the square root of the quark mass on a 6^4 lattice at gauge coupling $\beta = 5.1$. As at strong coupling there is a strong signal that this onset μ is dependent on the mass of a Goldstone boson for quark mass $m > 0.01$. At some smaller mass the system (on a 6^4 lattice at this β) becomes 'deconfined'. We checked this behaviour by determining the Lee-Yang zeros in the complex m-plane and they were found to be complex with non-zero real part < 0.01 as shown in Fig. 5.9. Eliminating the data point corresponding to the smallest quark mass we see that scaling with the square root of the bare quark mass is clearly preferred. Thus by investigating the scaling of the onset chemical potential with the bare quark mass and relating it to the Goldstone pion we have given further credence to the direct link between the pathologies of finite density QCD and the mass poles of the quark propagator.

5.2 Summary of Intermediate Coupling Simulations

Simulation of standard lattice QCD at finite density seems to be plagued by the problems of the naive quenched version of the theory, namely the chemical potential at which the fermion number begins to differ from zero (μ_o) appears to be controlled by a Goldstone pion rather than by the lightest baryon. However the features observed in the strong coupling simulations also carry over to the intermediate coupling regime. In particular, at intermediate coupling, in addition to the pathological early onset, we observe a clear signal for μ_c from the distribution of zeros in the e^μ plane which is reflected in the histogram of the real parts of the zeros. The susceptibilities of the fermion number and energy densities exhibit a peak in the region $\mu \sim \mu_c$ and scaling of the fermion number and energy densities appears to be continuum like for $\mu > \mu_c$. The observed signal for μ_c is encouraging

but the persistence of μ_o is still a puzzle. It will be instructive to perform a very high statistics simulation and to monitor the evolution of μ_o as the statistics are increased to determine whether or not it moves towards μ_c. This work is in progress.

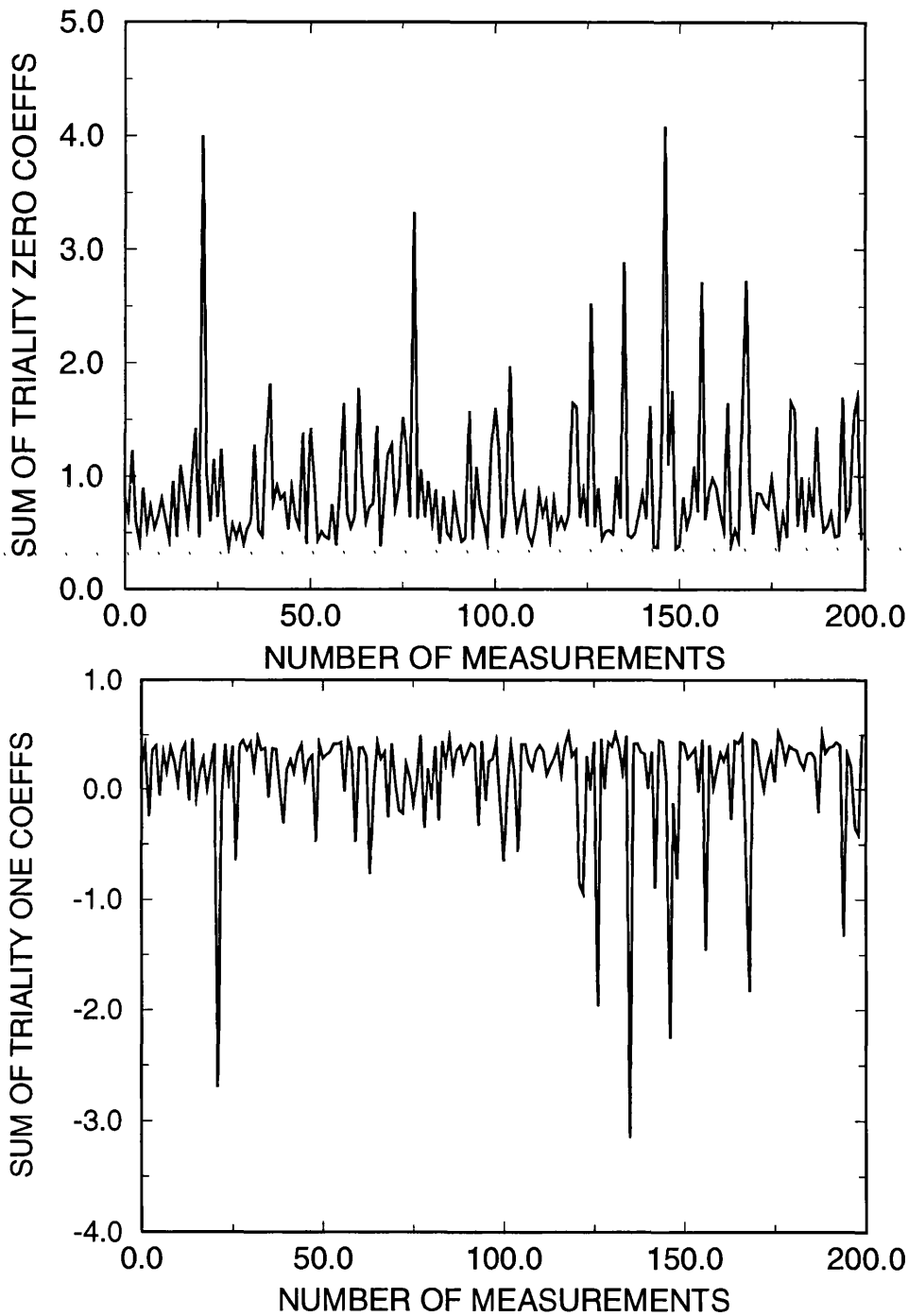

Figure 5.1: The HMC time evolution of the expansion coefficients on an 8^4 lattice at $\beta = 5.1$ and $ma = 0.01$. The behaviour of the triality 2 coefficients is similar to that of the triality 1 coefficients.

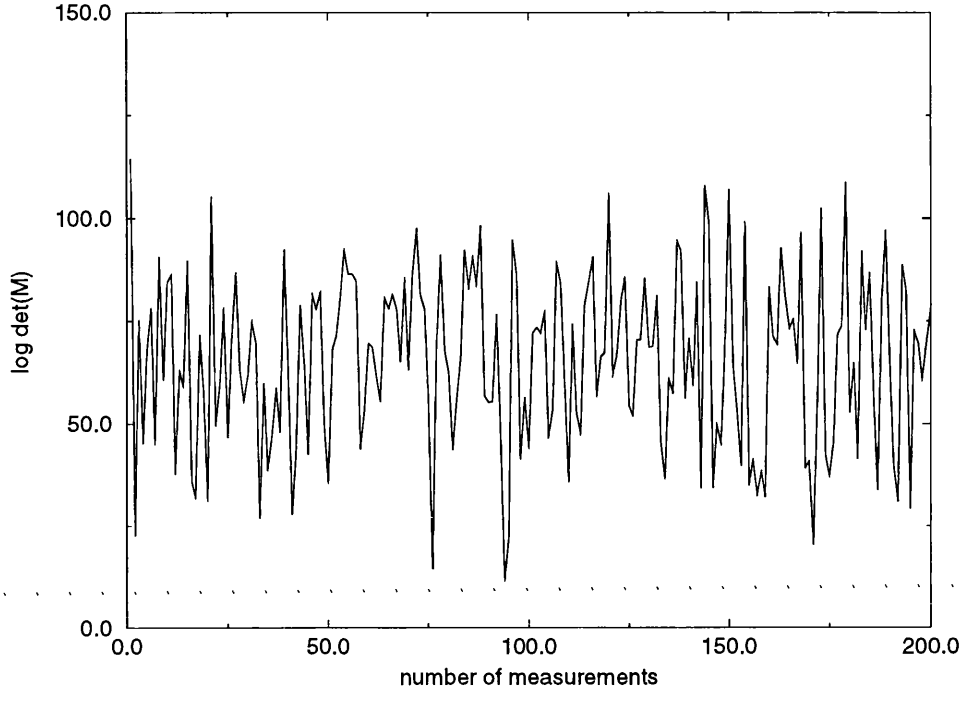

Figure 5.2: The HMC time evolution of $\ln|\det M|$ on an 8^4 lattice at $\beta = 5.1$ and $ma = 0.01$.

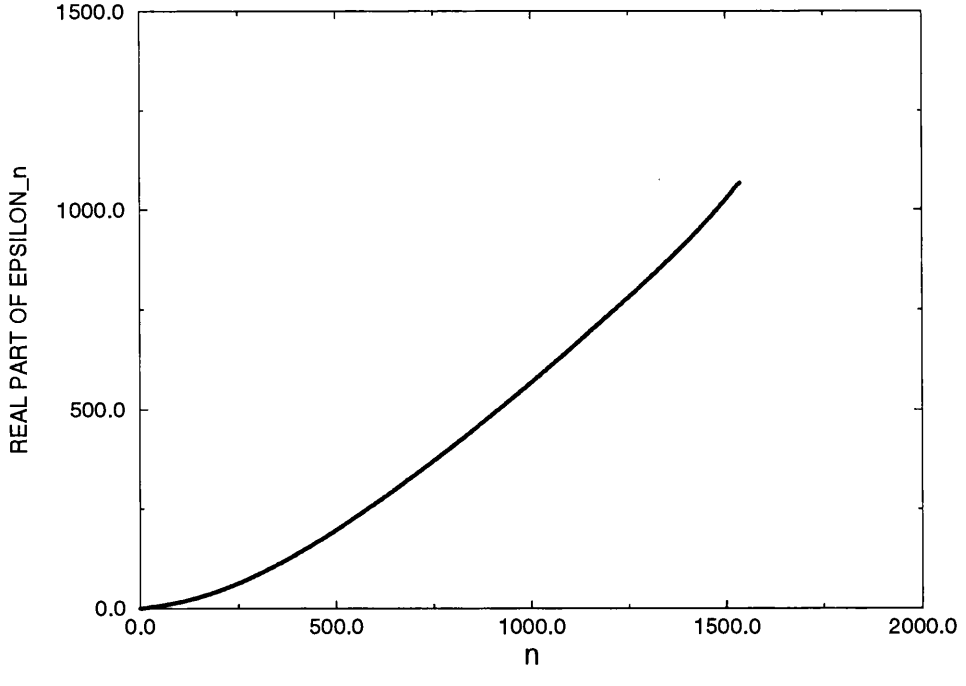

Figure 5.3: Plot showing the continuity of the coefficients on an 8^4 lattice at $\beta = 5.1$ and $ma = 0.01$.

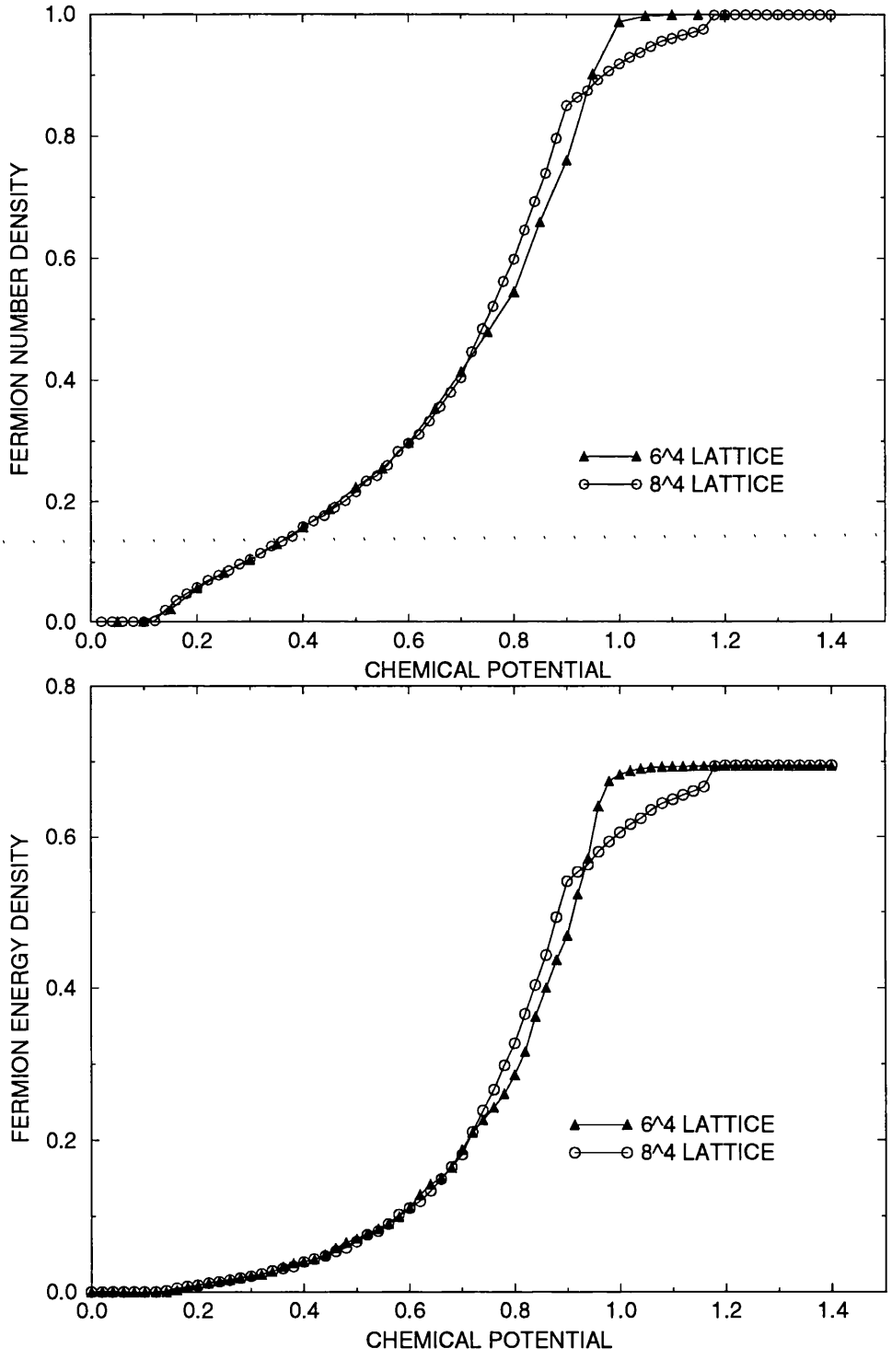

Figure 5.4: Comparison of fermion number density and fermion energy density on 6^4 and 8^4 lattices at $\beta = 5.1$ and $ma = 0.01$.

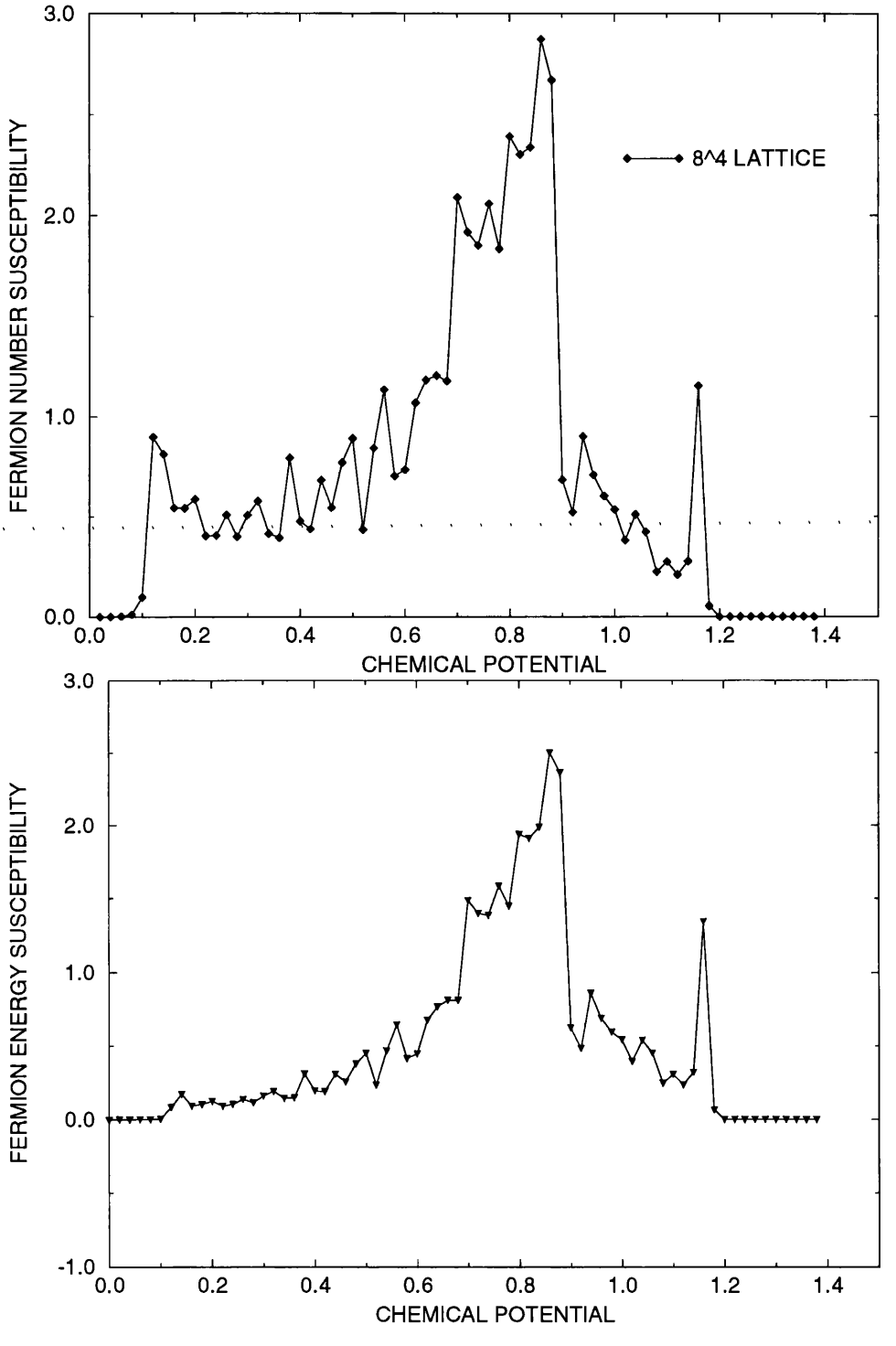

Figure 5.5: Susceptibility of fermion number density and fermion energy density on an 8^4 lattice at $\beta = 5.1$ and $ma = 0.01$.

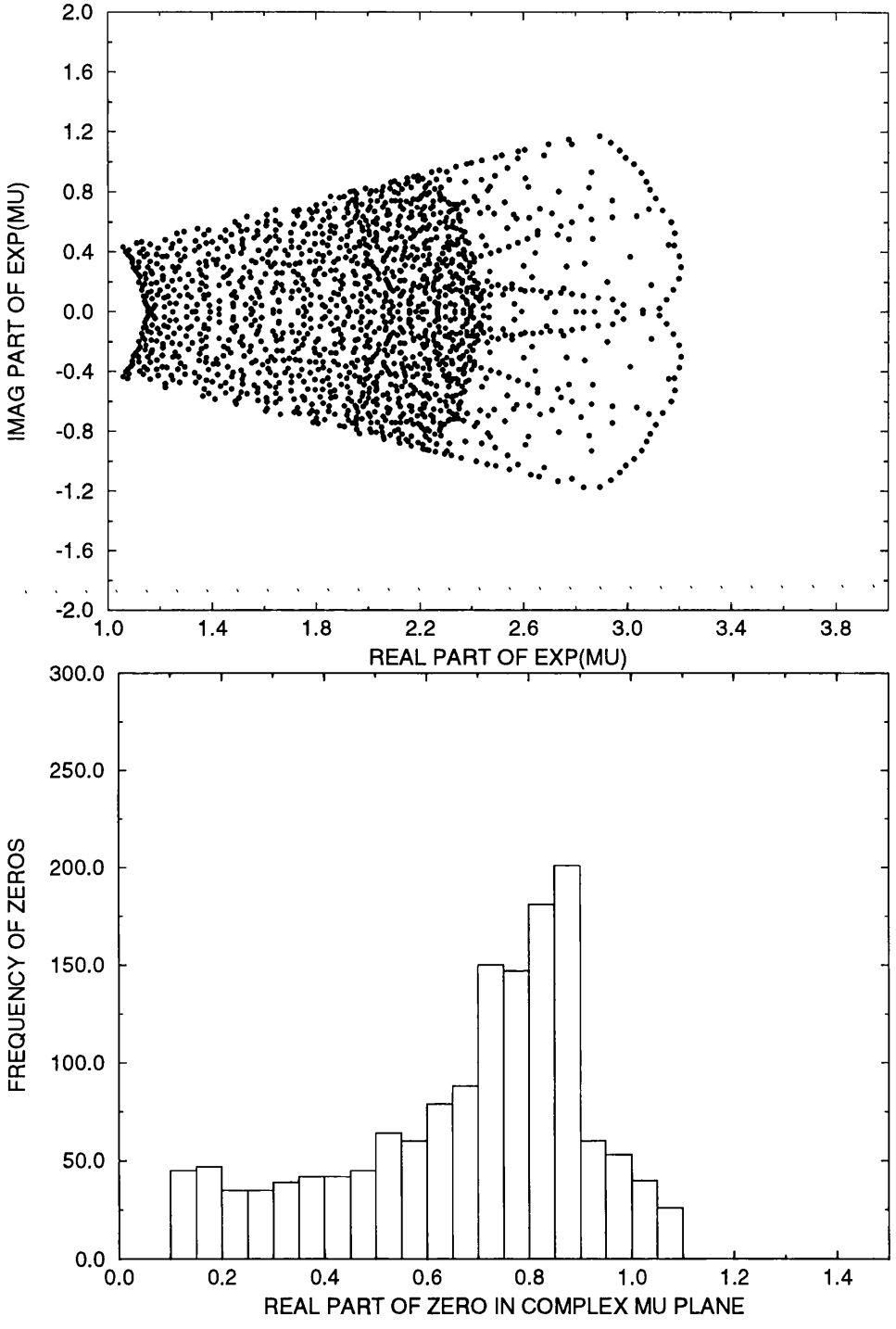

Figure 5.6: Data for the zeros on an 8^4 lattice at $\beta = 5.1$ and $m = 0.01$. The upper diagram is a plot of the zeros in the complex e^{μ} plane and the lower diagram is the corresponding histogram of the real parts of the zeros in the complex chemical potential plane. The general features are very similar to the zeros analysis of the strong coupling ($\beta = 0$) simulations

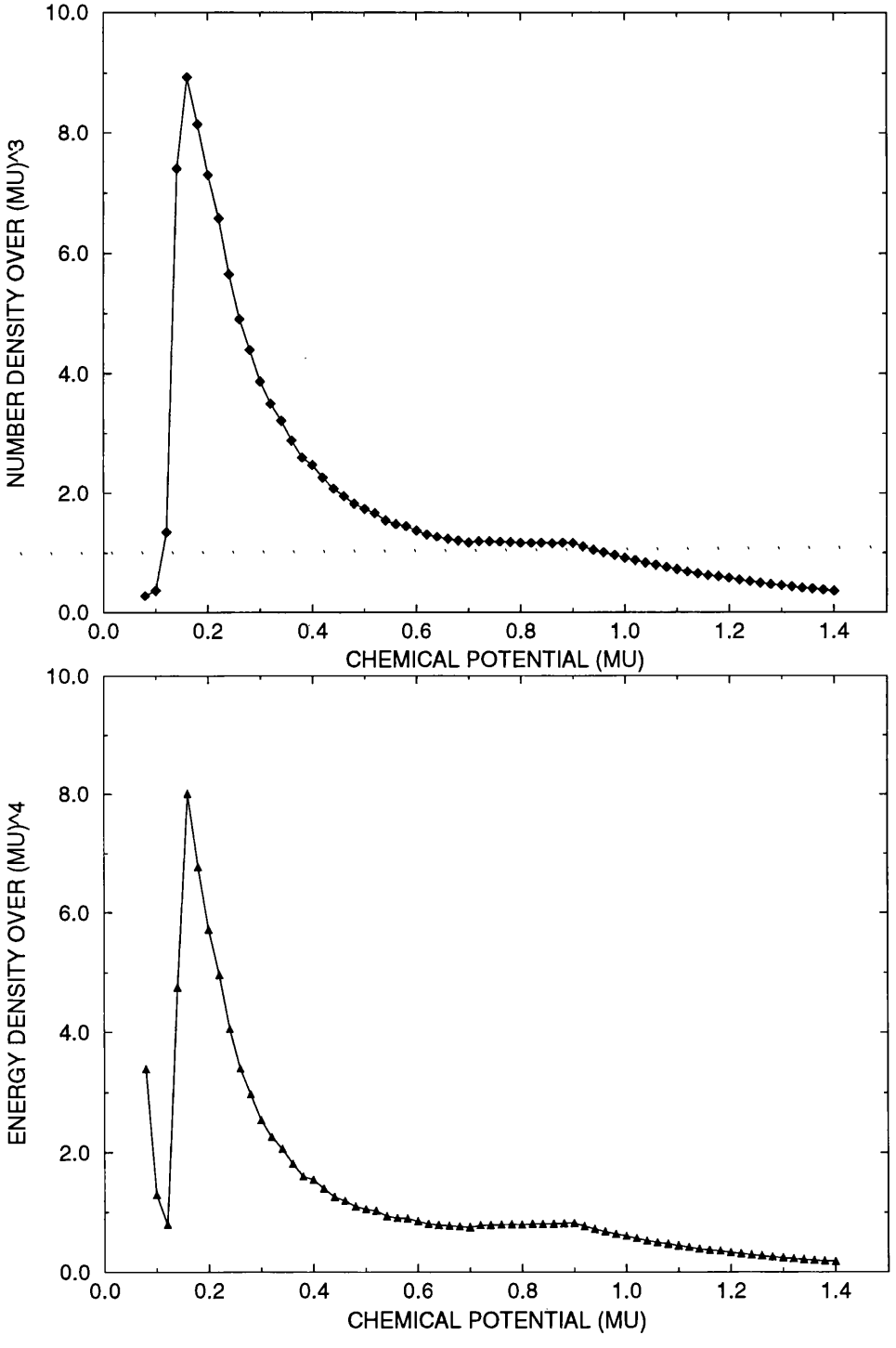

Figure 5.7: Comparison with the expected continuum behaviour of the scaling of the number density (top) and energy density (bottom) for simulation data from an 8^4 lattice with $\beta = 5.1$ and $m = 0.01$

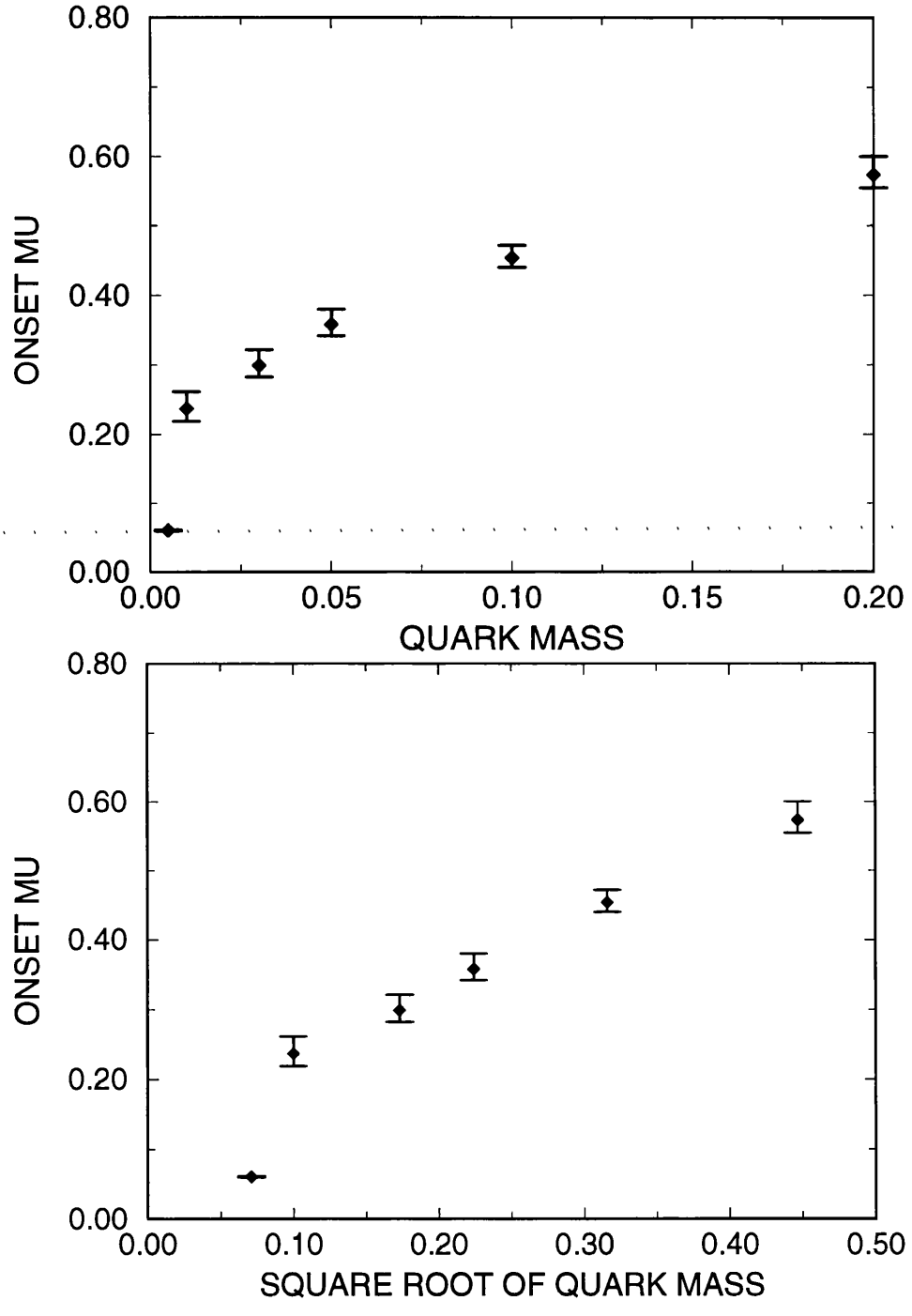

Figure 5.8: The quark mass dependence of the onset μ ($\beta = 5.1$ on a 6^4 lattice).The bare quark masses were $ma = 0.005$, 0.01, 0.03, 0.05, 0.1, 0.2

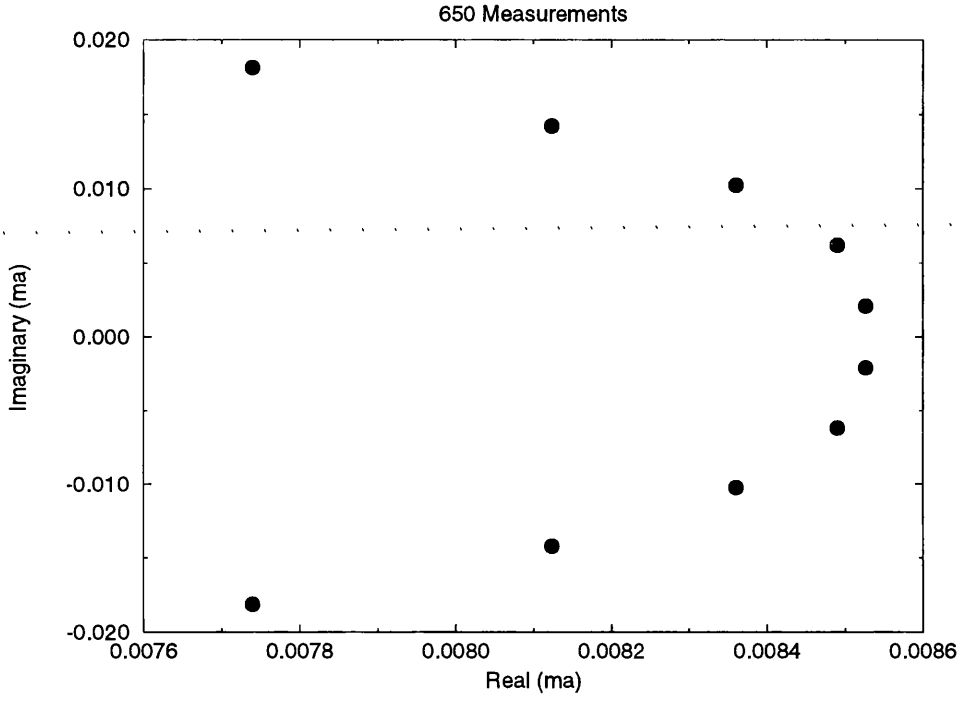

Figure 5.9: The zeros in the complex mass plane on an 6^4 lattice at $\beta = 5.1$ and $ma = 0.01$. These zeros confirm that the system is in the deconfined phase at $\mu = 0$ for $ma \lesssim 0.01$.

Chapter 6

Exploratory study of the 3 Dim $U(1)$ Gross-Neveu Model at $\mu \neq 0$

6.1 Introduction

The original motivation for studying four-fermion interaction models was the fact that they offer considerable insight into the phenomenon of *dynamical chiral symmetry breaking* in strong interaction physics [57]. The only degrees of freedom involved correspond to fermions which are coupled through a short-range interaction. At strong couplings, realisation of the Nambu-Goldstone mechanism of chiral symmetry breaking results in the appearance of scalar bound states in the particle spectrum. The fermions interact by exchanging these scalar bound states analogous to the case of the linear σ-model where the fermions are coupled to scalars by a Yukawa interaction. The Gross-Neveu model is the simplest relativistic theory of interacting fermions.

We have seen that the simulations of full QCD using the Glasgow algorithm reweighting method, the initial onset of the critical behaviour at non-zero μ appears to be controlled by the pion mass rather than the mass of the lightest baryon. Since the inclusion of the fermion determinant in the simulations was expected to eliminate the anomalous early onset of criticality first observed in the quenched theory (which replaces the complex fermion determinant by unity), the question of whether the reweighting procedure is sufficiently effective in its implementation

of dynamical fermions must be addressed. To check whether the persistence of μ_o is an artifact arising from measuring our observables on an ensemble generated at $\mu = 0$ we have implemented our reweighting method in an exploratory study of the 3 dimensional $U(1)$ Gross-Neveu model at finite density. The lattice formulation of this model is described in ref.[2]. In this paper Hands, Kim and Kogut present a thorough study of chiral symmetry restoration using an *exact* algorithm which generates the statistical ensemble at $\mu \neq 0$ (i.e. at the μ at which the measurement of the thermodynamic observable was made). Such exact simulations are possible because in this simple model the fermion determinant is real and non-negative even when $\mu \neq 0$. Therefore standard Monte-Carlo algorithms can be used to study its critical behaviour as a function of μ. The 3-dim $U(1)$ Gross-Neveu model lacks two important features of QCD

- the model does NOT confine quarks.
- model does NOT have a COMPLEX fermion determinant when $\mu \neq 0$.

However the GN model is known to have a chiral transition and **does have a massless pion** in the broken phase ($\mu < \mu_c$) in the chiral limit ($m_q \to 0$). Quantitative studies are possible since analytic predictions from the leading order $1/N_f$ expansion can be compared with Monte Carlo simulations. Hands, Kim and Kogut addressed the question of whether the presence of the massless Goldstone pion in the theory was possibly responsible for the pathologies linked with m_π in QCD simulations . Their simulations of the GN model were completely successful producing physical results in agreement with the predictions of the $1/N_f$ expansion. Their study concluded that the presence of a massless pion is **not** the source of difficulties in lattice QCD. Validation of the full QCD reweighting technique requires confirmation that the onset of non-zero fermion number density is in agreement with the results of the exact simulation i.e. that the onset is unrelated to the Goldstone pion in this simple model. Note that the gauge fields are effectively unity in the GN model so that the variation of $\det M(\mu)$ as μ is increased through the chiral transition region is largely determined by the expectation values of the σ and π auxiliary fields. Sigma acts like a dynamical fermion mass in this four-fermi theory so we expect $\langle\sigma\rangle$ to fall sharply for $\mu > \mu_c$ and this will inevitably affect the observables via the "reweighting factor" $\frac{\det M(\mu \neq 0)}{\det M(\mu=0)}$. In QCD the situation is more complicated since the gauge fields **do** contribute to the dynamics via the probability measure $\det M(\mu = 0)e^{-S_G}$.

6.1.1 The Lattice Formulation

The lattice action for the bosonized Gross-Neveu model with U(1) chiral symmetry is

$$\begin{aligned} S &= \sum_{i=1}^{N_f/4}\Big[\sum_{x,y}\bar{\chi}_i(x)\mathcal{M}_{x,y}\chi_i(y) \\ &+ \frac{1}{8}\sum_x \bar{\chi}_i(x)\chi_i(x)\Big(\sum_{<\tilde{x},x>}\sigma(\tilde{x}) + i\varepsilon(x)\sum_{<\tilde{x},x>}\pi(\tilde{x})\Big)\Big] \\ &+ \frac{N_f}{8C^2}\sum_{\tilde{x}}(\sigma^2(\tilde{x})+\pi^2(\tilde{x})). \end{aligned} \tag{6.1}$$

Here, χ_i and $\bar{\chi}_i$ are complex Grassmann-valued staggered fermion fields defined on the lattice sites, the auxiliary scalar and pseudoscalar fields σ and π are defined on the dual lattice sites, and the symbol $\langle\tilde{x},x\rangle$ denotes the set of 8 dual sites $\tilde{x}$ adjacent to the direct lattice site x. N_f is the number of physical fermion species and $1/C^2$ is the four-fermi coupling. The symbol $\varepsilon(x)$ denotes the alternating phase $(-1)^{x_0+x_1+x_2}$.

The fermion kinetic operator $\mathcal{M}$ is given by

$$\mathcal{M}_{x,y} = \frac{1}{2}\Big[\delta_{y,x+\hat{0}}e^{\mu} - \delta_{y,x-\hat{0}}e^{-\mu}\Big] + \frac{1}{2}\sum_{\nu=1,2}\eta_\nu(x)\Big[\delta_{y,x+\hat{\nu}} - \delta_{y,x-\hat{\nu}}\Big] + m\delta_{y,x}, \tag{6.2}$$

where m is the bare fermion mass, μ is the chemical potential, and $\eta_\nu(x)$ are the Kawamoto-Smit phases $(-1)^{x_0+\cdots+x_{\nu-1}}$.

This lattice model (at non-zero lattice spacing) has the symmetry: $\mathrm{U}(N_f/4)_V \otimes \mathrm{U}(N_f/4)_V \otimes \mathrm{U}(1)_A$. It is the $\mathrm{U}(1)_A$ symmetry which is broken, either spontaneously by the dynamics of the system, or explicitly by a bare fermion mass. We simulated the $N_f = 12$ model corresponding to three lattice species.

The expansion of this GCPF is very similar to that described above for standard QCD. At finite density the Dirac fermion matrices M and $\hat{M}$ are given by:

$$\begin{aligned} 2iM_{xy}(\mu) &= Y_{xy} + G_{xy} + V_{xy}e^{\mu} + V^{\dagger}_{xy}e^{-\mu} \\ -2i\hat{M}_{xy}(\mu) &= Y^{\dagger}_{xy} + G_{xy} + V_{xy}e^{\mu} + V^{\dagger}_{xy}e^{-\mu}. \end{aligned}$$

where

$$Y = 2i(m_q + \frac{1}{8}\sum_{<x,\tilde{x}>}(\sigma(\tilde{x}) + i\epsilon\pi(\tilde{x})))\delta_{xy}. \tag{6.3}$$

The determinants of these fermion matrices are related to that of the propagator matrix

$$P = \begin{pmatrix} -GV - YV & V \\ -V & 0 \end{pmatrix} \tag{6.4}$$

by

$$\begin{aligned} \det(2iM) &= e^{3\mu n_s^3 n_t} \det(P - e^{-\mu}) \\ \det(2i\hat{M}) &= e^{3\mu n_s^3 n_t} \det((P^{-1})^\dagger - e^{-\mu}) \end{aligned} \tag{6.5}$$

As for standard QCD, determination of the eigenvalues of P^{n_t} gives the expansion for the GCPF:

$$Z = \sum_{n=-2n_s{}^2}^{2n_s{}^2} < b_{|n|} > e^{n\mu n_t} = \sum_{n=-2n_s{}^2}^{2n_s{}^2} e^{-(\epsilon_n - n\mu)/T}. \tag{6.6}$$

6.1.2 Results

We performed simulations developing the ensemble at $\mu = 0$ to confirm that evaluation of the grand canonical partition function via reweighting does give an extrapolation which predicts the correct critical behaviour. The number density for a 16^3 lattice at a four-fermion coupling of $1/C^2 = 0.5$ and a bare fermion mass $m = 0.01$ is shown in Fig. 6.1. The chemical potential at which the number density, $\langle n \rangle$, becomes non-zero, μ_o, is correctly predicted. Note that from our simulation $\mu_o \sim 0.5$ but $\frac{m_\pi}{2} \sim 0.1$ (from ref. [2]) so the reweighting procedure is consistent with the exact simulations in that there is no evidence for an anomalous onset connected with the Goldstone pion.

Comparison with the exact simulation [2] (in which generation of the ensemble was at the μ at which the measurement was made) clearly shows that in this model the reweighting procedure results in an underestimation of the number density at $\mu > \mu_o$. In fact the discontinuity in $\langle n \rangle$ corresponding to μ_c is absent in the number density estimated from the coefficients of the GCPF generated on an ensemble at $\mu = 0$.

In the GN model the gauge fields do not contribute to the dynamics so that the gauge links are effectively identity matrices. In this case it is instructive to compare our simulation data for the fermion number density as a function of chemical potential with the predicted behaviour of a free fermi gas.

The expression for a free Fermi gas is obtained by summing over the finite set of Matsubara frequencies [58] that arises in the lattice thermodynamics. The appropriate expressions for the momentum sums for a 3-dimensional free lattice gas are :-

$$n_{free} = 2i \int_{-\pi}^{\pi} \frac{d^3p}{2\pi^4} \frac{\sin(p_0 + i\mu)\cos(p_0 + i\mu)}{\sum_{i=1}^{2} \sin^2 p_i + sin^2(p_0 + i\mu)} \tag{6.7}$$

and

$$\epsilon_{free} = 2 \int_{-\pi}^{\pi} \frac{d^3p}{2\pi^4} \frac{\sin^2(p_0 + i\mu)}{\sum_{i=1}^{2} \sin^2 p_i + sin^2(p_0 + i\mu)} - \frac{1}{2} \tag{6.8}$$

where p_0 is associated with the temporal direction. Exact simulations showed that for the above four-fermi coupling and fermion mass the theory has a critical chemical potential $\mu_c = 0.725(25)$ at which the chiral symmetry is restored. The profile of the number density and energy density in the exact simulations corresponds to that of a free lattice gas of mass m_q for $\mu > \mu_c$ so it is consistent with a free fermion gas in the chiral limit. Using the Glasgow reweighting algorithm it was only possible to achieve free-fermion gas behaviour in the number density for an *update* chemical potential $\mu > \mu_c$. Note that in the Gross-Neveu model it is possible to generate an ensemble at a non-zero update chemical potential whereas in QCD we are restricted to updating at $\mu = 0$ because the determinant is complex for finite density QCD.

The influence of the update chemical potential is illustrated in the upper portion of Fig. 6.1 which shows the number density obtained from an ensemble generated at an update $\mu = 0.8$, which is greater than μ_c. In the chiral limit the number density is consistent with that of a free gas of massless fermions whereas the number density from the $\mu = 0$ update is that of a free gas of massive fermions. The exact results show the transition between these two phases at μ_c.

The Lee-Yang zeros in the complex μ plane are the zeros of Eqn. 6.6 and should signal the critical μ associated with the chiral transition transition. They are shown in Fig. 6.1 There is a line formed by 6 zeros, two of which are isolated from the rest of the distribution. The line intersects the real μ axis at $\mu = 0.72$, in agreement with the critical μ found by the exact method.

Hence we find that for four-fermi coupling $1/C^2 = 0.5$ and $m = 0.01$ the onset μ found via the number density is not controlled by the Goldstone boson, and the critical μ is given by the distribution of the Lee-Yang zeros.

We repeated our simulations with the reweighting method for $1/C^2 = 0.8$ and the same quark mass ($m = 0.01$). At this coupling the results from exact simulations were much less well-defined with the fermion number and energy densities forming smooth curves with a much less obvious discontinuity than in the case of $1/C^2 = 0.5$. The simulation results showed the same general features as the $1/N$ calculation although the μ_c is much more difficult to locate especially from the number and energy densities. The transition was shown with greater clarity in the model's spectroscopy. From the exact simulations Hands et. al. concluded that the transition was in the vicinity of $\mu_c = 0.295(3)$ and again there was no evidence for pathological behaviour at $\mu = m_\pi/2 \simeq 0.11(1)$. Our own results are plotted in Fig. 6.2. Again the Glasgow algorithm underestimates the number density based on a comparison with the exact simulation. The zeros which correctly predicted μ_c in

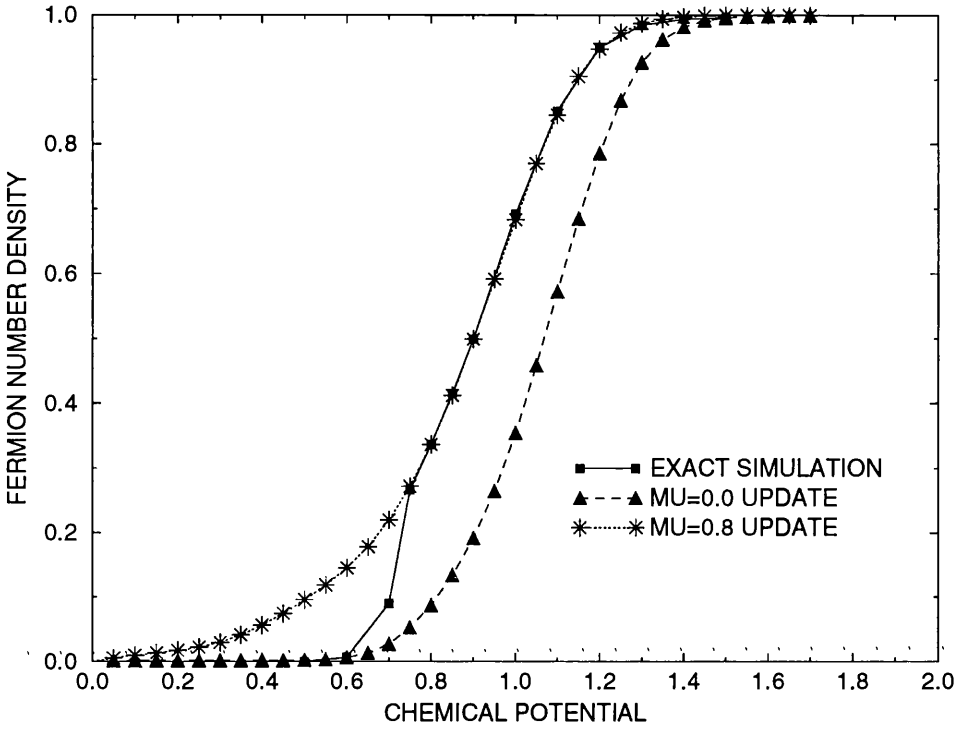

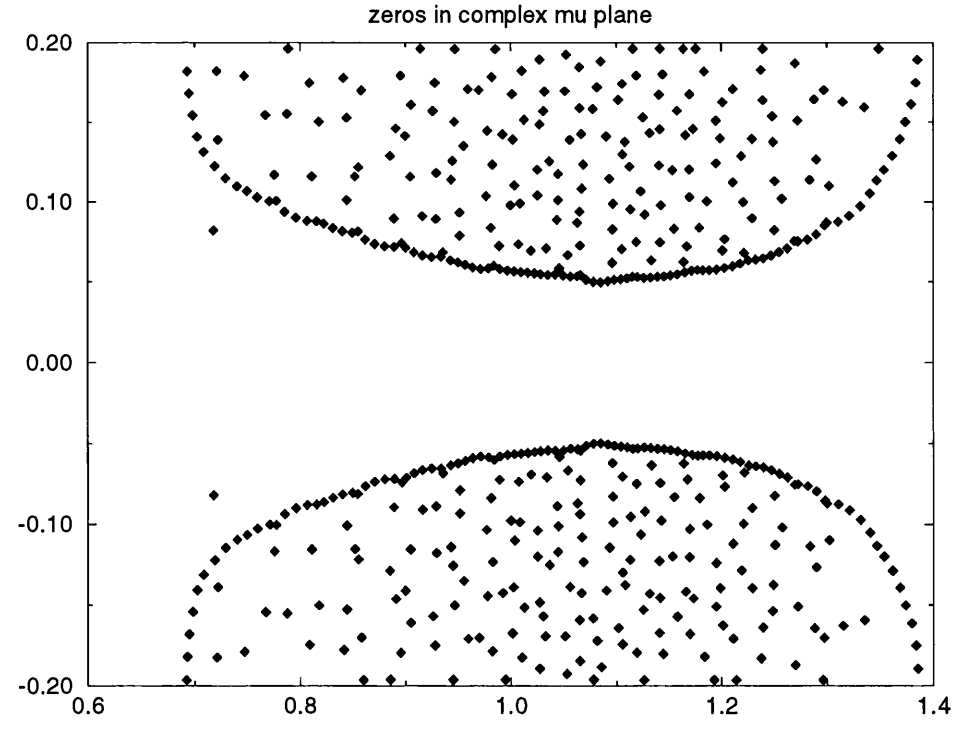

Figure 6.1: The upper diagram shows the fermion number density vs. the chemical potential, μ, on a 16^3 lattice. The lower diagram shows the Lee-Yang zeros in the complex μ plane for the Gross-Neveu model with $1/C^2 = 0.5$ and fermion mass 0.01 on a 16^3 lattice

the case of $1/C^2 = 0.5$, this time indicate $\mu_c \sim 0.4$ which differs slightly from the value from the exact simulations. This could however be due to the difficulty in locating the transition point at this particular four-fermi coupling.

A comparison of the predictions of the lattice gap equation for the fermion number density with the profile for a free lattice gas is made in Fig. 6.3. For both four-fermi couplings the behaviour for $\mu > \mu_c$ is very well approximated by a free lattice gas. Note that for four-fermi coupling of 0.8 the gap equation starts to agree with the free lattice gas behaviour for $\mu \sim 0.4$ which is consistent with the estimate of μ_c from the zeros of the Glasgow reweighting method. The upper portion of Fig. 6.4 shows the effect of a finite bare-quark mass in the simulations. As the bare quark mass is increased μ_c gradually increases and the number density takes longer to converge with the free lattice gas curve.

It is easily shown from a numerical evaluation of the gap equation that the onset in the Gross-Neveu model is simply a finite size effect i.e. as the lattice size is increased μ_o increases accordingly as the transition sharpens up. This is demonstrated in Fig. 6.4 where the number density profiles for four-fermi coupling 0.8 with $m = 0.01$ and for 8^3, 16^3 and 32^3 lattices have been plotted. Note that even on a 32^3 lattice the transition is not particularly sharp yet.

6.2 Summary of Gross-Neveu Model Simulations

Exploratory simulations of the 3 dimensional Gross-Neveu model using the Glasgow reweighting procedure have confirmed the findings of the exact simulations in that there is no evidence for the pathologies connected with the pion mass which appear in standard QCD at finite chemical potential. There is good evidence that μ_c can be accurately predicted from the zeros distribution (as long as the update chemical potential is less than the critical value) and this is certainly true at four-fermi coupling $1/C^2 = 0.5$ where the transition is strongly first order. The general vicinity of the transition can be confidently predicted for $1/C^2 = 0.8$. The fermion number density is inconsistent with that from the exact simulations for both four-fermi couplings tried and for $1/C^2 = 0.5$ the Glasgow algorithm did not pick up the discontinuity. The efficiency of the reweighting algorithm should certainly increase as higher statistics are obtained and in both of the simulations described above only a modest number of measurements (around 300) were made. The problems with the number density profile must originate from the fact that we have generated the configurations at zero chemical potential. However a very high statistics simulation

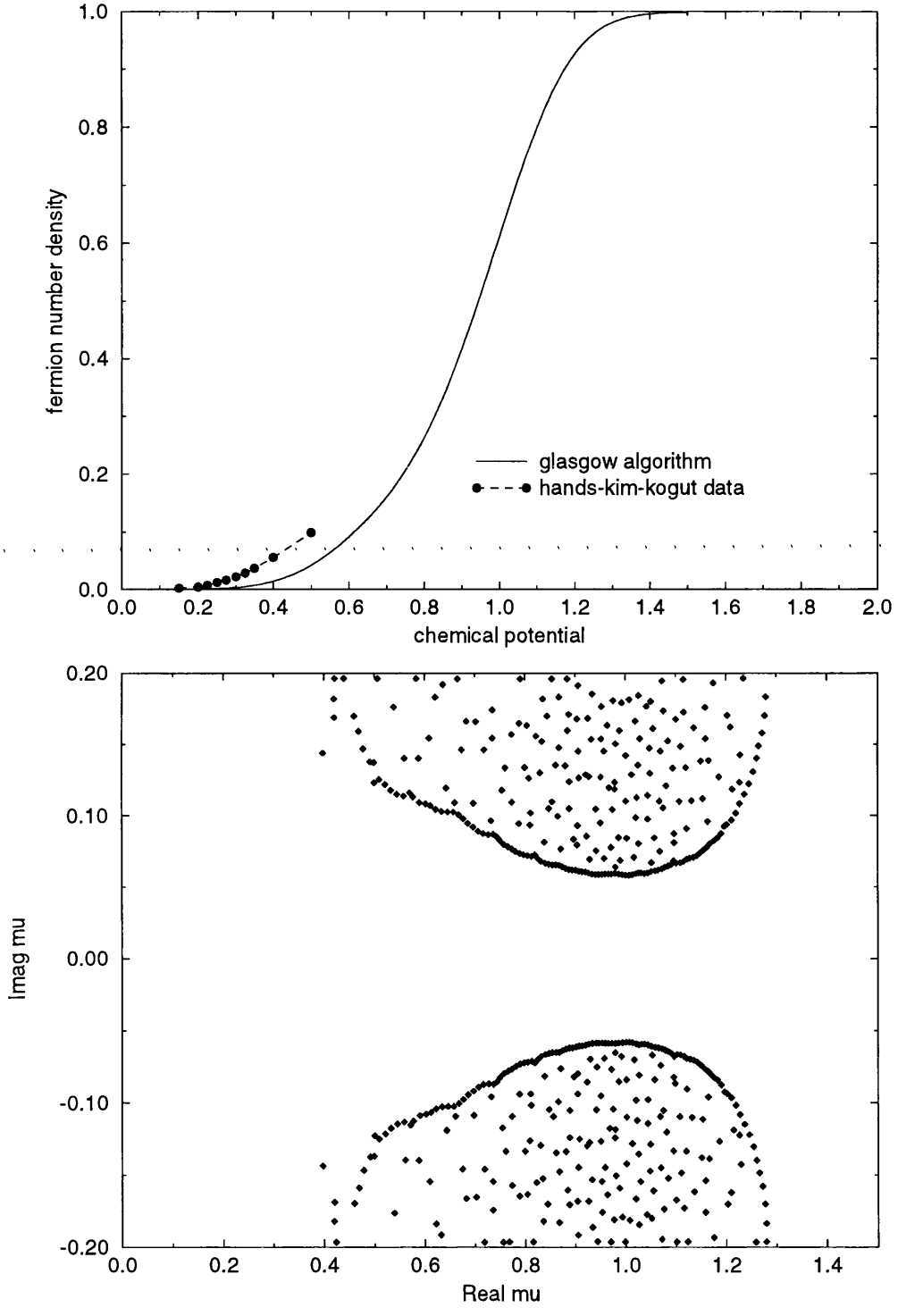

Figure 6.2: The upper diagram shows the number density estimated using the Glasgow reweighting algorithm alongside the results from the exact algorithm. The lower figure shows the zeros in the complex μ plane for the same data set for a 16^3 lattice with $1/C^2 = 0.8$ and $m = 0.01$

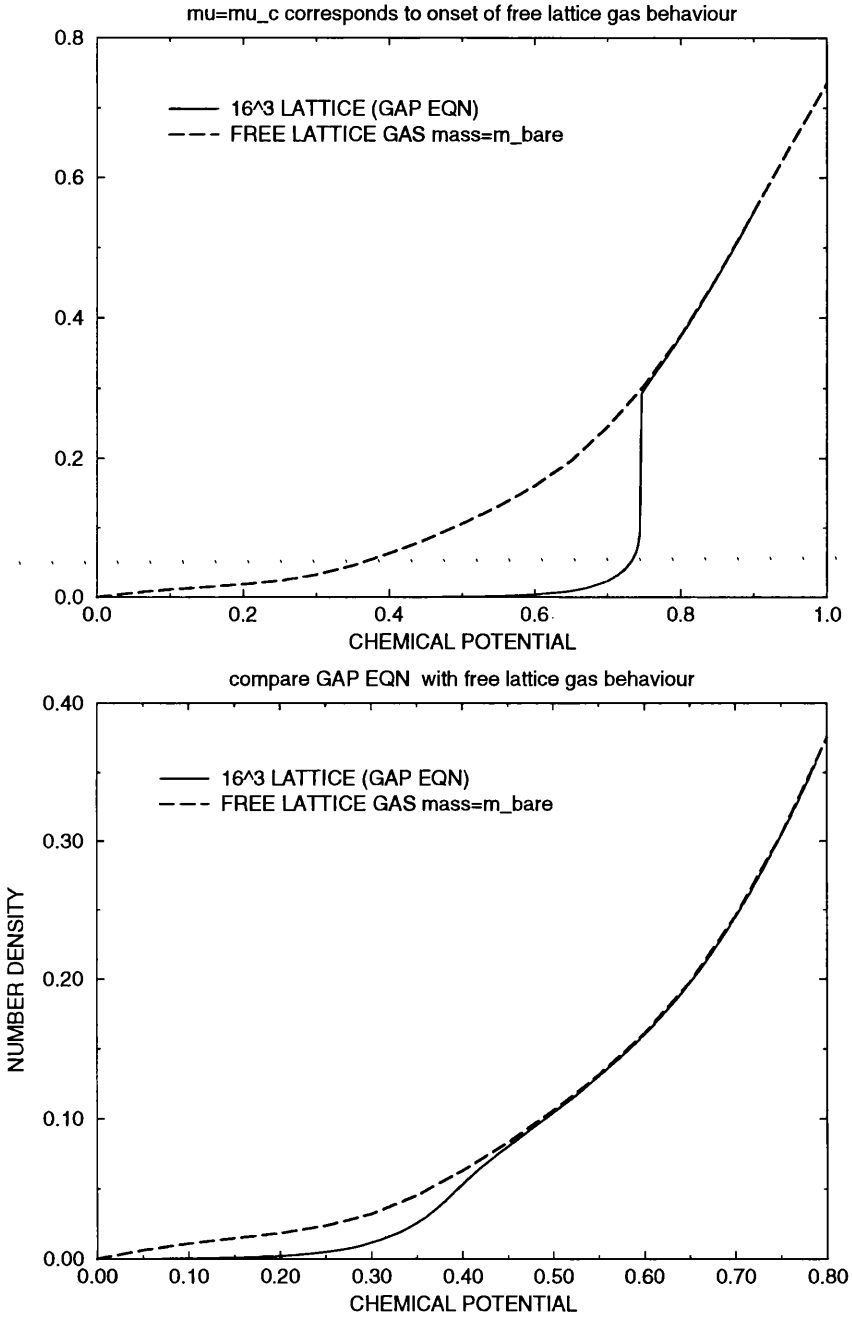

Figure 6.3: The upper diagram shows the number density profile from the lattice gap equation on a 16^3 lattice for $m = 0.01$ and four-fermi coupling 0.5 and the lower diagram gives the same for $1/C^2 = 0.8$. In both cases a comparison with the free lattice gas behaviour is given and the gap equation results are seen to agree with the lattice gas for $\mu > \mu_c$

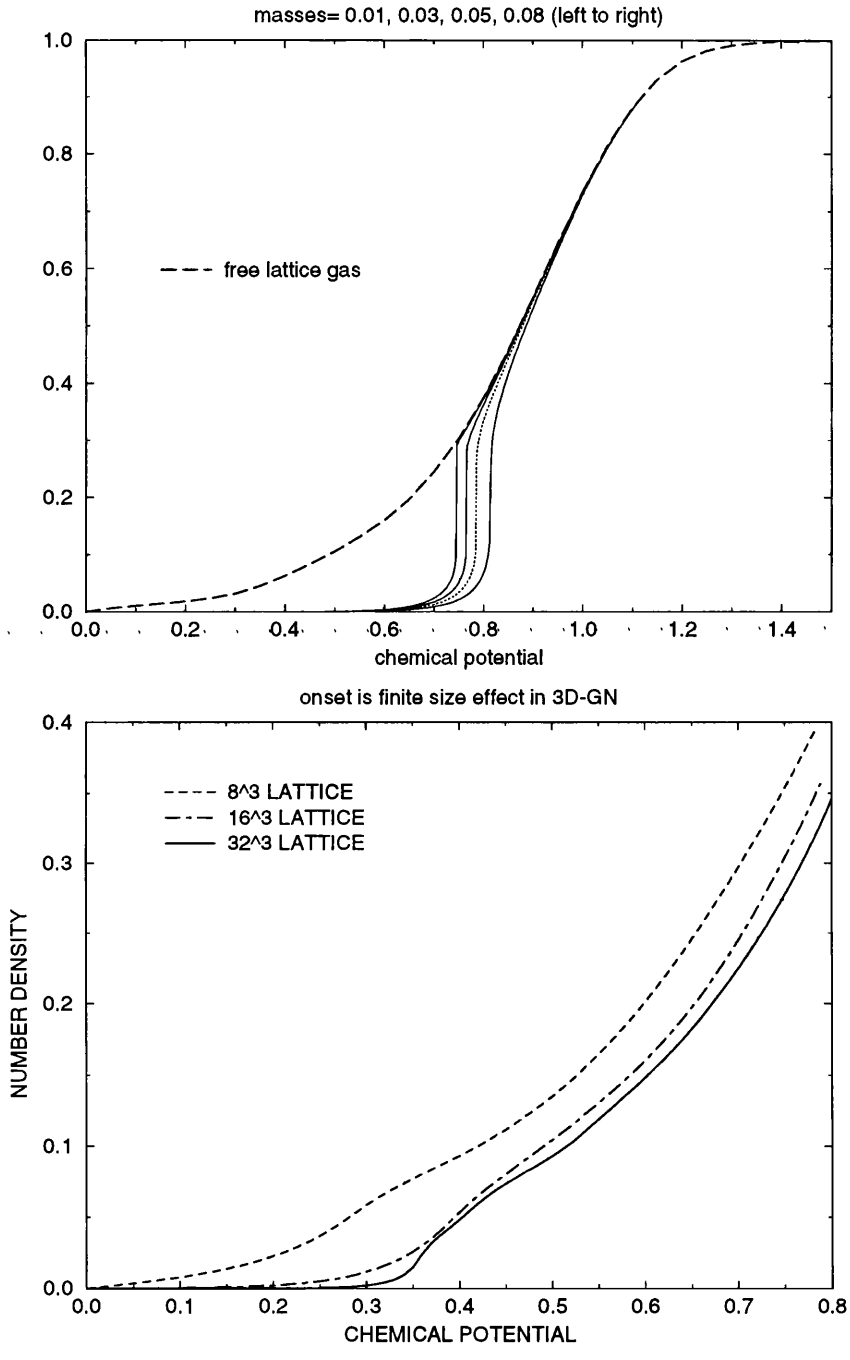

Figure 6.4: The upper diagram shows the effects of a finite bare quark mass on the gap equation prediction for the number density as a function of chemical potential for a 16^3 lattice with $1/C^2 = 0.5$ and $m = 0.01$. We expect the chiral transition to be washed out for sufficiently large bare quark masses. The lower diagram shows the number density profile as predicted by the gap equation with $1/C^2 = 0.8$, $m = 0.01$ and for three lattice sizes: 8^3, 16^3 and 32^3. The onset of non-zero number density is clearly a finite size effect in this model.

may well eliminate this problem. Alternatively the reweighting method could be improved if a better starting point were invented.

It is important to bear in mind that the outcome of this exploratory study cannot be translated directly to finite density QCD because as already mentioned some of the key ingredients of QCD are missing in the Gross-Neveu model. Unfortunately the GN model does not allow us to assess the crucial role which quark confinement plays in relation to the chiral transition. The most significant comparative factor in terms of the reweighting procedure is that in the Gross-Neveu model the gauge fields are all equal to unity whereas in QCD they make an important contribution to the dynamics. Although with limited statistics we certainly cannot trust the numerical values for the number and energy densities obtained from the reweighting method in the Gross-Neveu model we have shown that the zeros do correctly predict the critical chemical potential for the chiral transition and there is no evidence that the pion causes pathologies in this model.

Chapter 7

χQCD - Lattice Simulations at Non-Zero Chemical Potential in the Chiral Limit

7.1 Introduction to Four-Fermion Interaction Models

The unphysical results of early quenched QCD simulations at finite density whereby an infinitesimal chemical potential led to chiral symmetry restoration in the theory with massless quarks have taught us that simulation studies of QCD at $\mu \neq 0$ **must incorporate dynamical fermions.** It is believed that a correct implementation of dynamical fermions should result in the disappearance of the early pathological onset, μ_o, first observed in the quenched theory.

As described in Chapters 4 and 5, in the simulations of full QCD (using the Glasgow algorithm which involves generation of the statistical ensemble at $\mu = 0$ in conjunction with reweighting w.r.t. $\frac{\det M(\mu \neq 0)}{\det M(\mu=0)}$) the initial onset of the critical behaviour at non-zero μ was controlled by the pion mass rather than that of the lightest baryon. This result was unexpected. To assess whether this is an artifact of measuring our observables on an ensemble generated at $\mu = 0$, an implementation of the above reweighting method in a study of the 3-dimensional Gross-Neveu model at finite density has been investigated. This has shown that the chemical potential at which the number density, becomes non-zero, μ_o, is correctly predicted and there is no evidence for pion dependence in this simple four-fermion interaction model.

Due to the persistent dependence of the quenched onset of criticality in full QCD simulations at non-zero μ, and in the wisdom of experience with the Gross-Neveu model simulations where the anomalous pion-dependence is absent, we have investigated a new approach to QCD at finite density which has several important features. We add a chiral invariant four-fermi interaction terms to the standard QCD lattice action. These additional four-fermi interaction terms become irrelevant (in the renormalization group sense) as the lattice spacing is reduced to zero and thus should not affect the critical properties of QCD in the continuum limit. However at finite lattice spacings the four-fermi terms favour the generation of a dynamical fermion mass [59]. Since this dynamical mass removes the singularity in the Dirac operator it allows us to study the behaviour of the theory in the chiral limit of **exactly massless quarks.** This is not practical in standard QCD simulations where we rely on an extrapolation to zero bare quark mass. We refer to this modified version of QCD with an additional four-fermi interaction as χQCD [54].

An additional advantage of the χQCD algorithm is that it runs more efficiently and more than an order of magnitude faster than the standard QCD algorithm. In addition, at $m_q = 0$ there is a **massless** Goldstone pion in χQCD.

Note that at zero gauge coupling χQCD reduces to a Nambu-Jona-Lasinio model.

7.2 QCD with an additional Four-Fermi Interaction

In the following formulation we will add an irrelevant four-fermi interaction term to the standard QCD action. This additional term is of the form:

$$C^2 \left((\bar{\psi}\psi)^2 + (\bar{\psi}\gamma_5\psi)^2 \right) \tag{7.1}$$

For the purposes of analysis and simulations we require an action which is formally quadratic in the staggered fermion fields. The standard process of *bosonization* is used to linearize this four-fermion interaction term. We use the fact that the path integral of Gaussian functions can be performed exactly by applying following identity:-

$$\int D\Theta \exp\left[i \int d^4x \left(\pm A\Theta - B\Theta^2 \right) \right] = \frac{1}{Z'} \exp\left[i \int d^4x \, \frac{A^2}{4B} \right] \tag{7.2}$$

where Θ represents the auxiliary field; A will be associated with $(\bar{\psi}\psi)$ or $(\bar{\psi}\gamma_5\psi)$ and Z' is an infinite normalisation constant which need not be known explicitly.

This explains the origin of the auxiliary pseudoscalar fields σ and π in the χQCD Lagrangian below.

The molecular dynamics Lagrangian for this lattice theory with staggered quarks is

$$\begin{aligned} L &= -\beta\sum_{\square}[1-\frac{1}{3}\mathrm{Re}(\mathrm{Tr}_{\square}UUUU)]+\sum_{\dot{s}}\dot{\psi}^{\dagger}M^{\dagger}M\dot{\psi} \\ &\quad -\sum_{\bar{s}}\frac{1}{8}N_f\gamma(\sigma^2+\pi^2)+\frac{1}{2}\sum_{\bar{s}}(\dot{\sigma}^2+\dot{\pi}^2) \\ &\quad +\frac{1}{2}\sum_{l}(\dot{\theta}_7^2+\dot{\theta}_8^2+\dot{\theta}_1^*\dot{\theta}_1+\dot{\theta}_2^*\dot{\theta}_2+\dot{\theta}_3^*\dot{\theta}_3) \end{aligned} \tag{7.3}$$

where

$$M = \not{D}+m_q+\frac{1}{16}\sum_i(\sigma_i+i\epsilon\pi_i) \tag{7.4}$$

$\epsilon=(-1)^{x+y+z+t}$ and the θ_i parametrize the SU(3) link variables U,

The dual sites on the lattice of volume $n_t\times n_s^3$ are labelled by $\tilde{s}$ [60] and the auxiliary fields σ and π linearize the 4-fermi term. This Lagrangian describes $N_f=8$ flavours. For N_f which is not a multiple of 8 we use "noisy fermions" [29] and multiply the fermion kinetic term by $N_f/8$.

After integrating over the auxiliary fields, the lattice model approximates to the continuum theory

$$L=\bar{\psi}\left(\gamma^{\mu}D_{\mu}+\mu\gamma_0+m_0\right)\psi-\frac{C^2}{2N_f/4}\left[\left(\bar{\psi}\psi\right)^2-\left(\bar{\psi}\gamma_5\psi\right)^2\right]-\frac{1}{2g^2}Tr\left(F_{\mu\nu}F^{\mu\nu}\right) \tag{7.5}$$

where $\beta=2N_c/g^2$ and $C^2=1/\gamma$. The continuum theory (Eqn. 7.5) is invariant under the global $U(1)$ chiral symmetry

$$\bar{\psi}\rightarrow\bar{\psi}e^{i\gamma_5\theta}\ ,\ \psi\rightarrow e^{i\gamma_5\theta}\psi \tag{7.6}$$

Now consider the lattice model where for simplicity we consider a theory where the 4-fermion operator has a

$$U(1)\times U(1)\subset SU(N_f)\times SU(N_f)$$

flavour symmetry generated by $(1,i\gamma_5\xi_5)$ [61]. The component of the chiral symmetry generated by 1 is trivial since it is invariant under the following global transformation which holds for all values of the quark mass and leaves fermion bilinears (and quadrilinears) invariant

$$\dot{\psi}(n)\rightarrow e^{i\zeta}\dot{\psi}(n) \tag{7.7}$$

The most interesting component (which is only a symmetry when the quark mass is zero) is generated by $i\gamma_5\xi_5$. Under this symmetry the fields transform as

$$\begin{aligned} \dot{\psi}(n) &\rightarrow e^{-i\frac{1}{2}\phi\epsilon(n)}\dot{\psi}(n) \\ \sigma(n)+i\pi(n) &\rightarrow e^{i\phi}\left[\sigma(n)+i\pi(n)\right] \end{aligned} \tag{7.8}$$

from which we find that

$$\begin{aligned} \sigma(n)+i\epsilon(n)\pi(n) &\rightarrow e^{i\phi}\epsilon(n)\left[\sigma(n)+i\epsilon(n)\pi(n)\right] \\ A\dot{\psi}(n) &\rightarrow e^{i\frac{1}{2}\phi\epsilon(n)}A\dot{\psi}(n) \end{aligned} \tag{7.9}$$

and it follows that if $m_q = 0$, the Lagrangian is chirally invariant. The $U(1)$ chiral symmetry is spontaneously broken in the low density hadron phase through the dynamics of the colour gauge fields. The chiral condensate is defined by

$$\langle\bar{\chi}^a\chi^a\rangle = \frac{N_f}{4}\gamma\langle\sigma\rangle \tag{7.10}$$

where $\bar{\chi}^a$ and χ^a are the staggered fermion fields and each χ^a represents four degenerate flavours of fermions so that the sum over the flavour index a runs from 1 to $N_f/4$. The chiral condensate is nonzero in the broken phase and serves as the order parameter for the chiral transition. Consider how the addition of the four-fermi term facilitates simulations *directly* in the chiral limit. The Dirac operator of standard lattice QCD becomes singular as $m_q \rightarrow 0$ simply because m_q sits on the diagonal of the fermion matrix. By inspecting Eqn. 7.4 it is evident that the auxiliary scalar field σ appears on the diagonal in addition to the bare quark mass term. The Dirac operator in χQCD remains non-singular at $m_q = 0$ because the expectation value of σ is always non-zero. One might naively expect that as we approach the limit of QCD as we take $\gamma \rightarrow \infty$ that we would obtain $\langle\sigma\rangle \sim 0$, however this should not be the case. In fact in χQCD the QCD sector acts as an external symmetry breaking source to the auxiliary field scalar sector (analogous to an external magnetic field for a paramagnetic material) . Note that any gauge coupling is sufficient to drive chiral symmetry breaking on sufficiently large lattices. Therefore the expectation value of σ is always non-zero in χQCD even when the four-fermi coupling is chosen so small that it alone is insignificant dynamically.

The Lagrangian of χQCD, $L(C^2)$, has a simple dependence on the four-fermi coupling C^2 and when $C^2 \rightarrow 0$ or equivalently $\gamma \rightarrow \infty$, $L(C^2)$ becomes formally equivalent to the standard QCD Lagrangian. How small must C^2 be in order to be confident that we are extracting only QCD dynamics from the χQCD simulations and not physics which is dominated by the influence of the four fermion interaction

term ? We must ask for what threshold value of C^2 does the four-fermion interaction cease to dominate the physics? When the gauge coupling is taken to zero so that we are considering a pure four-fermi model, the simulations indicate that for $\gamma > 1.7$ [54] the chiral condensate vanishes so that the pure four-fermi model is already in the chirally symmetric phase for $\gamma > 1.7$. Therefore provided we choose $\gamma \gg 1.7$ the simulation results should correspond entirely to physical phenomena controlled by QCD dynamics.

Conjugate gradient inversion of the standard QCD Dirac operator requires a number of iterations which diverges as $V \to \infty$ and $m_q \to 0$. Inversion of the χQCD Dirac operator requires a finite number of iterations even at $m_q = 0$. In addition the scale of the 'time' step in the molecular dynamics algorithm of χQCD is set by the dynamical quark mass and thus can be chosen several times larger in χQCD than in QCD for the same systematic error or acceptance rate.

7.2.1 Formulation

The expansion of the GCPF for χQCD is very similar to that described above for standard QCD. The Dirac fermion matrices M and $\hat{M}$ are given by:

$$\begin{aligned} 2iM_{xy}(\mu) &= Y_{xy} + G_{xy} + V_{xy}e^{\mu} + V^{\dagger}_{xy}e^{-\mu} \\ -2i\hat{M}_{xy}(\mu) &= Y^{\dagger}_{xy} + G_{xy} + V_{xy}e^{\mu} + V^{\dagger}_{xy}e^{-\mu}. \end{aligned} \tag{7.11}$$

where

$$Y = 2i\left(m_q + \frac{1}{16}\sum_{<x,\tilde{x}>}(\sigma(\tilde{x}) + i\epsilon\pi(\tilde{x}))\right)\delta_{xy}. \tag{7.12}$$

The determinants of these fermion matrices are related to that of the propagator matrix

$$P = \begin{pmatrix} -GV - YV & V \\ -V & 0 \end{pmatrix} \tag{7.13}$$

by

$$\begin{aligned} \det(2iM) &= e^{3\mu n_s^3 n_t}\det(P - e^{-\mu}) \\ \det(2i\hat{M}) &= e^{3\mu n_s^3 n_t}\det\left((P^{-1})^{\dagger} - e^{-\mu}\right) \end{aligned} \tag{7.14}$$

As for standard QCD, determination of the eigenvalues of P^{n_t} gives the expansion for the GCPF:

$$Z = \sum_{n=-6n_s{}^3}^{6n_s{}^3} < b_{|n|} > e^{n\mu n_t} = \sum_{n=-6n_s{}^3}^{6n_s{}^3} e^{-(\epsilon_n - n\mu)/T}. \tag{7.15}$$

7.3 Preliminary results of simulations of χQCD at finite density

The above equation provides an expansion of the GCPF in terms of the canonical partition functions for fixed particle number [62]. Hence the chemical potential is given as a function of fermion number by the local derivative with respect to n of ϵ_n, the energy of the state with n fermions.

$$\mu(\rho) = \frac{1}{6n_s^3}\frac{\partial \epsilon_n}{\partial \rho} \tag{7.16}$$

where ρ is the fermion density, $\frac{n}{6n_s^3}$.

We have measured the energies ϵ_n for χQCD at strong and intermediate gauge couplings and varying 4-fermi couplings (parametrized by γ) on 4^4 and 6^4 lattices with $m_q = 0$.

Given sufficient measurements, the ϵ_n with $\mathrm{mod}(n,3) = 0$ should be real and finite whereas the ϵ_n with $\mathrm{mod}(n,3) \neq 0$ should tend to ∞ (so that $b_n \to 0$) because of the $Z(3)$ tunnelling described above. We do see in our simulations that this tunnelling is occurring, with the strongest signal around the small n levels. However, although some of the triality zero levels are determined with large error, it is clear that their real parts are approximating to a continuous curve with respect to n, as shown in Fig. 7.1.

We therefore made a cubic spline fit to a randomly selected subset of $n_s^3/3$ of the $2n_s^3$ ϵ_n's with $n > 0$ and triality zero and evaluated the derivative. This process was performed $n_s^3/3$ times and an estimate of the fitting error and the mean was obtained from the distribution of the corresponding $\mu(\rho)$'s. The continuity of the coefficients allows us to obtain profiles of the number density and energy density even on samples with limited statistics. The process is illustrated for a sample data set on a 6^4 lattice with $\beta = 5.0$ and $\gamma = 3$ by Figs. 7.2 and 7.3 . A total of 433 triality zero GCPF expansion coefficients from the coefficient corresponding to the zero quark ($n = 0$)CPF up to the coefficient corresponding to a fully populated lattice with $n = 2{n_s}^3 n_t$ quarks. A random number generator was used to select 80 distinct values of n and the corresponding 80 coefficients were used to obtain the chemical potential as a function of the fermion number density from the local derivative of the coefficients with respect to n (with appropriate normalisations). The derivative was calculated in the simplest possible way from the actual data points. This analysis was repeated on 300 sets of 80 coefficients and the results were plotted in the top diagram in Fig. 7.2. Since we expect the estimates of the

coefficients to improve as the statistics are increased we investigated the effects of excluding those coefficients in the sample of 433 which were known to have large statistical errors and those which were not strictly positive (remembering that the coefficients must be positive if their interpretation as canonical partition functions is to be valid). We call this subset of 129 relatively accurate coefficients the "filtered set". The results of the same analysis on the filtered set are shown in the bottom diagram in Fig. 7.2. Clearly we have achieved a more clear-cut number density curve and comparison of the upper and lower plots in Fig. 7.2 inspires confidence in our analysis procedure since we can see that as the statistical errors are reduced we can expect the outlying data points on the number density profile to converge towards the fitted curve. The results of our splinefit to the data set are shown in Fig. 7.3.

In Fig. 7.4 we show the number density at strong gauge coupling, $m_q = 0$ on a 4^4 lattice for varying 4-fermi couplings given by γ. The pion is massless and mean field analyses [48] predict the critical μ to be about 0.60. Standard QCD would give the particle number becoming non-zero at very small μ whereas our simulation of χQCD is in good agreement with the mean field prediction. Note that we expect the fermion number density curves to become progressively closer as γ is increased since for large γ values (weaker four-fermi couplings) the four-fermi term ceases to dominate so the number density should become characteristic of standard finite density QCD. The simulation results are consistent with this trend.

Fig. 7.5 shows the number density at a weaker gauge coupling $\beta = 5.0$ and $m_q = 0.0$ for varying γ on a 6^4 lattice. Simulations at $\mu = 0$ indicate that there is a finite 'temperature' quark gluon plasma transition for γ between 5.0 and 6.0. Our results were totally consistent with this prediction - Fig. 7.5 shows this transition very clearly with the critical $\mu > 0.5$ for $\gamma < 5.0$ and falling suddenly to zero for $\gamma = 6.0$. For $\gamma = 1, 2, 3, 4, 5$ our results were consistent with those on the 4^4 lattice at $\beta = 0.5$ i.e. μ_o was significantly larger than the onset μ for the number density in standard QCD. The six sets of zeros for the 6^4 lattice are plotted in Fig. 7.6. The inclusion of the four-fermi coupling means that we expect a zeros pattern which is distinct from the simple pattern observed for the standard QCD simulations. It can be seen that for $\gamma = 1$ where the four-fermion interaction is dominant and for $\gamma = 6$ where the QCD sector is deconfined the zeros have general features resembling those in the Gross-Neveu simulations. For $\gamma = 2, 3, 4, 5$ the innermost circular arc of zeros has a radius which decreases gradually and the corresponding fermion number density curves become progressively closer as gamma increases.

The histograms of the real part of the zeros are plotted in Fig. 7.7. The histograms should be compared with those obtained for standard QCD at $\beta = 5.01$. Although the onset μ is distinctly larger for χQCD it is possible that there is a signal for a secondary peak is developing at $\mu \sim 0.8$ in the $\gamma = 5$ and $\gamma = 6$ data sets. This is supported by Fig. 7.8 which shows the fermion number susceptibility for the 6^4 lattice at $\gamma = 5$ and for the 8^4 lattice at $\gamma = 8$, both at intermediate gauge coupling. The susceptibility plots for the two lattices are remakably similar and there seems to be an increase in gradient at $\mu \sim 0.8$. We have also checked the μ^3 scaling of the number density and the μ^4 scaling of the energy density which is the behaviour expected in the continuum limit. For the range of chemical potential where the scaling is continuum-like the quantities plotted in Fig. 7.9 should have zero gradient – this seems to be a good approximation for $\mu \sim 0.8-1.0$. Furthermore the continuum scaling behaviours of both standard QCD and χQCD appear to be consistent as shown for the fermion number density in Fig. 7.10. Clearly the onset μ is significantly larger for χQCD than for QCD however both data sets have zero gradient (consistent with μ^3 scaling) in the region marked mu_X to mu_Y. Comparing with Fig. 5.6, $mu_X = 0.72$ corresponds to the inner circle and $mu_Y = 0.89$ to the outer circle of the band of increased density associated with μ_c and the second peak in the histogram of the real parts of the zeros. The real parts of the zeros for χQCD (8^4 lattice) are plotted in the lower portion of Fig. 7.10. The development of a secondary peak is more difficult to distinguish than for standard QCD because the onset is much larger for χQCD however it is possible that an additional signal (corresponding to the true transition) at $\mu > \mu_o$ could also be present in this case.

Stochastic estimators were implemented for χQCD at $\gamma = 8$ and $\beta = 4$ on an 8^4 lattice (see Figs. 7.11 and 7.12). The operators used for the stochastic estimators are defined in Eqns. 2.44, 2.45 and 2.46. For the 8^4 lattice, the expectation value of the operator $\mathcal{O}$ was calculated from the following ad. hoc. definition:

$$\langle \mathcal{O} \rangle = \frac{\langle \mathrm{Abs}\left(\mathcal{O} \frac{\det(\mu \neq 0)}{\det(\mu = 0)} \right) \rangle}{\langle \mathrm{Abs}\left(\frac{\det(\mu \neq 0)}{\det(\mu = 0)} \right) \rangle} \tag{7.17}$$

Although the above definition is non-standard, it was necessary to use the **absolute value** of the (appropriately normalised) determinant to eliminate the effects of the fluctuations in sign.

The profiles of the fermion number and energy densities were completely consistent with those obtained from the coefficients of the grand canonical partition function. For this 8^4 lattice with the given parameters we found $\mu_o \sim 0.5$. It was also possible to obtain the chiral condensate using a stochastic estimator. As seen

in Fig. 7.12 the chiral condensate starts to fall at $\mu \sim \mu_o$ indicating the onset of the chiral transition however the gradient becomes distinctly less negative for $\mu \sim 0.6 - 1.0$ the interpretation of this effect is unclear at present.

The effects of the fluctuations in sign mentioned above can be seen from the stochastic estimator results on the 4^4 lattice for $\beta = 0.5$ and $\gamma = 9$ (see Fig. 7.13) where the absolute value of the determinant was **not** taken.

7.4 Summary of χQCD Simulations

We have seen in previous chapters that the finite density simulations which include dynamical fermions give a clear signal for the expected transition at μ_c but retain the pathological quenched onset μ_o. It is still conceivable that μ_o may not cancel with high statistics in which case a satisfactory simulation of finite density QCD requires an algorithm which produces physical results *on each configuration.* This has motivated our study of χQCD where we have added a perturbatively irrelevant four fermion interaction term to the lattice QCD Lagrangian. χQCD has the advantage that chiral symmetry breaking and the generation of a dynamical quark mass occurs **configuration-by-configuration** and the pion and sigma excitations are explicitly free of μ dependence. We have seen that χQCD simulations do not appear to suffer from the severe μ_o pathologies seen in standard QCD. We note that the introduction of a four-fermi interaction can also speed up spectroscopy and matrix element calculations for QCD with dynamical fermions at light quark masses because of the dynamical quark mass it introduces.

Certainly additional analytical and numerical work is required to see if χQCD really produces only physical results. In particular, it will be necessary to explore the interplay between the gauge coupling and the four-fermi coupling to determine definitively the range of couplings for which QCD dynamics is dominant. The condition $\gamma > 1.7$ is a necessary but not necessarily a sufficient condition to ensure that the chiral symmetry breaking is entirely due to the QCD sector of the theory. Additional simulations should be able to clarify whether $\mu_o = \mu_c$ for χQCD. In future work it will be important to establish how the critical points of QCD and of χQCD are related. For example, does the χQCD onset scale like $m_\pi(\langle\sigma\rangle)/2$ or like $m_B(\langle\sigma\rangle)/3$? Addressing such questions should help to reveal the origin of the pathologies of finite density QCD simulations. If we find that $\mu_o < \mu_c$ in χQCD as well as QCD we will have to reconsider the role of the quark propagator in a colour confined system and attempt to understand how the poles in the propaga-

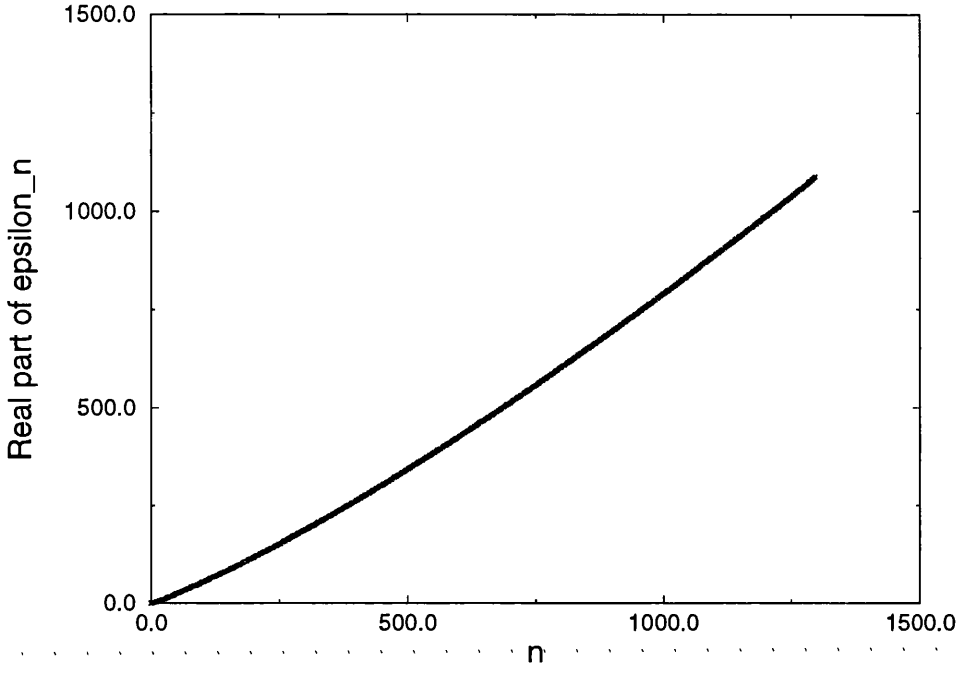

Figure 7.1: The energy levels ϵ_n vs. n on a 6^4 lattice at $\beta = 5.0$ and $\gamma = 5.0$.

tor for $\mu_o \to \mu_c$ could be cancelled by the fermion determinant. These questions can be addressed by exploring the phenomenology of the χQCD algorithm and by performing very high statistics QCD simulation to see how μ_o evolves in relation to the signal for μ_c.

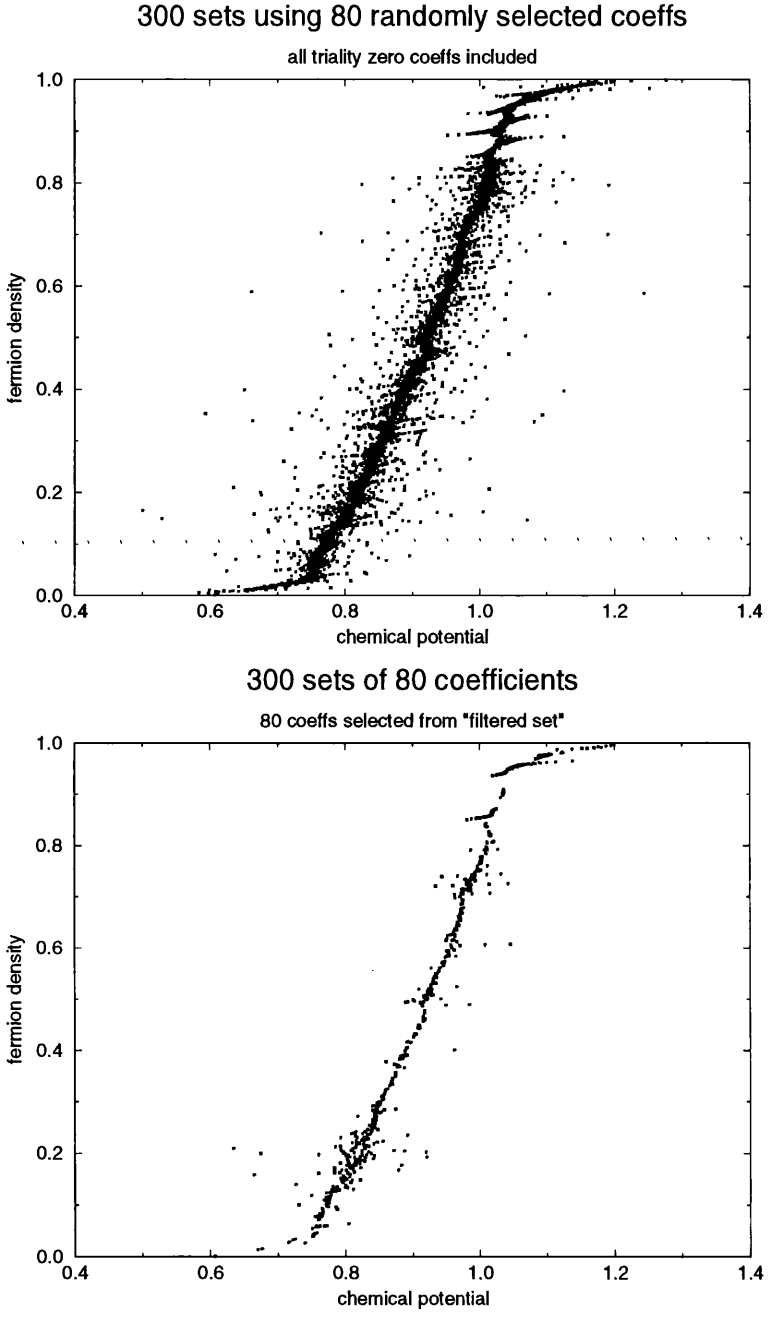

Figure 7.2: The fermion number density vs. the chemical potential, μ, on a 6^4 lattice at β=5.0 for $\gamma = 3$. In the upper diagram all triality zero coefficients have been included whereas in the lower diagram the coefficients which were not strictly positive and those with large statistical error were excluded.

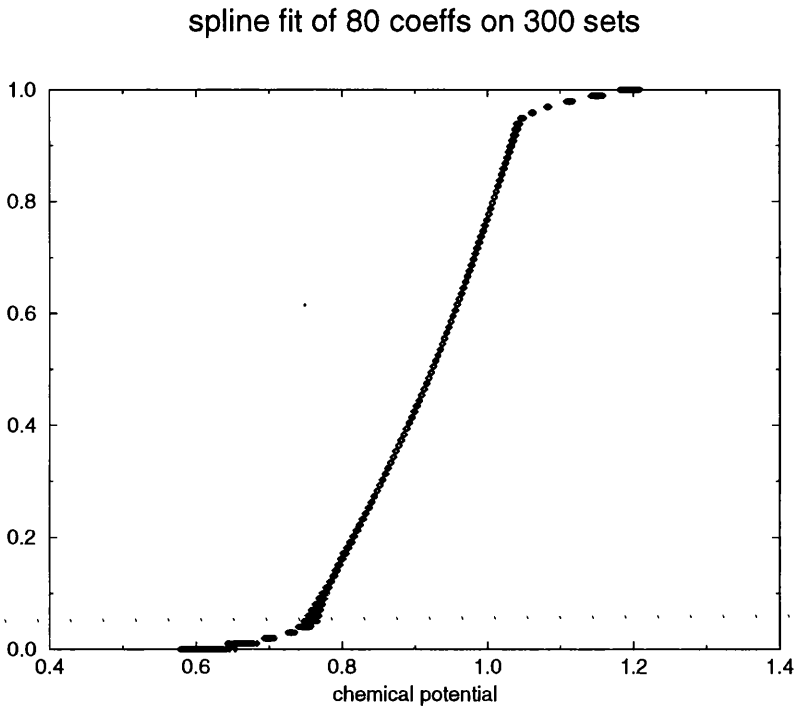

Figure 7.3: A splinefit to the same data set used in Fig. 7.2.

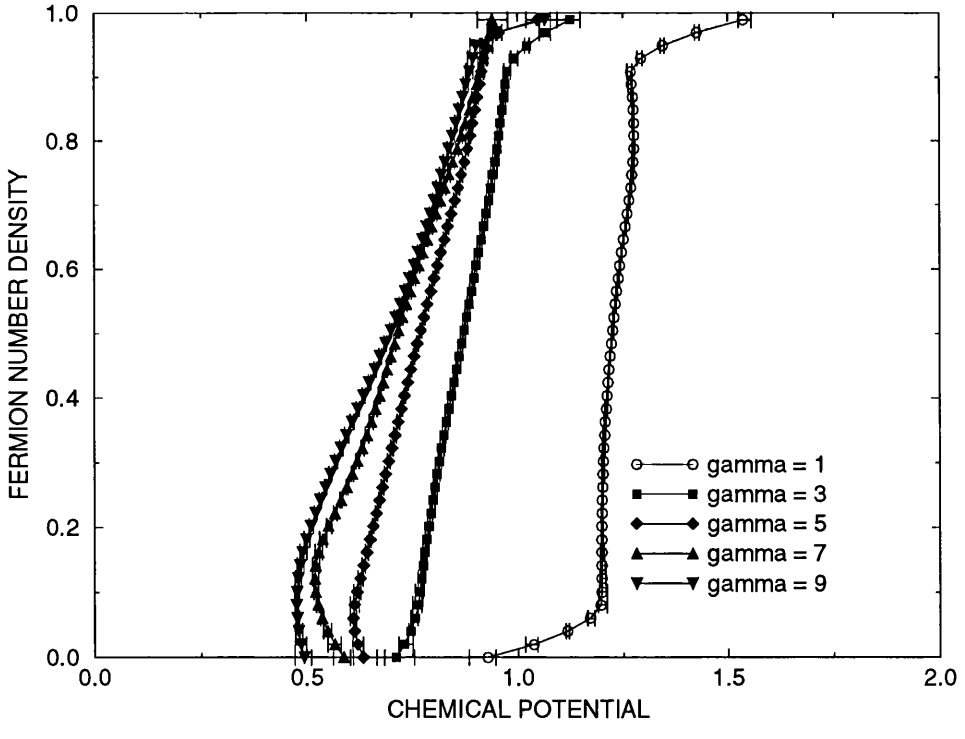

Figure 7.4: The fermion number density vs. the chemical potential, μ, on a 4^4 lattice at $\beta = 0.5$ for varying γ.

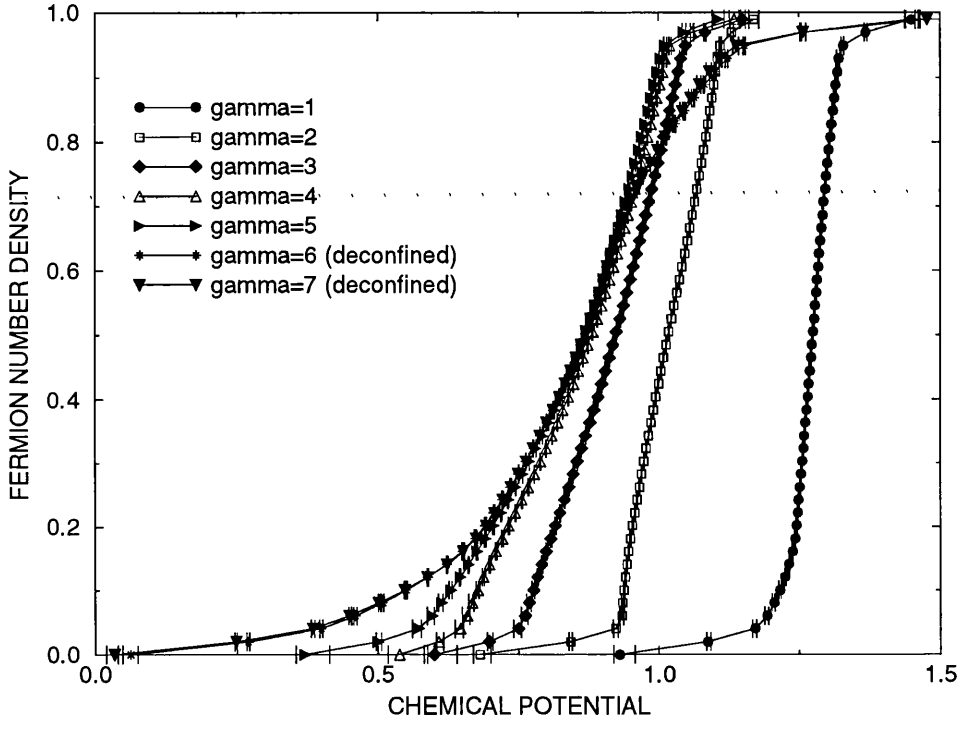

Figure 7.5: The fermion number density vs. the chemical potential, μ, on a 6^4 lattice at β=5.0 for varying γ.

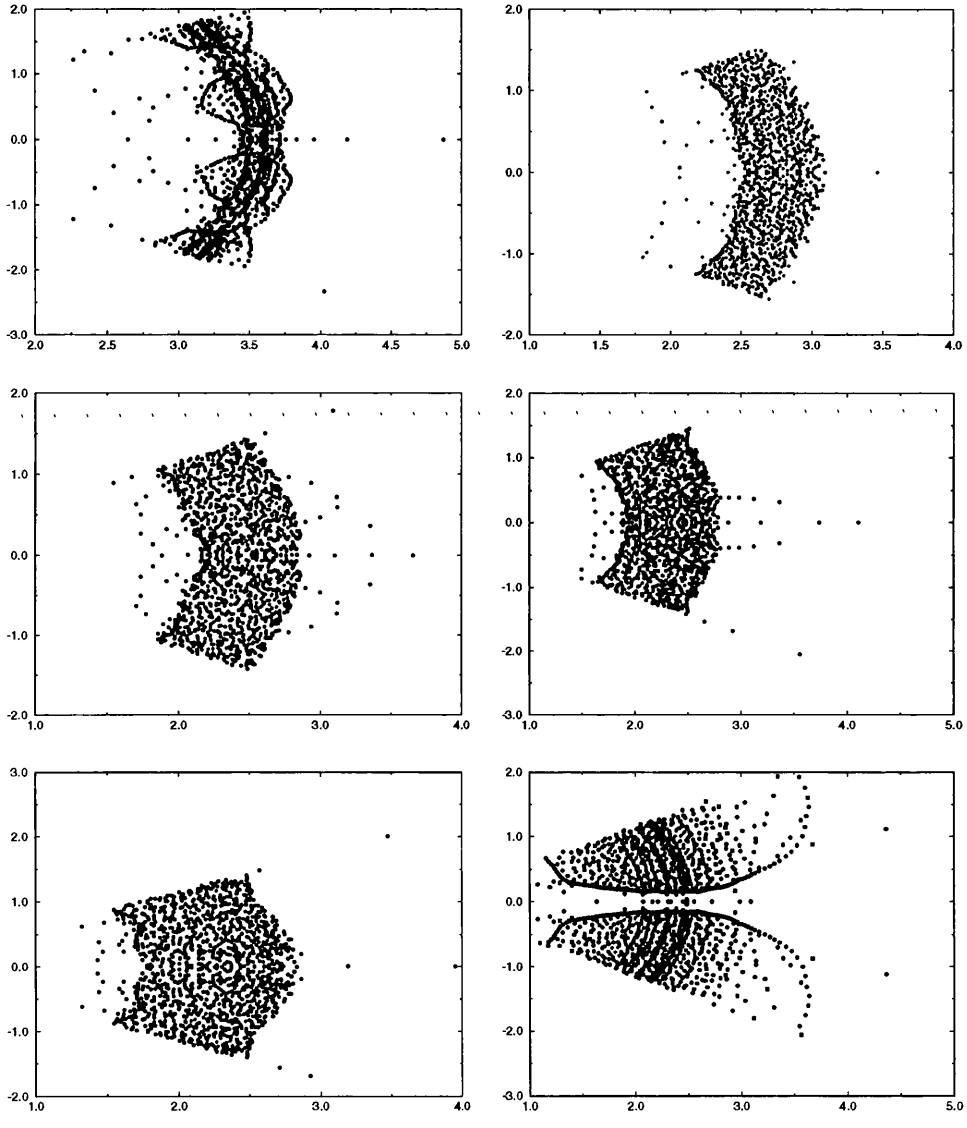

Figure 7.6: e^{μ} PLANE ZEROS FOR CHIRAL QCD ON A 6^4 LATTICE AT $\beta = 5.0$ AND $\gamma =$ 1,2 (top);3,4(middle);5,6(bottom)

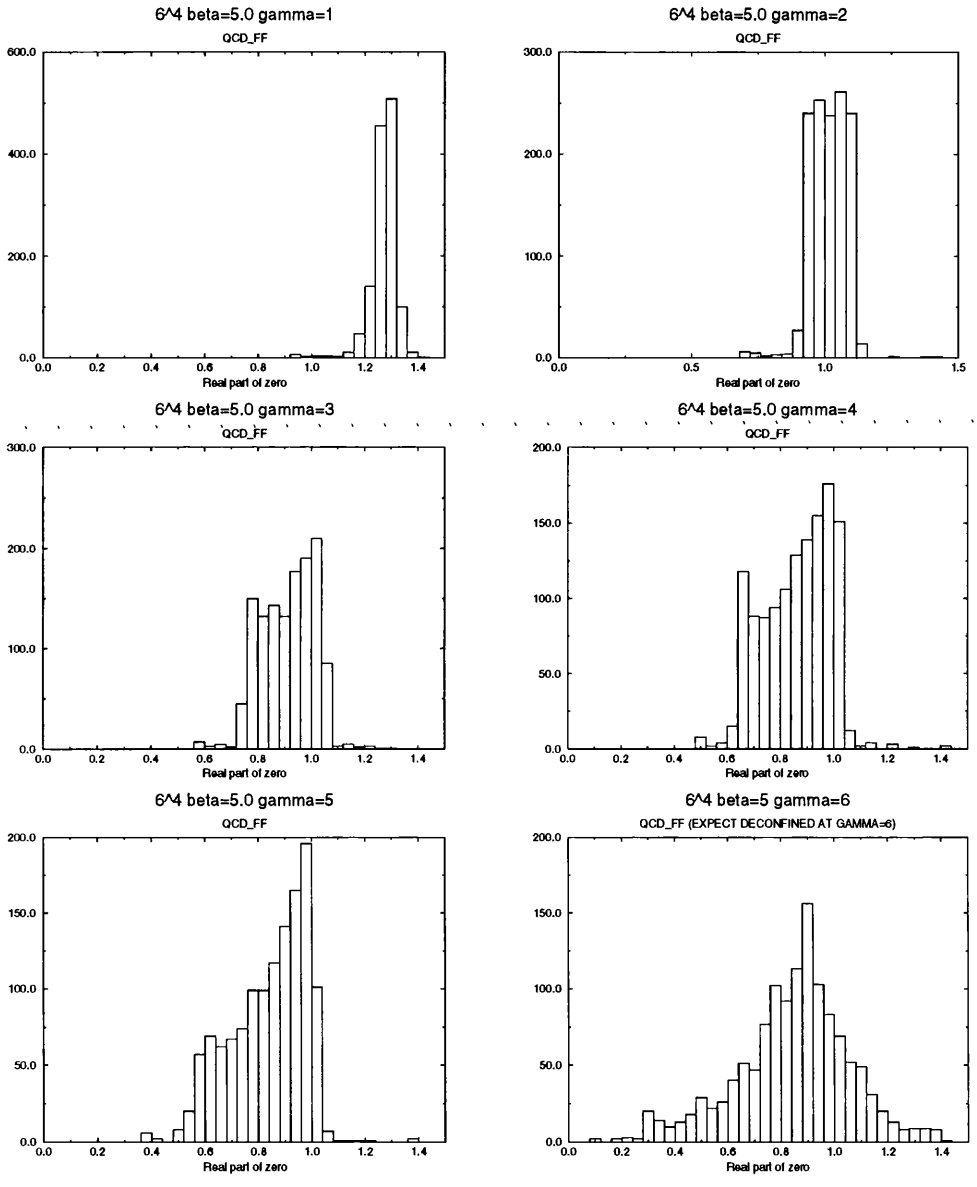

Figure 7.7: Histograms of real parts of zeros in complex μ plane, on a 6^4 lattice at β=5.0 for various values of γ.

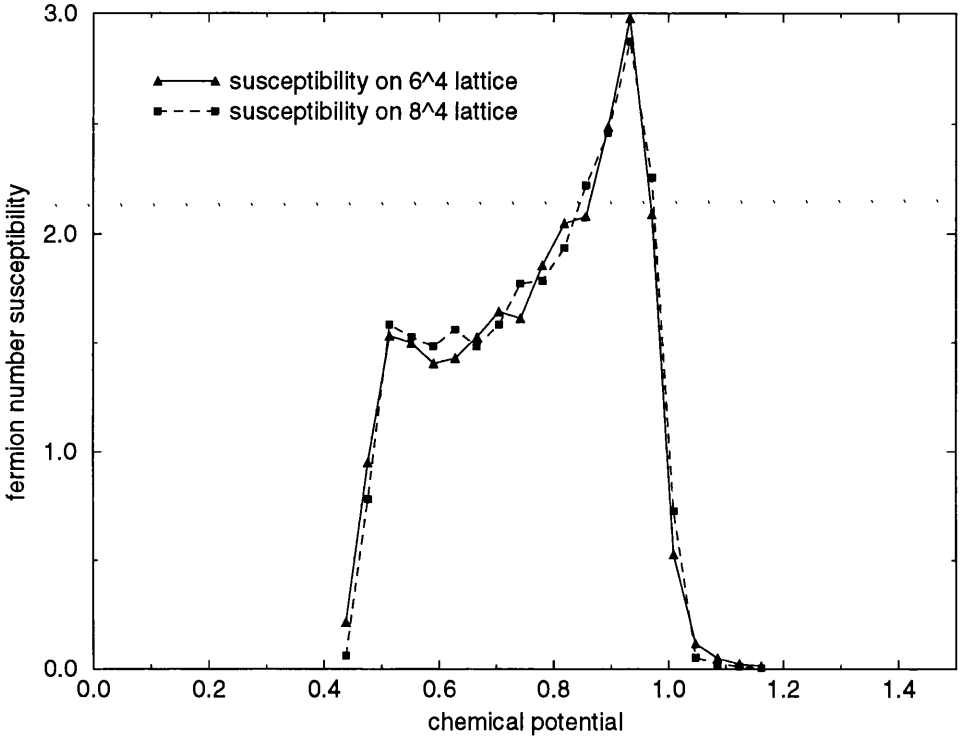

Figure 7.8: Comparison of fermion number susceptibility on a 6^4 lattice with $\beta = 5.0$, $\gamma = 5$ and an 8^4 lattice at β=4.0 with $\gamma = 8$.

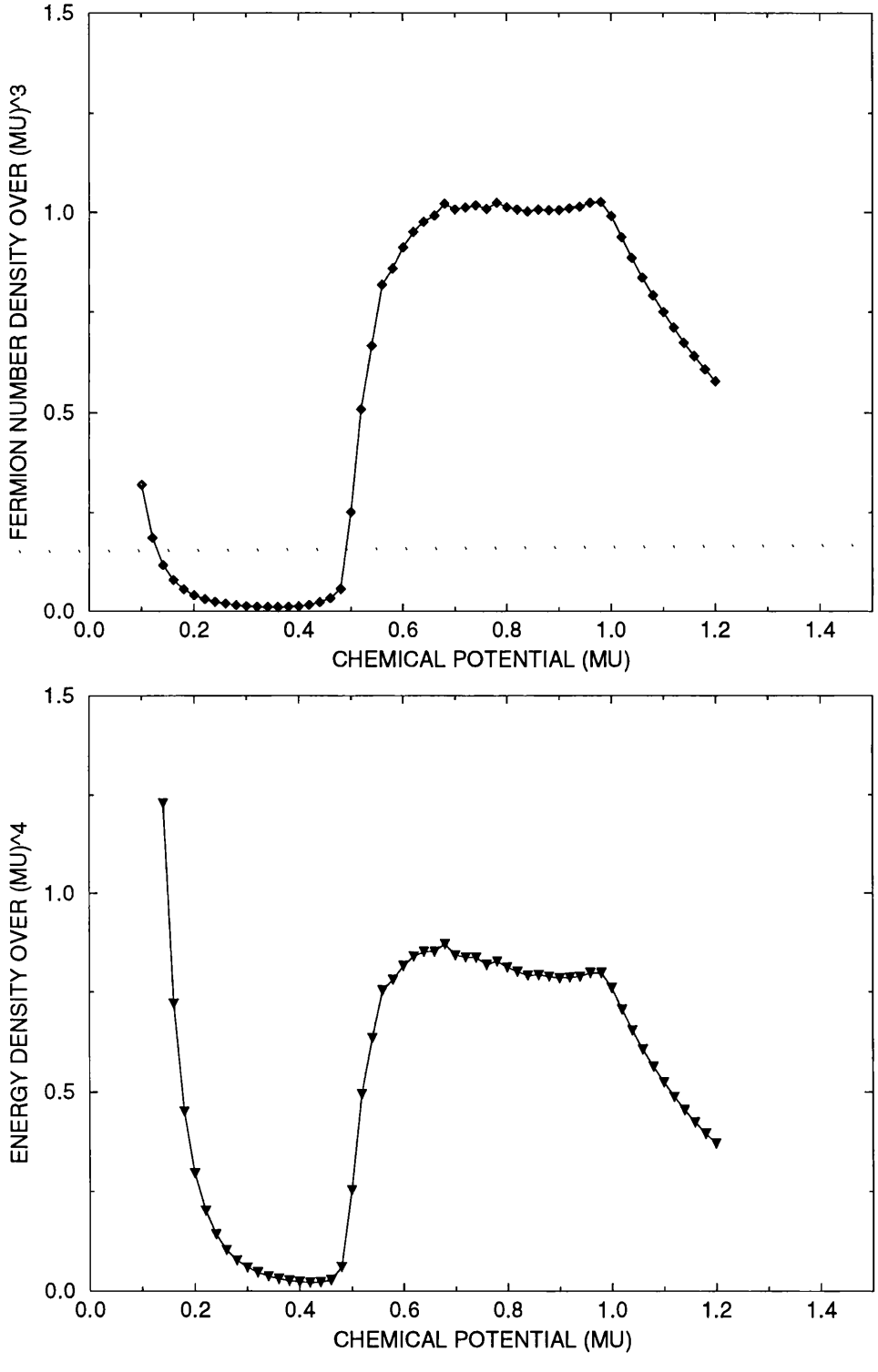

Figure 7.9: Plots showing the range of chemical potential for which we appear to have continuum-like scaling of the fermion number density (top) and fermion energy density (bottom) for χQCD on an 8^4 lattice at $\beta = 4.0$ and $\gamma = 5$

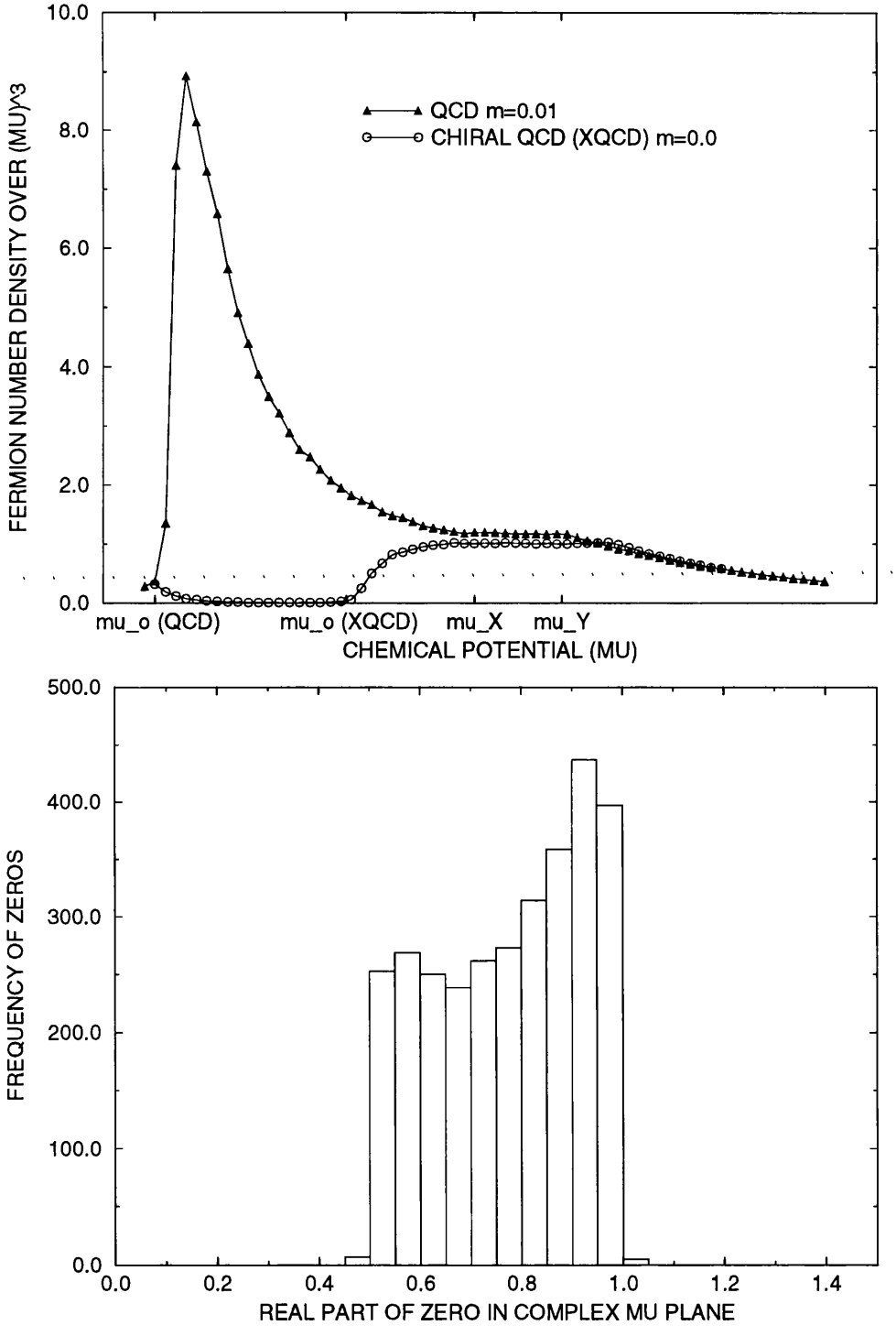

Figure 7.10: The top diagram provides a comparison of the scaling behaviours of the fermion number density for χQCD (m=0.0, $\beta = 4.0$) and for standard QCD (m=0.01, $\beta = 5.0$) on an 8^4 lattice. The bottom diagram shows the histogram of the real parts of the zeros in the complex μ plane corresponding to the same 8^4 χQCD data set

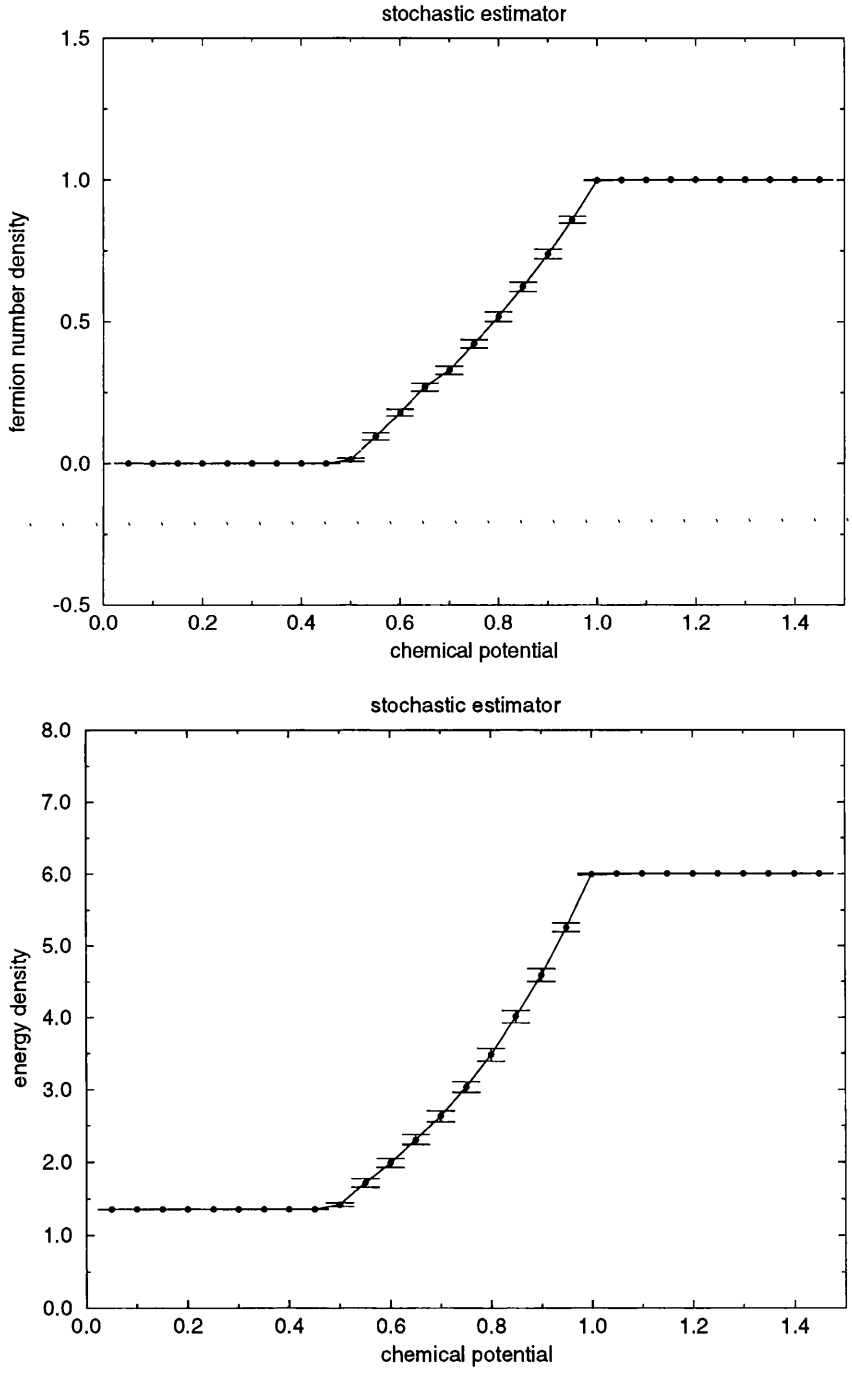

Figure 7.11: Results from stochastic estimators, on an 8^4 lattice at $\beta = 4.0$ for $\gamma = 8$: fermion number density (top), fermion energy density (bottom).

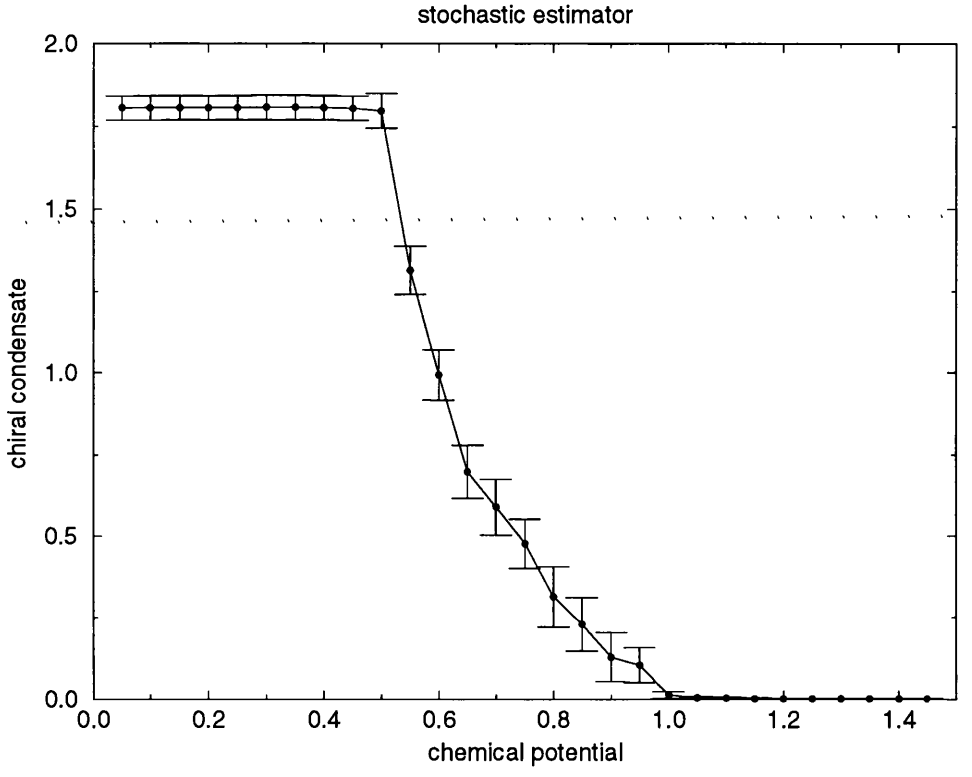

Figure 7.12: Chiral condensate from stochastic estimator, on a 8^4 lattice at $\beta = 4.0$ for $\gamma = 8$.

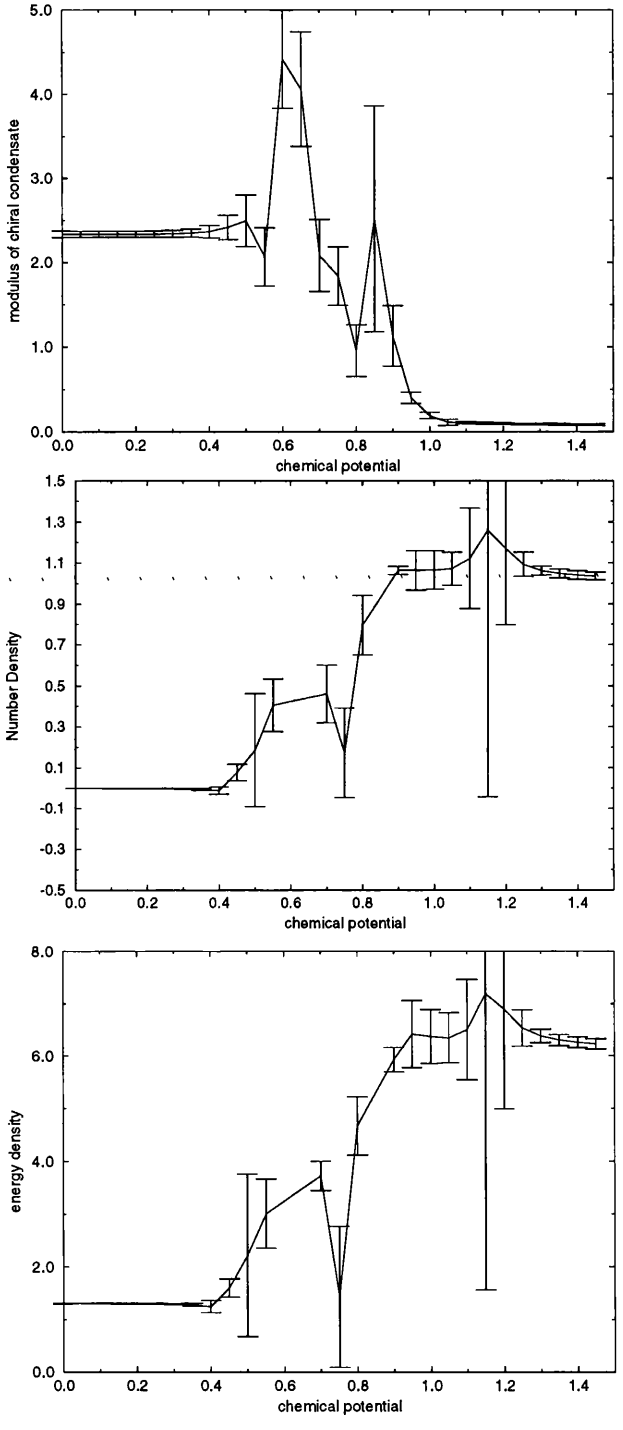

Figure 7.13: Results from stochastic estimators, on a 4^4 lattice at $\beta = 0.5$ for $\gamma = 9$: chiral condensate (top), fermion number density (middle) and fermion energy density (bottom).

Conclusions

The pathologies of quenched lattice QCD at non-zero chemical potential are well-known. However the explanations for the failure of the quenched theory have been the focus of debate ever since the problem was first exposed in 1986 [31]. Gibbs [35] showed that the failure of the quenched theory could be explained by the mass poles in the fermion propagator on isolated configurations and the more recent work of Stephanov [37] using a random matrix model strongly suggests that the phase of the fermionic determinant is important and that the true physical nature of the deconfinement/chiral transition at $\mu \neq 0$ will only be revealed with a simulation which correctly implements dynamical quarks. This task is a difficult one since the fermion determinant becomes complex for $\mu \neq 0$ and standard Hybrid Monte Carlo simulation algorithms cannot be directly applied.

This thesis describes an attempt to implement dynamical fermions in finite density QCD simulations by using a reweighting method where the statistical ensemble is generated at zero chemical potential thereby avoiding the problem of the complex action. The grand canonical partition function is expanded in powers of the fugacity variable and from the coefficients of this expansion the fermion number density and energy density are obtained. The coefficients are also used to perform a Lee-Yang zeros analysis of the partition function which gives us additional information on the phase structure of the theory.

The Glasgow method was applied to simulations at infinite coupling where our results could be compared with analytical results from the strong coupling expansion [48] and simulation results from the monomer-dimer algorithm [49]. By extending the arguments of Gibbs and developing an improved complex zeros analysis we have shown that the reweighting method gives clear signs of the critical point μ_c which should be the point of chiral symmetry restoration. The method also gives an onset, μ_o, in the number density which is much less than μ_c. This onset is most likely unphysical since it is not seen in the monomer-dimer results and it coincides with

the pathological onset first seen in the quenched theory. We have demonstrated by an analysis of the probability distributions for particle number that μ_o is the threshold of a phase characterised by forward quark propagation.

Simulations at intermediate gauge coupling $\beta = 5.1$ where $S_G \neq 0$ showed features very similar to the infinite coupling simulations with an early onset μ_o for the transition and a signal for the true critical point μ_c in the zeros. The susceptibilities of the number and energy densities supported this scenario. An investigation of the scaling of μ_o with the bare quark mass revealed scaling with the square root of the bare quark mass which suggested that a Goldstone pion was controlling the onset. This result was unexpected because a pion has zero baryon number and therefore should not propagate in the temporal direction for $\mu \neq 0$. Unfortunately since the thermodynamic observables in our simulations deviate from zero at the unphysical μ_o point, their values near μ_c cannot be trusted which means that although the Glasgow algorithm gives μ_c accurately, it does not make any other *phenomenologically* reliable predictions.

We have attempted to address the question of whether the persistence of μ_o originates from having generated configurations at zero chemical potential. This explanation is suggested from the standard problems encountered by reweighting procedures and from the behaviour observed in our exploratory simulations of the 3 dimensional Gross-Neveu model at $\mu \neq 0$. Implementation of the reweighting procedure in this simple model indicated that (with limited statistics) the discontinuity in the number density at the chiral transition point μ_c was not observed. The discontinuity was clearly observed in the exact simulations at four-fermi coupling of $1/C^2 = 0.5$. However by generating our ensemble at $\mu < \mu_c$ we were able to accurately predict the critical chemical potential from the Lee-Yang zeros analysis. We verified the findings of the exact simulations in that we did not observe an early onset of the chiral transition despite having a non-zero bare quark mass in our simulations in a theory with pion which is massless in the chiral limit.

It is expected that the onset in the QCD simulations should disappear in a correct calculation. This would require cancellation of the poles of the fermion propagator by the fermion determinant. It may well be that a very high statistics run of the Glasgow reweighting algorithm will cancel the early onset μ_o and in this case a strategy should be developed to monitor the convergence of the method to the correct statistical ensemble. If the unwanted onset μ_o can be cancelled with high statistics then implementation of the reweighting method would be CPU intensive although not conceptually wrong. An unpleasant possibility which must be

considered if the unwanted onset cannot be cancelled is that the Hybrid Monte Carlo approach to finite density QCD is flawed. The monomer-dimer algorithm involves first integrating over the gauge fields and then the fermion fields. Hybrid Monte-Carlo algorithms integrate the fermion fields first. It is clear from the work presented in this thesis that ensemble averaging does not help to suppress the pathologies of isolated configurations.

It may be the case that a satisfactory simulation of finite density QCD requires an algorithm which produces physical results on each configuration. A promising development of this sort is χQCD [54], where an irrelevant four fermi term is added to the standard QCD action used here. χQCD has the advantage that chiral symmetry breaking and the generation of a dynamical quark mass occurs configuration-by-configuration and the pion and sigma excitations are explicitly free of μ dependence. In fact preliminary simulations of χQCD at non-zero chemical potential described in Chapter 7 of this thesis do not seem to suffer from the severe μ_o pathologies seen here but additional work, both theoretical and practical, is needed to see if χQCD really produces only physical results. Certainly the forbidden region $\mu_o \leq \mu \leq \mu_c$ (characterised by large fluctuations in the observables) is significantly smaller for χQCD than for standard QCD. In future χQCD simulations it will be necessary to explore the interplay between the gauge coupling and the four-fermi coupling in order to determine the range of couplings for which QCD dynamics is dominant. The condition $\gamma > 1.7$ is a necessary but not a sufficient condition to ensure that the chiral symmetry breaking is entirely due to the QCD sector of the theory. Additional simulations should be able to clarify whether $\mu_o = \mu_c$ for χQCD

Simulations of Lattice QCD at finite baryon density continue to pose a challenge for theoretical physics and although steady progress has been made towards understanding the pathologies of the theory, increased computing power and more theoretical effort are required before we can make confident predictions for critical densities an energies associated with the deconfinement/chiral phase transition.

List of Figures

List of Tables

Bibliography

[1] I.M. Barbour and A.J. Bell. *Nuclear Physics*, B372:385, 1992.

[2] S. Hands, S. Kim, and J.B. Kogut. *Nuclear Physics*, B442:364, 1995.

[3] D.J. Gross, R.D. Pisarski, and L.G. Yaffe. *Reviews of Modern Physics*, 53:43, 1981.

[4] J.H. Applegate, C.J. Hogan, and R.J. Scherrer. *Physical Review*, D35:1151, 1987.

[5] B. Muller and J.W. Harris. *Proceedings of the NATO Advanced Study Institute on Particle Production in Highly Excited Matter.* Plenum, 1993.

[6] J.B. Kogut, H. Matsuoka, M. Stone, H.W. Wyld, S. Shenker, J. Shigemitsu, and D.K. Sinclair. *Nuclear Physics*, B225 [FS9]:93, 1983.

[7] L.H. Karsten and J. Smit. *Nuclear Physics*, B183:103, 1981.

[8] H.B. Nielsen and M. Ninomiya. *Nuclear Physics*, B185:20, 1981.

[9] H.B. Nielsen and M. Ninomiya. *Nuclear Physics*, B195:541, 1981.

[10] H.B. Nielsen and M. Ninomiya. *Nuclear Physics*, B193:173, 1981.

[11] H. Kluberg-Stern, A. Morel, O. Napoly, and B. Petersson. *Nuclear Physics*, B220:447, 1983.

[12] Iwasaki *et. al. Nuclear Physics B (Proc. Suppl.)*, 53:449, 1997.

[13] Karsch *et. al. Nuclear Physics B (Proc. Suppl.)*, 53:413, 1997.

[14] F. Karsch and E. Laermann. *Physical Review*, D50:6954, 1994.

[15] R. Pisarski and F Wilczek. *Physical Review*, D29:339, 1984.

[16] P. Hasenfratz and F. Karsch. *Physics Letters*, 125B:308, 1983.

[17] S Weinberg. *The Quantum Theory of Fields*, volume II. Cambridge University Press, 1996.

[18] Y. Nambu. *Physics Review Letters*, 4:380, 1960.

[19] Y. Nambu and G. Jona-Lasinio. *Physical Review*, 122:345, 1961.

[20] J. Goldstone. *Nuovo Cimento*, 9:154, 1961.

[21] J. Goldstone, A. Salam, and S. Weinberg. *Physical Review*, 127:965, 1962.

[22] Cheng Ta-Pei and Li Ling-Fong. *Gauge theory of elementary particle physics.* Oxford University Press, 1983.

[23] A. Casher. *Physics Letters*, 83B:395, 1979.

[24] R.V. Gavai. *Physical Review D*, D32(2):519, 1985.

[25] N. Bilić and R.V. Gavai. *Z. Phys.*, C 23:77, 1984.

[26] P.H. Damgaard, D. Hochberg, and N. Kawamoto. *Physics Letters*, 158B:239, 1985.

[27] E. Dagotto, Karsch F., and Moreo A. *Physics Letters*, 169B No. 4:421, 1986.

[28] S. Duane, A.D. Kennedy, B.J. Pendleton, and D. Roweth. *Physics Letters*, B195:216, 1987.

[29] S. Duane and J.B. Kogut. *Physics Review Letters*, 55:2774, 1985.

[30] S. Gottlieb, W. Liu, D. Toussaint, R.L. Renken, and R.L. Sugar. *Physical Review*, D35:2531, 1987.

[31] I.M. Barbour, N-E. Behilil, E. Dagotto, F. Karsch, A. Moreo, A. Stone, and H.W. Wyld. *Nuclear Physics*, B275 [FS17]:296, 1986.

[32] J.B. Kogut, M.-P. Lombardo, and D.K. Sinclair. *Physical Review*, D51:1282, 1995.

[33] J.B. Kogut, M.-P. Lombardo, and D.K. Sinclair. *Physical Review*, D54:2303, 1996.

[34] C.T.H. Davies and E. G. Klepfish. *Physics Letters*, 256B:68, 1991.

[35] P.E. Gibbs. *Physics Letters*, 172B:53, 1986.

[36] A. Gocksch. *Physical Review*, D37:1014, 1988.

[37] M.I. Stephanov. *Physics Review Letters*, 76:4472, 1996.

[38] A. Vladikas. *Nuclear Physics B (Proc. Suppl.)*, 4:322, 1988.

[39] D. Toussaint. *Nuclear Physics B (Proc. Suppl.)*, 17:248, 1990.

[40] A. Gocksch. *Physics Letters*, B61:2054, 1988.

[41] T. Blum, J.E. Hetrick, and D. Toussaint. *Physics Review Letters*, 76:1019, 1996.

[42] G.H. Golub and C.F. Van Loan. *Matrix Computations.* Hopkins, 1985.

[43] J.H. Wilkinson. *Rounding errors in algebraic processes.* Notes on applied science: No.32. London: H.M.S.O., 1963.

[44] C.N. Yang and T.D. Lee. *Physical Review*, 87:404, 1952.

[45] C.N. Yang and T.D. Lee. *Physical Review*, 87:410, 1952.

[46] Kerson Huang. *Statistical Mechanics.* Wiley, 1987.

[47] C. Itzykson, R.B. Pearson, and J.-B. Zuber. *Nuclear Physics*, B220:415, 1983.

[48] N. Bilić, K. Demeterfi, and B. Petersson. *Nuclear Physics*, B377:615, 1992.

[49] F. Karsch and K.H. Mütter. *Nuclear Physics*, B313:541, 1989.

[50] I.M. Barbour, C.T.H. Davies, and Z. Sabeur. *Physics Letters*, B215:567, 1988.

[51] J.H. Wilkinson. *Num. Math.*, 1:150, 1959.

[52] I.M. Barbour, E.G. Klepfish, J.B. Kogut, and S.E. Morrison. The Critical Points of Strongly Coupled Lattice QCD at Nonzero Chemical Potential. *Physical Review*, D:(to be published), 1997.

[53] I.M. Barbour, S.E. Morrison, E. Klepfish, J.B. Kogut, and M.-P. Lombardo. review talk given by I.M. Barbour at *lattice qcd on parallel computers.*

[54] J.B. Kogut and D.K. Sinclair. *Nuclear Physics B (Proc. Suppl.)*, 53:272, 1997.

[55] I.M. Barbour, S.E. Morrison, and J.B. Kogut. *xxx.lanl.gov preprint*, hep-lat/9612012, 1996.

[56] I.M. Barbour, S.E. Morrison, and J.B. Kogut. *Nuclear Physics B (Proc. Suppl.)*, 53:456, 1997.

[57] S.P. Klevansky. *Reviews of Modern Physics*, 64(3):649, 1992.

[58] H. Matsuoka and M. Stone. *Physics Letters*, 136B:204, 1984.

[59] B. Rosenstein, B.J. Warr, and S.H. Park. *Physics Reports*, 205(2):60, 1991.

[60] Y. Cohen, S. Elitzur, and E. Rabinovici. *Nuclear Physics*, B220:102, 1983.

[61] S. Hands, A. Kocic, and J.B. Kogut. *Ann. of Phys.*, 224:29, 1993.

[62] R.P. Feynmann. *Statistical Mechanics.* W.A. Benjamin, 1972.